ENGINEERING DESIGN AND OPTIMIZATION OF LARGE-SCALE SOLAR PHOTOVOLTAIC AND WIND TURBINE INSTALLATION IN AN URBAN ENVIRONMENT

FARIBORZ MANSOURI KOUHESTANI
Master of Science, University of Tabriz, 2005

A Thesis
Submitted to the School of Graduate Studies
of the University of Lethbridge
in Partial Fulfilment of the
Requirements for the Degree

DOCTOR OF PHILOSOPHY

Department of Geography
University of Lethbridge
LETHBRIDGE, ALBERTA, CANADA

ENGINEERING DESIGN AND OPTIMIZATION OF LARGE-SCALE SOLAR
PHOTOVOLTAIC AND WIND TURBINE INSTALLATION IN AN URBAN
ENVIRONMENT

FARIBORZ MANSOURI KOUHESTANI

Date of Defence: April 11, 2019

Dr. James Byrne Supervisor	Professor	Ph.D.
Dr. Dan Johnson Thesis Examination Committee Member	Professor	Ph.D.
Dr. Locke Spencer Thesis Examination Committee Member	Associate Professor	Ph.D.
Dr. Bryson Brown Thesis Examination Committee Member	Professor	Ph.D.
Dr. Paul Hazendonk Thesis Examination Committee Member	Associate Professor	Ph.D.
Dr. Amir Akbary-Majdabadno Internal Examiner	Professor	Ph.D.
Dr. Tim Weis External Examiner University of Alberta	Professor	Ph.D.
Dr. Greg Pyle Chair, Thesis Examination Committee	Professor	Ph.D.

Dedication

This study is earnestly dedicated to my wife, Shaghayegh for all her patience, support, and

friendship.

Abstract

Wind turbine and photovoltaic (PV) technologies will play a significant role in the world energy future. However, a lack of awareness of the potential of renewables is a significant challenge in sustainable energy development. The potential of solar and wind energy sources in producing electricity to meet the electrical demands of the University of Lethbridge was evaluated. Furthermore, expanding the research to a large area, a multi-criteria approach based on geographic information systems (GIS) and light detection and ranging (LiDAR) was developed to estimate rooftop photovoltaic potential of buildings in an urban environment, the City of Lethbridge. The unreliability of renewable resources is an impediment to developing renewable projects. An optimal sizing strategy was developed using a particle swarm optimization (PSO) technique to determine the optimum configuration of photovoltaic panels, wind turbines and battery units minimizing the annual system cost while maximizing the reliability of the hybrid system.

Acknowledgements

Table of Contents

List of Tables

List of Figures

Chapter 1: Introduction and Study Scope

Extensive energy generation and consumption are the main anthropogenic sources of greenhouse gas emissions and air pollution (two-thirds of all human-induced GHG emissions) (International Energy Agency 2015). Unless sufficient countermeasures are taken in the energy sector, the progressive deterioration of the environment related to these emissions will continue (International Energy Agency 2015). The world energy sector is facing dramatic structural and technological changes. The transition is driven by concerns for the environment, for energy supply security and independence, and global and regional energy availability, cost and competitiveness. Fossil fuels production and use have immense environmental impacts. Establishing a new energy system that supplies sufficient, reliable energy while protecting global and regional environments is imperative. The global significance of anthropogenic climate warming is driving rapid adoption of renewable energy sources. While this transition is just beginning, it creates enormous opportunities and similar scale challenges due to the complexity of design and installation of sophisticated renewable energy technologies and resources (World Energy Council 2016).

In general, renewable energy sources have lower adverse environmental impacts than fossil fuels particularly greenhouse gas emissions. Engineers, scientists, investors, decision makers, and society recognise we must transition to large scale renewable energy utilization (Shahzad 2012). The development of renewable energy sources as the main component of energy transition plays a vital role in reducing reliance on fossil fuels, combats climate change, preserves the environment, and reduces energy poverty by providing local clean energy (Jacobson et al. 2017). The renewable energy transition requires the allocation of all available resources from all sectors.

Investment in renewable energy sources has increased in many countries (L. Sawin et al. 2018). Globally, 178 GW of renewable energy capacity was added worldwide in 2017, representing 70% of the new energy generation capacity constructed. This is the highest ever global annual increase in renewable power production capacity to date – but this is not at all satisfactory progress (L. Sawin et al. 2018). Humanity needs a rapid transition off carbon-based fuels.

1.1 Alberta's Role in Reducing Electrical Sector GHG Emissions

Canada has one of the highest GHG per capita emissions globally, and emitted 1.6% of total global GHG emissions in 2014 (Government of Canada 2018). As a first world nation, Canada must take responsibility for dramatic reductions in per capita emissions. Canada ranked fourth globally in renewable power generation in 2015, and from 2005 to 2015, the share of power produced from all renewable energy sources in the country's total generated power increased from 60% to 65% (Lis et al. 2016). Existing hydro is the biggest source of electricity in Canada - 59.6% of total electricity generation from 2005 to 2016. Other renewable energy sources increased from 1.5% to 7.2% of total electricity generation since 2005 (Canada National Energy Board 2018). The increase is mostly wind energy, which grew from 684 MW capacity in 2005 to 12 GW in 2016 (Canadian Wind Energy Association 2017).

The electricity sector accounted for 11% of greenhouse gas emissions (GHGs) in Canada in 2015 (Lis et al. 2016). In Alberta 87.7% of electricity generation was from coal and natural gas in 2016 (Canada National Energy Board 2018). Because of this heavy reliance on fossil fuels for power generation, 57% of Canada's electricity GHG emissions were produced by Alberta in 2014 (Lis et al. 2016). Emitting 790 g of GHGs per kWh

electricity generation, Alberta has the highest GHG generation intensity in Canada (Canada's average is 140 g GHG/kWh) (Canada National Energy Board 2018). Renewables accounted for 12.3% of Alberta's electricity generation in 2016, with wind as the primary renewable power source (Canada National Energy Board 2018).

Alberta has a deregulated market and renewable facilities may not always be able to adjust and sell their produced power when electricity prices are higher, leading to lower average income compared with other power generators (Lis et al. 2016). Furthermore, the intermittent nature of wind and solar induces these resources to fail on demand power production for Alberta's large industrial sector, and makes backup supply sources a vital factor for reliable renewable energy deployment (Lis et al. 2016).

Alberta is endowed with outstanding wind and solar resource potential. Wind in Alberta is now the cheapest and most affordable source of new electricity. Wind now meets 7% of the province's electricity demand approximately, sufficient electricity for 380,000 average sized homes (Canadian Wind Energy Association 2018). The annual solar energy resource in Alberta is estimated at about one million-billion kWh. Canada consumed 1,784 petajoules (about 496 billion kWh) total electricity energy in 2015 (Natural Resources Canada 2018a). The solar energy resource in Alberta is approximately 2000 times the total annual electricity consumption in Canada! Alberta is a sunny province. Edmonton, at the same latitude (53.5° N) as Manchester, UK, has a yearly solar energy resource 20% larger. Solar electricity is expected to satisfy 100,000 Albertan households annual power demand on average by the end of 2018. The role of solar energy in Alberta's energy mix is expected to grow considerably due to continuous rapid reductions in cost of solar electricity (Canadian Solar Industries Association and Energy Efficiency Alberta 2018).

The Alberta climate leadership plan (CLP, November 2015) is designed to stimulate more renewable energy development and higher energy efficiency investments (Government of Alberta 2017). The CLP targets were new carbon pricing, phasing out emissions from coal electricity power plants, and increasing the share of renewables in Alberta's total electricity generation by 30% by 2030 (Government of Alberta 2017). The government of Canada is also committed to phase out coal power plants by 2030 to reduce GHGs (Natural Resources Canada 2018b).

To facilitate the deployment of solar photovoltaic (PV) and wind energy technologies and achieve higher solar PV and wind penetrations, exhaustive research on these systems' regional and local performance, potential, and cost is required. Accurate and reliable renewable energy resource evaluation is the cornerstone of any renewable energy planning and transition (Hermann et al. 2014). In fact, spatial and temporal availability assessment of renewable energy resources is necessary to utilize these resources efficiently (Ramachandra 2006). GIS and Remote Sensing (RS) are two key tools that are used to evaluate renewable energy resources temporally and spatially (Ramachandra 2006). An accurate and complete assessment of renewable energy capacity can be created by incorporating GIS and RS in energy system modeling (Resch et al. 2014). This research developed a series of energy models for assessing the local potential of solar and wind energy; and for optimal engineering development and design of renewable generation capacity.

1.2 Thesis structure

This is a refereed paper format thesis. Chapter 1 presents the introduction, background, scope and objectives. Chapter 2, currently under review, is titled: *A

comprehensive assessment of solar and wind energy potential at the University of Lethbridge campus. Chapter 3, titled: *Evaluating solar energy technical and economic potential on rooftops in an urban setting: the city of Lethbridge, Canada* is published in the International Journal of Energy and Environment Engineering (Kouhestani et al. 2018). Chapter 4, titled: *Multi-criteria PSO-based optimal design of grid-connected hybrid renewable energy systems* will be submitted shortly for publication. Chapter 5 provides an overall summary and conclusions for all chapters.

Chapter 2 employs light detection and ranging (LiDAR) data, aerial photography, and historical weather data to conduct a feasibility assessment of solar photovoltaic (PV) and wind turbine electricity potential for the University of Lethbridge campus, southern Alberta.

Three essential factors that govern solar PV energy generation include local solar resource, the size of PV systems, and the performance ratio of the systems (Sun et al. 2017). Two types of general solar PV electricity generation application models include large-scale PV facilities for non-built up suitable areas and rooftop PV systems for built-up areas (Sun et al. 2017). For wind energy, power curves can be employed to evaluate the wind turbine energy potential using measured wind speed data (Sohoni et al. 2016). Wind energy is gaining more attention among researchers and investors as the efficiency of wind turbines is increasing and their cost is reducing. Feasibility study concerning both energy production analysis and economic analysis is the most essential factor in higher wind deployment (Quan and Leephakpreeda 2015). This research investigates the ability of local renewables electricity generation to meet local demand based on measured local weather data and local geographic and land use characteristics.

Chapter 3 addresses rooftop PV energy production assessment in a large urban environment with intricate natural and built-up structures. A simulation and modelling framework and strategy for evaluating the potential of solar PV over a large area, City of Lethbridge's rooftops, is presented. City level energy reorientation is an indispensable element for efforts and plans that target energy and climate change crises (Byrne et al. 2015). Cities consume much electricity, but within cities, many areas provide opportunities for local infrastructures for solar energy production. Rooftops are often a neglected location for solar electricity generation in cities (Byrne et al. 2015).

Urban environments can enhance their sustainability by employing renewable energy resources, and PV, among different micro-generation technologies, has the highest potential to contribute in future energy mix (International Renewable Energy Agency 2016, Gooding et al. 2013). Widespread utilization of rooftop distributed PV systems can technically supply a substantial amount of cities' annual electricity consumption, for example 30% of the annual electricity consumption of the City of Seoul, South Korea (Byrne et al. 2015). In Canada, installing solar panels on the residential building rooftops could supply approximately 50% of residential electricity demand (Natural Resources Canada 2017a) . In addition, electricity distribution and transmission costs and losses can be reduced by onsite PV electricity production (Gagnon et al. 2016).

Cities' intricate and dense environments consist of diverse artificial and natural elements which make it challenging to model and evaluate rooftop PV electricity potential (Byrne et al. 2015, Kanters and Davidsson 2014). This intricacy increases the rooftops attractiveness as a valuable location for harnessing solar energy (Redweik et al. 2013). Urban rooftop PV potential evaluation is complicated and requires the consideration of

factors such as building heights and trees, urban morphology, and urban densities (Byrne et al. 2015, Huang et al. 2015).

The scale of the study area and data availability are two important factors that usually determine the methodology employed for rooftop PV potential estimation (Byrne et al. 2015, Gooding et al. 2013). Sample methodology, multivariate sampling-based methodology, and complete census methodology are three primary categories for different methods used to estimate PV potential in urban settings (Byrne et al. 2015). Sample methodology which is usually used for large areas evaluates the available roof surfaces, and allows meaningful extrapolation of results to a larger total area. A multivariate sampling-based methodology evaluates PV available rooftop surface area based on relationship(s) between population density, building densities, and rooftop areas (Byrne et al. 2015, Gooding et al. 2013). Complete census methodology uses statistical data sets (e.g. buildings footprint area), cartographic data sets (digitized model of the study area), and software packages (e.g. GIS) to estimate the whole rooftop surface in the study area (Byrne et al. 2015).

LiDAR technology has the ability to provide a wealth of information about the complex environment of urban areas and can be used to model various features of cities (Huang et al. 2015). The effective and suitable roof area for solar PV cell installations can be assessed more effectively by utilizing LiDAR data.

In Chapter 2 and 3, the solar radiation resources are evaluated using a new methodology that employs measured solar data and ArcGIS. Accurate estimation of the solar resource is always a crucial task in solar PV energy generation assessments and solar

PV systems design (Mohanty et al. 2016). The diffuse proportion of global radiation and the transmittivity as two essential inputs of ArcGIS's Solar Analyst tool are computed for the study region employing this new methodology.

In Chapter 4, the discussion recognizes renewable energy generation often cannot be estimated accurately due to intermittency (Bhandari et al. 2015). Therefore, renewables are known as unreliable energy sources which need large capital investments (Bhandari et al. 2015, Wang and Singh 2008). A hybrid renewable energy system (HRES) that integrates various renewable energy sources is considered as a propitious solution to this unreliability (Nafeh 2011). Chapter 4 returns to solar and wind electricity generation potential assessment at the University of Lethbridge campus. To achieve a balance among costs, emissions, and load availability, the feasibility of integrating these renewable sources with battery storage is evaluated in chapter 4. Cost-effective grid-linked hybrid systems with reliable energy generation are designed.

Battery storage mitigates renewable intermittency – a highly complementary design (Wang and Singh 2008). By restricting the amount of purchased electricity from fossil fuel-based utility grid, the potential for reducing a consumer's greenhouse gas emissions is also evaluated. Particle swarm optimization (PSO) is an evolutionary stochastic population-based heuristic optimization method, a powerful intelligence technique capable of solving large-scale nonlinear optimization problems for multiple components of the hybrid systems (Maleki et al. 2017, Poli et al. 2007, Del Valle et al. 2008). Solving large-scale multi-objective nonlinear optimization problems usually requires dealing with conflicting objectives where improving one worsens another (Ranjithan et al. 2001, Khalkhali et al. 2010). Discovering a set of solutions known as non-dominant or non-inferior solutions is a

practical way to solve multi-objective problems (Sharafi and ElMekkawy 2014, Khalkhali et al. 2010).

The performance of the proposed PSO method implemented in the Python programming language is investigated and nearly optimum solutions are extracted for different conditions. This research is an attempt to shed light on different aspects of renewable energy potential in Sothern Alberta, the University of Lethbridge, and the City of Lethbridge, and provides background information for stimulating the successful and effective implementation of sustainable sources of energy.

1.3 Thesis objectives

This research has four primary objectives to better realise the potential of wind and solar energy resources at the University of Lethbridge campus and the City of Lethbridge.

1- Quantify the full potential of solar and wind energy sources in generating electricity to meet the electrical demands of the University of Lethbridge (a feasibility assessment for campus solar PV and wind turbine installations).

2- Estimate rooftop photovoltaic electricity potential of buildings in an urban environment, the City of Lethbridge, employing a multi-criteria approach using geographic information systems (GIS) and LiDAR.

3- Conduct an economic assessment utilizing present market prices to determine economically attractive rooftop PV systems in the City of Lethbridge.

4- Develop an optimal sizing and design strategy based on a heuristic particle swarm optimization (PSO) technique to determine the near optimum number and configuration of

photovoltaic (PV) panels, wind turbines and battery units minimizing the annual system cost while maximizing the reliability of the hybrid system in matching the electricity supply and demand.

Chapter 2: A comprehensive assessment of solar and wind energy potential at the University of Lethbridge campus

2.1 Introduction

Our current industrialized world relies heavily on conventional energy resources such as coal, oil, and natural gases (Pachauri et al. 2014). Humanity's insatiable appetite for the consumption of fossil fuels and the consequent pollution threatens our environment and natural resources (Pachauri et al. 2014). At current global population and economic growth, the total world consumption of energy is expected to grow by 48% from 2012 to 2040, and fossil fuels will still supply 78% of energy use in 2040 (U.S. Energy Information Administration 2016). This dependence on carbon-based fuels produces large amounts of CO_2 (Pachauri et al. 2014). CO_2 emissions from fossil fuel combustion and industrial processes account for about 78% of the rise in the total greenhouse gas emissions from 1970 to 2010 (Pachauri et al. 2014). The climate system has undoubtedly been influenced by anthropogenic activities, and human-induced increases in GHG concentrations are extremely likely to be the principal cause of the observed warming since the mid-20th century (Pachauri et al. 2014). The production and use of energy is by far the primary contributor to producing GHG emissions (two-thirds of all anthropogenic GHG emissions) and CO_2 is the main released gas from fossil fuel combustion (van der Hoeven 2015) .

Although the elimination of fossil fuels is not feasible at this time, new energy strategies should be implemented targeting the transition to alternative energy supplies, the improvement of the efficiency of facilities and wise use of energy, in part to reduce the negative impacts of climate change (Devabhaktuni et al. 2013, Izquierdo et al. 2008). Implementing renewable energy as an alternative to fossil fuels is not a new concept, but it

is receiving more attention because of this climate consideration (Devabhaktuni et al. 2013). Renewables are now well recognized globally as key sources of energy because of the improved cost-competiveness of these technologies, improved financing conditions, energy security importance, and environmental concerns (Seyboth et al. 2016). In principle, renewable energy sources can generate much more energy than the total global energy demand (Devabhaktuni et al. 2013).

Solar photovoltaic (PV) technologies collectively represent an important renewable energy source due to improving efficiencies, functionality in different locations, and applicability to both individual homes and utility-scale power plants (Devabhaktuni et al. 2013). For example, solar provided 7.8% and 6.4% of electricity demand in Italy and Germany, respectively, during 2015 (Seyboth et al. 2016). One important advantage of solar technologies is onsite power generation (Izquierdo et al. 2008). Solar energy generation can be easily employed in urban settings where electricity generated is consumed by the local population (Aznar et al. 2015). PV systems can be mounted on rooftops and façades, and in other available locations such as abandoned or unutilized municipal lands not needed for urban development, agriculture, or conservation (Martín et al. 2015).

Wind energy also plays a significant role in the world energy future due to technological maturity, and relative cost competitiveness (Herbert et al. 2007). By 2020, about 10% of the world's electricity demand can be met by wind energy (Herbert et al. 2007). Technology advances have led to a 5% annual rise in the power output of wind turbines since 1980 (Herbert et al. 2007). In 2015, wind power was the most cost-effective source of energy for new grid-based power in many countries including Canada (Seyboth

et al. 2016). Globally, the average cost of land–based wind and solar PV dropped by about 35% and 80% respectively between 2008 and 2015 (Seyboth et al. 2016). In 2015, wind and solar PV installations set new records, composing about 77% of new installations in the global power sector (Seyboth et al. 2016).

The scientific community is increasing efforts in the applied study of renewables as a clean and sustainable energy supply (Martín et al. 2015). The assessment of the renewable energy potential is the first step in understanding the value of clean sources of energy, and in supporting policies to encourage renewable energy development (Martín et al. 2015). However, the rapid growth of renewable electricity creates concurrent challenges for electric grid system management, new regulations, and market design (Seyboth et al. 2016). Balancing demand and supply requires understanding the characteristics of local renewable generation, and sufficiently precise monitoring and forecasting of clean electricity generation (Kausika et al. 2014).

The objectives herein are to quantify the full potential of solar and wind energy sources in generating electricity to meet the electrical demands of the University of Lethbridge. The focus includes a feasibility assessment for campus solar PV and wind turbine installations. This research will:

- merge LiDAR data and aerial photography with GIS software to evaluate the suitable available rooftop, parking lot, and open spaces for PV installation;

- calculate electricity output possible with available solar radiation data;

- calculate the wind energy potential for the study site using local wind data and turbine characteristics;

- and compare the resulting solar and wind generation over five years to typical university hourly electrical demand.

Generating green energy will showcase University of Lethbridge's environmental responsibility and sustainability; and will also allow development of a full-scale research facility to encourage and support the transition to renewable energy sources for other sectors of society. The present study will examine how local clean electricity generation may meet local demand, based on data characterizing local demand over time.

2.2 Background

2.2.1 Solar PV potential

Many studies state that PV systems can meet much of our electrical needs. The adoption of PV technology in Canada is comparatively slow (Rosenbloom and Meadowcroft 2014). There is limited information about technical parameters such as solar insolation rates and variability, and land area that might be assigned to this technology in Canada in coming decades (Rosenbloom and Meadowcroft 2014). Advanced alternative energy simulations, modeling, and forecasting play an important role to help local communities to increase their knowledge and assessment ability with respect to renewable energy planning and utilization (Izquierdo et al. 2008). Previous studies have employed GIS techniques, LiDAR data, and aerial images to investigate solar energy potentials. Given the total available land and rooftop area, it is important to understand the amount and characteristics of suitable space that is available for installing PV systems (Melius et al. 2013). Some studies have used constant-value methods of rooftop-area estimation which calculates a multiplier that can be applied to the entire study area (Martín et al. 2015). For example, using geographic information systems capabilities and object-specific image

recognition, Wiginton et al. (2010) proposed a five-step method for estimating total rooftop PV potential by finding a relationship across the region between total roof area and population. Another technique to identify suitable locations is by manually selecting areas from sources such as aerial imagery; this protocol is time-intensive, especially for large regions (Melius et al. 2013). Nguyen and Pearce (2013) presented a methodology to provide urban solar PV resource assessments in which roof outlining is carried out on aerial images. The majority of potential analyses utilize GIS-based methods for evaluating available area for PV installation (Melius et al. 2013). Izquierdo et al. (2008) estimated the potential of roof-integrated PV systems applying a statistically representative stratified sample of vector GIS maps of urban areas. Chow et al. (2014) created a 3D model in ArcGIS at a fine spatiotemporal resolution to evaluate solar potential on the facades and rooftops of buildings at a community level.

In this research, taking into account the size of the study region and the data availability, insolation incident on the PV modules sloped surface is modeled and area selection has been done by means of both GIS-based methods and manually selecting areas. In order to increase the accuracy, the present study combines these methods. In addition to the improvement in methodology by employing multiple techniques, this research will contribute to the literature by investigating the solar PV potential in the study region and exploring the ability of solar energy to match electricity demand over time.

2.2.2 Wind energy potential

Various studies have been carried out to predict wind energy potential worldwide. Because of the uncertain and stochastic nature of wind, having a precise knowledge of wind regime and evaluating the potential of wind energy in the region of study is an important

initial step for the efficient planning and cost optimization studies of any wind energy project (Mathew 2006). Once one has the wind speed at the turbine hub height, converting the wind kinetic energy to turbine energy output is a crucial step. One of the common methods to estimate the energy production is to use the characteristic power curve of a particular wind turbine as provided by the manufacturers in conjunction with wind distribution data (Sohoni et al. 2016). A detailed review of various wind turbine power curve modeling methods is presented by Sohoni (Sohoni et al. 2016). The power curve illustrates the energy output of a wind turbine at various wind speeds. Describing the actual shape of the power curve by appropriate equations is a challenging task (Sohoni et al. 2016). Power curve models are mostly deterministic models which demonstrate a fixed relation between wind velocity and the turbine power yield (Sohoni et al. 2016). The relationship between wind speed and wind turbine power output can be approximated by various polynomial functions (Sohoni et al. 2016). Yang et al. (2007) implemented the most simplified model to simulate the selected wind turbine power output based on a linear curve which represents the power curve by a straight line. In our study, hourly available wind data was used to estimate wind energy potential in the study region employing the power curve method.

2.3 Study Area

The University of Lethbridge campus is situated in the west side of the City of Lethbridge, southern Alberta, Canada (49° 40' 38" N, 112° 51' 51" W) (Figure 2-1). There are twelve buildings on campus with wide flat rooftops potentially suitable for installing PV panels. The campus has abundant, level parking lots and fields with unobstructed solar exposure. The campus coulees are complex high slope topography constituting a large part

of the east side of the campus, which have extensive southern exposure faces that could host PV panels.

Southern Alberta receives an enormous amount of annual global solar radiation (Rosenbloom and Meadowcroft 2014). In fact, Alberta has some of the best solar resources in Canada (Canadian Solar Industries Association and Energy Efficiency Alberta 2018). Furthermore, Southern Alberta has many ideal sites suitable for wind energy production (Weis et al. 2010). Wind energy has been the most installed of new electricity generation capacity in Canada over the past decade (Canadian Wind Energy Association 2016). Currently, wind meets about 7% of Alberta's electricity demand (Canadian Wind Energy Association 2018). Solar and wind electricity are poised to be a huge part of the province's electricity supply; and Southern Alberta holds the majority of that generation capacity.

Historically, coal has been the largest and cheapest electricity generation source in Alberta (Alberta Government 2017b). Electricity power plants produced 16% of Alberta's total greenhouse gas emissions in 2014 (Alberta Government 2017b). To shift towards a low-carbon energy future, the Alberta government began a transformation of the electricity sector. The Alberta Climate Plan, released November 22, 2015, says Alberta will decommission all coal fired power plants by 2030, and build renewable generation to meet 30% of the provincial electricity demand (Alberta Government 2017b). Regarding the provincial government's new climate change plan, Alberta is expected to install at least 4,500 MW of new wind energy capacity (Canadian Wind Energy Association 2018).
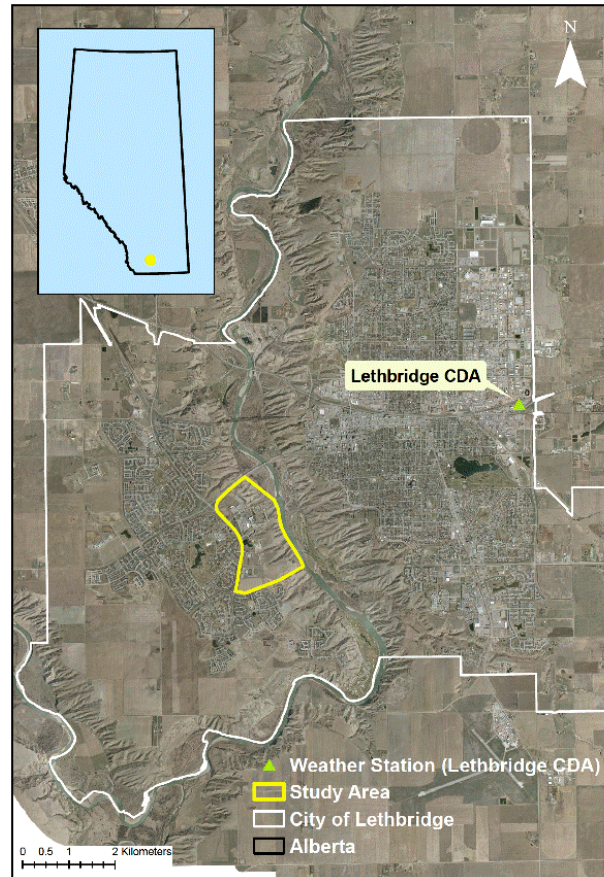
Figure 2-1: Study area, the University of Lethbridge campus.

2.4 Data

The availability of high quality LiDAR data and meteorological data from a nearby station was critical in determining the methodology employed for this research. The source for hourly values of the global solar radiation on a horizontal surface, air temperature, and wind speed was the Alberta Climate Information Service (ACIS) (http://agriculture.alberta.ca/acis, 2016). The data were obtained at a nearby station, Lethbridge CDA, located at 49° 42' 0" N, 112° 46' 60" W (Figure 2-1). The meteorological data for the period 2010-2014 was used in accordance with the available university electricity consumption provided by the university utility service. LiDAR point cloud data were obtained from the City of Lethbridge through the University of Lethbridge for this

project area. In addition, aerial images provided by the City of Lethbridge were used to understand the texture of the study region.

2.5 Methodology

2.5.1 Solar electricity potential

The estimation of solar electricity potential usually requires knowledge of available suitable area for installing PV panels (geographic potential), the available solar insolation (physical potential), the capability (efficiency) of a particular technology in converting solar energy to electricity considering the technical limitations (technical potential), and the costs related to employing solar systems and the energy generation (economic potential) (Martín et al. 2015). Additionally, social and environmental impacts should be assessed, but that is beyond the scope of this paper (Izquierdo et al. 2008).

2.5.1.1 Geographic potential (site assessment)

Optimum planning needs to evaluate the potential of solar radiation received at spots that will be covered by PV panels. Wise PV panel positioning and orientation decreases the probability of losses in solar gain due to obstructions from neighboring buildings and topographic features and makes the project more cost effective. Adjustment and changing the position of PV arrays relative to sun for maximum output is usually expensive and impractical, especially for utility scale installations (Piragnolo et al. 2015).

Utilizing aerial imagery and hand digitizing in ArcGIS, key rooftop, parking lot, and flat abandoned open areas without neighboring obstructions were identified. In case of building rooftops, the situation and size of buildings, and the shape of their rooftops (flat or inclined) are important factors in calculating incoming radiation (Martín et al. 2015). To

understand the physical characteristics of the study area and evaluate the area of buildings' rooftop and parking lots, and to assess how much of the roof top area is assigned to other applications such as air conditioning systems, aerial images of the campus were used. Aerial images are a useful tool for checking study area textures (Kausika et al. 2014).

The extensive open coulee area located in the east side of the campus provides a substantial area for placing PV systems. Factors such as latitude, the time of day, season, topography, and weather influence the insolation that strikes the surface of earth (Hofierka and Suri 2002). On regional and local scales, available radiation is mostly modified by terrain (relief) due to variability in elevation, surface orientation (slope and aspect) and shadow cast by topographic features (Hofierka and Suri 2002). ESRI Solar Analyst was used to identify coulee areas that have good solar exposure throughout the year.

Solar Analyst is an extension for ArcGIS that creates a solar irradiation map over an area for specific time periods (Chow et al. 2014). This tool takes into account the atmospheric attenuation, latitude and elevation of the area, slope and aspect, daily and seasonal changes of the sun position and angle, and effects of shadows cast by surrounding features and topography (Ruiz-Arias et al. 2009). Solar Analyst uses the topographic information contained in a digital elevation model (DEM) to estimate direct and diffuse components of solar irradiation for point locations or for entire geographic areas (Esri 2016c). The global solar radiation in Solar Analyst is the sum of direct and diffuse components (Esri 2016c). The results of this analysis are shown in Figure 2-2.

In assessing solar potential in a built area, most researches use LiDAR data to create DEMs for their solar radiation calculations because LiDAR provides the highest resolution

(Martín et al. 2015). The DEM of the study area with 1x1 m spatial resolution was generated using ground (or bare earth) LiDAR point clouds in ArcGIS. LiDAR data is usually stored in LAS format and typically does not have a defined spatial reference (Esri 2013). Therefore, using the 3D Samples extension of ArcGIS, LAS files were rewritten to contain the proper spatial reference information, which is NAD1983 3TM. Determining the special reference of each LAS file is critical for the following analysis in ArcGIS (Esri 2013). According to the LiDAR metadata, the vertical datum was defined as Canadian geodetic vertical datum of 1928 (CGVD28).
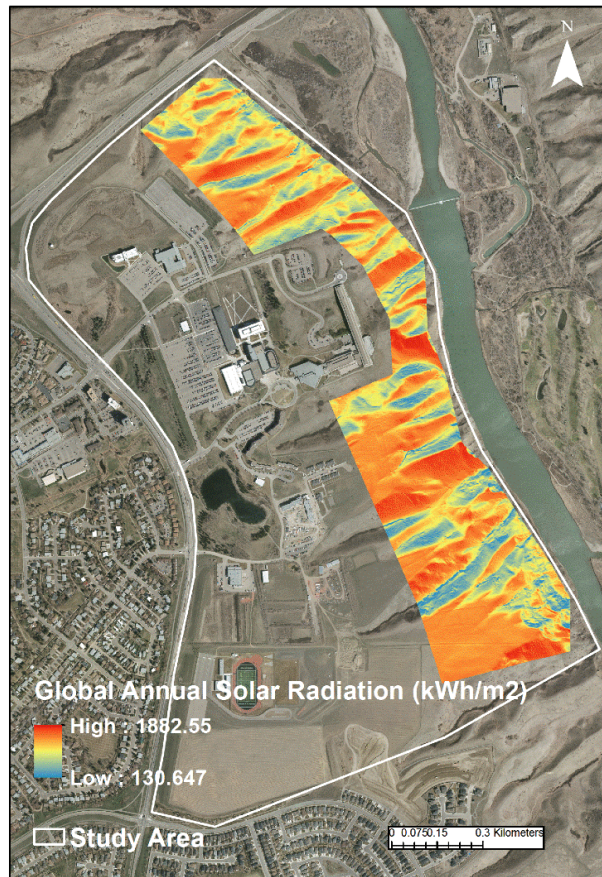
Figure 2-2: Global annual solar radiation for the coulees area.

The "Area Solar Radiation" tool was used to calculate the amount of radiant energy for the coulee area (Figure 2-2). Solar Analyst needs the proportion of exoatmospheric radiation transmitted as direct radiation along the shortest atmospheric path at sea level (τ_{sl}) and diffuse proportion (K_D) which is the ratio of measured defuse solar radiation on a horizontal surface against the global solar radiation (Fu and Rich 2000, Esri 2016a). However, to achieve better results we considered $K_{T_{sl}}$ (the ratio of measured global solar radiation on a horizontal surface against the extraterrestrial radiation at sea level) instead of τ_{sl} in global annual solar radiation calculation (Mirmasoudi et al. 2018). The hourly K_T was assessed for the selected nearby station between 11:30 and 12:30 hours for each day of the years 2010 to 2014. This K_T pertains to the shortest atmospheric path (in the direction of the zenith) (Ruiz-Arias et al. 2009). The average of these K_T values represents the annual mean K_T and was used for estimating the annual solar radiation. Using the Erbs et al. (1982) correlation represented by Equation 2.1, the fraction of the hourly radiation on a horizontal plane that is diffuse was evaluated (Duffie and Beckman 2013).

$$K_D = \begin{cases} 1.0 - 0.09K_T & ; K_T \leq 0.22 \\ 0.9511 - 0.1604K_T + 4.388K_T^2 - 16.638K_T^3 + 12.336K_T^4 & ; 0.22 \leq K_T \leq 0.8 \\ 0.165 & ; K_T > 0.80 \end{cases} \quad (2\text{-}1)$$

The Solar Analyst algorithm corrects for elevation effects, so transmissivity should always be given for sea level (Fu and Rich 2000). Therefore, K_{T_Z} was corrected by means of the Equation (2-2) for sea level, with z as the elevation (Ruiz-Arias et al. 2009).

$$K_{T_Z} = K_{T_{sl}} exp(-0.000118z - 1.638 \times 10^{-9}z^2) \quad (2\text{-}2)$$

To represent all participating locations and discard unsuitable places in the coulee area, some constraints were applied. A suitable location has an appropriate aspect, slope

(less than 60 degrees), and a minimum annual insolation. Investigating the generated solar radiation map, 1200 kWh/m^2/year was defined as the minimum threshold of solar radiation. To assure that there is no shading on selected areas from neighboring trees and buildings, the study site was visually inspected.

Some reduction factors are assumed in order to reduce the total suitable area available for solar photovoltaic applications to a realistic level. In case of rooftop area, this reduction has to be implemented considering the effects of shading from other parts of the roof or from surrounding buildings or trees (Wiginton et al. 2010). Significant areas of every roof are occupied by ventilation, air conditioning systems, chimneys and other apparatus (Wiginton et al. 2010). PV array installation requires extra area for maintenance (service area) and to avoid shading from neighboring panels (Amado and Poggi 2012). In the case of flat rooftops, this service area is usually a perimeter space with a width of 1 meter (Ordóñez et al. 2010). To estimate the fraction of rooftops that can be devoted to PV modules, aerial images were investigated. Furthermore, related literature was reviewed to obtain appropriate reduction values (Table 2-1).

Table 2-1: Fractions of total roof area assigned to PV modules estimated in different studies.

Study	Method utilized	Fraction of total roof area	Region
Ordonez et al.(2010)	simulation	0.74 (Detached houses) - 0.796 (Town Houses) - 0.654 (High rise buildings)	Andalusia (Spain)
Izquierdo et al. (2008)	inspection of satellite imagery	0.32 (All urban buildings)	Spain
Montavon et al. (2004)	computer simulation	0.49-0.95-0.73 (different urban sites)	Switzerland
Wiginton et al.(2010)	literature based	0.30	Canada

Ong et al. (2013) evaluated 72% of installed and under-construction utility-scale PV (ground-mounted photovoltaic) and CSP (concentrating solar power) capacity in the United States, and assessed the solar land use requirement and array spacing. They found that fixed-tilt systems have an average packing factor (the ratio of area actually covered by PV panels to the total land area occupied by the array system) of 47% (Ong et al. 2013, Horner and Clark 2013). They stated that there is large variability in packing factor and it ranges from 20% to 67% based on the research literature (Ong et al. 2013). For this research, taking into account the specific characteristics of our study area, the ratio of PV module area to the total available suitable area was assumed to be 0.30.

2.5.1.2 Physical potential

The physical potential is the assessment of the solar energy resource availability in the study site (Izquierdo et al. 2008). The availability of solar radiation data on oblique surfaces with different angles is a fundamental requirement in utilizing solar energy technologies. The knowledge of solar resource is very important in long term or short term assessment of PV power output, performance evaluation, and to make the best decisions in designing profitable solar systems (Mohanty et al. 2016). A weakness of the Solar Analyst tool is the assumption that sky transmissivity and diffuse coefficients are constant values over the year; this is not valid and can impact the amount of annual calculated radiation significantly (Jakubiec and Reinhart 2013). Generally, Solar Analyst underestimates the total insolation (Ruiz-Arias et al. 2009). It does not take into account radiation reflected from surrounding surfaces such as buildings, trees, or terrain features (Jakubiec and Reinhart 2013). Such radiation cannot always be ignored, especially when the site is surrounded by highly reflective objects such as snow (Rich et al. 1994). Accordingly,

measured hourly radiation data was used to calculate insolation incident on PV surfaces. Solar radiation data provided by weather stations are usually measured as global radiation on a horizontal plane while PV panels are inclined to maximize their received insolation (Tina et al. 2012). The inclination angle of a sloped surface (measured relative to the horizontal) and its orientation or azimuth angle (measured relative to south, with zero due south) are two important defining characteristics of the surface (Tina et al. 2012). The incident solar radiation received by the sloped surface is built of three components including beam radiation ($I_{T,b}$), diffuse radiation ($I_{T,d}$), and reflected radiation ($I_{T,ref}$) from the different neighbouring objects (Duffie and Beckman 2013). The total radiation on this surface is:

$$I_T = I_{T,b} + I_{T,d} + I_{T,ref} \qquad\qquad\qquad\qquad\qquad (2\text{-}3)$$

Many methods with various complexity have been presented for estimating I_T (Duffie and Beckman 2013, Tina et al. 2012). These methods utilize different approaches to treat the fraction of hourly radiation which is diffuse (Fu and Rich 2000). Based on various assumptions about the directional distribution of the diffuse component on the sloped surface, these models are classified as isotropic and anisotropic sky models (Shukla et al. 2015). The isotropic models are conservative and simple, where the intensity of the diffuse radiation stream is assumed to be uniform over the sky dome. The anisotropic models take into account the anisotropy of the diffuse radiation in the circumsolar region (Shukla et al. 2015). Several anisotropic models are proposed by different researchers (Perez et al. 1987, Perez et al. 1990, Skartveit and Olseth 1986, Steven and Unsworth 1980, Reindl et al. 1990). In this work, the Perez et al. (1990) model, which is based on more detailed analysis of diffuse radiation, is implemented (Duffie and Beckman 2013). Usually the results of this

model are very close to measurements for many locations worldwide and it is more comprehensive compared with many other models (Duffie and Beckman 2013, Tina et al. 2012). Based on this model, the total radiation on the oblique surface is given by (Duffie and Beckman 2013):

$$I_T = I_b R_b + I_d (1 - F_1) \left(\frac{1 + cos\beta}{2} \right) + I_d F_1 \frac{a}{b} + I_d F_2 sin\beta + I\rho \left(\frac{1 - cos\beta}{2} \right) \qquad \text{(2-4)}$$

where a and b are defined as $a = \max(0, cos\theta)$, $b = \max(cos85, cos\theta_z)$. The parameters F_1 and F_2 are circumsolar and horizon brightness coefficients and are functions of sky conditions (a set of these coefficients is given in (Duffie and Beckman 2013)). The parameter β is the tilt angle of the surface, $I_b R_b$ is the beam contribution on radiation on the sloped surface, and $R_b = \frac{cos\theta}{cos\theta_z}$ is the ratio of beam insolation on the sloped surface to that on a horizontal surface. The parameters θ and θ_z are the angle of incident and zenith angle, respectively. $I\rho \left(\frac{1 - cos\beta}{2} \right)$ is the reflected radiation from the neighbouring objects where ρ is the diffuse reflectance of the surroundings (Table 2-2) (Duffie and Beckman 2013). As it is not practical to estimate the reflected radiation from all surroundings, the common approach assumes that there is one extensive, horizontal ground in front of the collector which reflects this component in all directions equally (Duffie and Beckman 2013, Tina et al. 2012). The albedo coefficient ρ has a typical value of 0.2 for ordinary ground or grass (Tina et al. 2012).

Table 2-2: Reflection coefficient values for some materials (Piragnolo et al. 2015).

Material	ρ	Material	ρ
asphalt road	0.10	loam (with clay)	0.14
broad-leaf trees	0.26	roof	0.13
concrete	0.22	snow	0.75
conifers	0.07	stones, gravel	0.2
dark-colored building	0.27	water	0.07
dirt road	0.04	white-colored building	0.6
grass (dry + green)	0.23		

The parameters I_b, I_d are the beam and diffuse fractions of total horizontal radiation respectively. In order to determine the total radiation on surfaces of other orientations given global horizontal radiation, horizontal beam and diffuse radiation must be treated separately (Duffie and Beckman 2013). Several methods are developed to split total horizontal radiation into its constituents (Orgill and Hollands 1977, Boland et al. 2001, De Miguel et al. 2001, Erbs et al. 1982). Usually scientists try to establish an hourly correlation between I_d/I , where I is the total radiation on the horizontal surface, and $K_T = I/I_0$, the hourly clearness index. I_0 is the hourly extraterrestrial radiation on a horizontal plane (Duffie and Beckman 2013). In this research, the Erbs et al. (1982) model, as presented in Equation (2-1) was deployed.

To estimate hourly total solar radiation on inclined PV panels, these selected models were applied to global solar radiation data obtained from a nearby weather station from 2010 to 2014. Because any measurement brings some errors, radiation data were screened for quality following Ref. (Journée and Bertrand 2011) to eliminate questionable values. Global horizontal radiation data at the Earth's surface that was larger than the corresponding extraterrestrial value incident were filtered out. In addition, the direct and diffuse irradiance components must be smaller than the global horizontal radiation (Journée and Bertrand 2011).

2.5.1.2.1 Optimal PV orientations and tilt angles

The amount of generated electricity is a function of the orientation and tilt angle of the PV array (McKenney et al. 2008). The efficiency of a solar collector is optimum when oriented towards the sun (Handoyo and Ichsani 2013). As in the northern hemisphere the sun is due south at solar noon, south facing PV panels receive the maximum amount of irradiation. The yearly output of PV panels with tilt angle (angle of inclination away from horizontal toward the South) equal to latitude is greater than panels with other tilt angles (McKenney et al. 2008). PV Surfaces with higher tilt angles usually produce more constant energy, however, they receive less insolation on a yearly basis (McKenney et al. 2008). Lower tilt angles result in more electricity production in the summer months, while higher tilt angles are more appropriate for winter (McKenney et al. 2008, Rehman and Siddiqui 2012). The seasonal optimal tilt angles are location specific because they are influenced by climatic variations (Rowlands et al. 2011). The amount of solar radiation that a PV panel is exposed to is a function of the location latitude, the day of the year and the time of day, surface tilt angle, surface azimuth angle, and the angle of incident radiation (Vignola et al. 2008). Among these various factors, surface tilt and azimuth angles can be adjusted to maximise the radiation at the surface (Handoyo and Ichsani 2013). In principle, optimum values of tilt angles change every day and thus should be adjusted accordingly to their optimum values (Rehman and Siddiqui 2012). Researchers have carried out many studies for evaluating the local optimal tilt angle for a specific location (Rehman and Siddiqui 2012, El-Sebaii et al. 2010, Rowlands et al. 2011). El-Sebaii et al. (2010) calculated the total solar radiation on a sloped surface facing south with different tilt angles for Jeddah (Saudi Arabia), and inferred that in this location, the best yearly performance of a solar collector is obtained when it is oriented due south with a tilt angle equal to the latitude.

Rowlands et al. (2011) investigated, and modelled solar radiation data and subsequent PV panel performance to determine the optimum tilt angle and azimuth for a PV system in Ontario. They found that for all case studies, the ideal tilt angle is slightly less than the local latitude (7° and 9° less than the local latitudes in Ottawa and Toronto respectively) and the maximum power output is achieved when the PV panel is facing slightly east of due south (6° east of due south for Ottawa, and 2° east of due south for Toronto). In our study, PV panels were assumed to be oriented due south and a slope angle equal to the local latitude was utilized.

2.5.1.3 Technical potential

2.5.1.3.1 Solar panel selection

Wafer-based Solar cells made from crystalline silicon and thin-film products are two basic commercial PV module technologies available on the market today. For terrestrial applications, silicon based solar cells are the most common modules available as single-crystal, polycrystalline or amorphous solids (Mohanty et al. 2016). Single-crystal silicon has the best performance and amorphous silicon (a-Si) has the lowest efficiency among the three types (Mohanty et al. 2016). In 2016, about 94% of the total PV module production belonged to silicon-wafer based PV cells and multi crystalline modules represented about 70% of total production (Philipps and Warmuth 2017). The efficiency of commercial wafer-based silicon panels has increased in the past decade, from about 12% to 17% (Philipps and Warmuth 2017). With recent advancements, mono-crystalline silicon panels deliver 24.2% efficiency under standard test conditions (Philipps and Warmuth 2017). In this research, it was assumed that the PV cell efficiency is 15% (Nguyen and Pearce 2013).

2.5.1.3.2 Estimating PV electricity production potential

Photovoltaic system performance is influenced by the quality of the system and the weather (Dierauf et al. 2013). PV module performance ratings are usually supplied by manufacturers based on their performance at standard testing conditions (STC): 1000 W/m^2 solar irradiation, 25°C module temperature, and air mass 1.5 (McKenney et al. 2008). The potential power output of a module under these conditions is called module nominal power. In reality, photovoltaic panels produce less energy due unavoidable losses in various parts of the system. These losses are determined by the overall system design, the type of modules used, and operating conditions (solar radiation intensity, angle of incidence, temperature, etc.) (McKenney et al. 2008). Performance Ratio (PR) is an indicator of the effect of losses compared to the PV system's rated output and is defined as the ratio of actual system AC output per year to the expected DC yield, which can be used to quantify the overall system losses. The performance ratio is used to compare the system performance to that of an ideal system at the same place (Schmalensee 2015). With technology advancements, over the past decades, increased efficiencies of PV modules and other components of PV systems have led to dramatic improvement in performance. New systems have PR values ranging from 0.6 to 0.9 (Reich et al. 2012). Reich et al. (2012) have investigated the PR of about 100 German PV systems and stated that with help of cool climates in Germany, some systems' PR exceed 0.9.

Having cold weather conditions in our study region, we expect that the system proposed herein would operate at a high PR value. Canadian systems located on latitudes of 44° up to 64° have yearly average performance ratios ranging from 0.7 to 0.75 (McKenney et al. 2008). Del Cueto (2002) compared 14 photovoltaic modules installed at

fixed latitude tilt and stated that performance ratios fluctuate seasonally, mostly because of air or module temperature variations. This study showed that the η_{EFF} (effective efficiency) is significantly temperature-dependant (Del Cueto 2002). The operating temperature of the PV cell, which is the temperature of the PV array surface, is an important variable for the photovoltaic conversion process and the PV array output depends strongly on this factor (Brihmat and Mekhtoub 2014). PV systems are more efficient at lower cell temperatures (Brihmat and Mekhtoub 2014). Performance temperature changes during sunshine hours, exceeding ambient temperature by as much as 30 ℃ or more; however, at night it is at ambient temperature (Brihmat and Mekhtoub 2014). Having the estimated total global radiation on the surface of the tilted PV panel, using the ambient air temperature and wind data, the DC generated energy was calculated. The Skoplaika model was used to assess the operating temperature of photovoltaic cells (Skoplaki et al. 2008). The effect of temperature on the efficiency of the photovoltaic cell (where $\eta_c = P_m/AG$, P_m is the maximum power, A is the cell's area, and G is the irradiation) is given by:

$$\eta_c = \eta_{T_{ref}}[1 - \beta_{ref}(T_c - T_{ref})] \tag{2-5}$$

where $\eta_{T_{ref}}$ and β_{ref} are the module's electrical efficiency and the efficiency correction coefficient at temperature T_{ref} and at solar radiation of 1000 W/m² respectively that are usually provided by manufacturers. The average value for temperature coefficient at $T_{ref} = 25℃$ is usually taken as $\beta_{ref} \approx 0.004C^{-1}$ (Skoplaki et al. 2008). The PV cell operating temperature (T_c) is given as:

$$T_c = T_a + \left(\frac{0.32}{8.91 + 2.0V_f}\right)G_T \quad ; \qquad V_f > 0 \tag{2-6}$$

where V_f (m/s) is the wind speed in the windward side of the Photovoltaic array. The equation $V_f = V_w/0.67$ relates near the PV array wind speed (V_w) to the free stream wind speed (V_f). The ambient air temperature is shown by T_a in °C and G_T is the solar irradiance on the surface of the array (W/m²) (Skoplaki et al. 2008). The efficiencies at different irradiances and air temperatures were estimated and the maximum DC output power was calculated for the ith hour of the day using Equation (2-7) (Duffie and Beckman 2013).

$$P_i = A_c G_{T,i} \eta_{c,i} \tag{2-7}$$

Many factors may decrease the ideal DC power output, such as losses due to surface soiling and snow, module parameter mismatch, resistance in the DC circuit, and DC current ripple and algorithm error caused by the switching converter which performs the maximum power point tracking function (Ropp et al. 1997). The voltage and current at which a PV cell operates is a function of the load characteristics (a battery or a power grid) (Duffie and Beckman 2013). When generator and load characteristics are seriously inconsistent, power conditioning equipment (maximum power point trackers) can be used. For tracking maximum power points, these devices control voltage while sacrificing some power (Duffie and Beckman 2013). Mismatch power losses occur when PV cells do not have similar characteristics (are not identical perfectly) or do not operate under uniform conditions (Vijayalekshmy et al. 2014). Therefore, the following equation displays the system's efficiency taking into account the mentioned losses (Ropp et al. 1997):

$$\eta = \eta_c \cdot \eta_{Dust} \cdot \eta_{mismatch} \cdot \eta_{DClass} \cdot \eta_{MPPT} \tag{2-8}$$

The values represented in Table 3 were used to predict the power output.

Table 2-3: Values representing various losses used in system efficiency calculation (Equation (2-8)) (Ropp et al. 1997).

Parameter	Value
η_{Dust}	96%
$\eta_{mismatch}$	95%
η_{DClass}	98%
η_{MPPT}	95%

The generated DC power is converted to alternating power (AC) used in the electrical grid by an inverter. Inverters efficiency, usually provided by manufacturers, range from 92% to 95% (Vignola et al. 2008).

2.5.2 Wind energy potential

Areas with annual average wind speed of greater than 6-7 m/s at a height of 80 meters are economically suitable places for commercial wind turbine installations (Weis et al. 2010). The annual average wind speed at a height of 80 m above the ground surface was calculated for our study area using the wind speed data at a height of 10 m obtained from a nearby station over five successive years (Table 2-4). Results show that this study region is a favorable wind site.

Table 2-4: Annual average wind speed at a height of 80 m above the ground surface in the study site.

Year	2010	2011	2012	2013	2014
Average annual wind speed (m/s)	5.8	6.74	6.31	6.00	5.8

Wind power output is strongly dependent on the wind speed distribution across the region where wind turbines are placed and the type of wind turbines employed (Weis et al. 2010). Southern Alberta represented about 76% of total wind generation installed capacity in the province at the end of 2016. These wind facilities performed with an average capacity factor (the ratio of the annual average output to the nameplate output) of 35% in 2016

(Alberta Electric System Operator 2017). The annual energy that a wind turbine will generate can be estimated by multiplying the nameplate capacity by the capacity factor and by 8760 hours in a year (8784 hours in a leap year) (Weis et al. 2010). With increase in wind speed in conjunction of increase in height, and with better matching between wind spectra and the turbine, the capacity factor can be increased significantly (Mathew 2006).

In order to assess wind power generated from a wind turbine in a particular region, long term measurements of the local wind data are required. Due to continual change of wind distribution about the mean, average wind speeds do not reflect an accurate estimate of wind potential and are not sufficient to assess long term performance of wind turbines (Duffie and Beckman 2013). Accordingly, hourly wind data from 2010 to 2014 from a nearby station was used to predict wind energy potential using turbine power curve modeling method. Wind speed data are usually measured at 10 meters above the ground surface. In order to extrapolate wind speeds from the height of measurement to hub height of wind turbines, a power law equation of the following form was used:

$$\frac{V(Z_1)}{V(Z_2)} = \left(\frac{Z_1}{Z_2}\right)^{\alpha} \tag{2-9}$$

where $V(Z)$ is the wind speed at the height of Z and α is the wind shear coefficient and depends on many factors such as the velocity of wind, air temperature, surface roughness, season, and time of day (Staffell and Green 2014, Duffie and Beckman 2013). The parameter α can be calculated from measurements at two different heights and its typical value is 0.143 (Duffie and Beckman 2013). Wind profiles for sites without measured wind data are determined using the wind speed values from a nearby station (Sohoni et al. 2016). Extrapolating wind speeds to greater heights is probably one of the most important

uncertainty factors in evaluating the wind potential at a particular region (Schallenberg-Rodriguez 2013).

Models based on rudimentary equations of the wind power and models based on equations representing the power curve of wind turbines are two different approaches that are used to approximate the behaviour of wind turbines (Thapar et al. 2011). For example, Nelson et al. (2006) evaluated the wind turbine power response using average hourly wind velocity data and equation (2-10) derived from fundamental equations of the wind power.

$$P_e(t) = \frac{1}{2} \rho A v^3(t) C_p E f f_{ad} \qquad (2\text{-}10)$$

where, Eff_{ad} is the efficiency of AC/DC converter, ρ is the air density (kg/m³), A is the area swept by the turbine rotor blades (m²), v is the wind speed (m/s), and C_p is the power coefficient of the turbine (Nelson et al. 2006). Power curves of wind turbines supplied by manufacturers are also used to calculate the electrical power generated by turbines at a specific wind speed (Thapar et al. 2011). The aerodynamic, transmission and generation efficiencies of a wind turbine are reflected in its power curve (Mathew 2006). In this research a model based on the power curve concept is used to assess the turbine power output (Mathew 2006, Nelson et al. 2006). The power curve is modeled by an appropriate polynomial function (equation (2-11)) in each of the turbine's performance phases (turbines have four distinct performance phases as shown in equation (2-11)). Equation (2-11) demonstrates the turbine electrical power output versus wind velocity (Mathew 2006, Nelson et al. 2006):

$$P_W = \begin{cases} 0 & ; \ v < v_i \\ av^n + b = P_R \left(\frac{v^n - v_i^n}{v_r^n - v_i^n} \right) & ; \ v_i \leq v \leq v_r \\ P_R & ; \ v_r < v \leq v_o \\ 0 & ; \ v > v_o \end{cases} \qquad (2\text{-}11)$$

where v_i(cut-in velocity),v_r(rated velocity), and v_o(cut-out velocity) are the essential characteristic velocities of the wind turbine (Mathew 2006).The parameters P_R and n are the turbine's rated power (W) and the velocity-power proportionality respectively (Mathew 2006). At too low wind speeds turbines cannot operate, and also at too high wind velocities, due to extreme mechanical loads, turbines can be damaged (Duffie and Beckman 2013). To find the energy (kWh) produced in each hour, the assessed power for any specific hour is multiplied by one hour (Nelson et al. 2006). The reference wind turbine selected in this study rated at 3.05 MW, with rotor diameter of 101 meters and a hub height of 150 meters. Considering the extensive area available on the campus, it was assumed that three turbines could be installed on this site.

There are some losses that occur in wind power generation facilities including availability losses (2 - 5%), electrical losses (2 - 3%), turbine performance losses (1 - 3%), environmental losses such as icing (1 - 5%), soiling and damage (1 − 2%), and curtailment (4%). Making a precise estimation of the aforementioned losses is hard because they are highly site specific (Clifton et al. 2016). Studying the effects of aging in the wind turbine performance, Staffel and Green (2014) investigated the data from the UK's 282 wind farms and found that wind turbines lose $1.6 \pm 0.2\%$ of their energy output annually, leading to a reduction of 12% of energy production over a 20 year lifetime.

2.5.3 Uncertainties in solar PV energy production estimation

The uncertainty in solar radiation data and solar resource estimation is one of the most important factors affecting PV output prediction (Schnitzer et al. 2012, Myers et al. 2004). Usually, modeled data that has been historically used to evaluate the on-site solar radiation resource are not accurate enough (Schnitzer et al. 2012). Likewise, the spatial difference among reference networks and project sites and deficient station maintenance decrease the accuracy of the measured data at many projects (Schnitzer et al. 2012). Describing the sources of uncertainty associated with measurements, Myers et al. (2004) stated that the uncertainty in measured global horizontal radiation data could reach to 3-5%. In addition, horizontal radiation transposition to the plane of the PV array, and simulation and plant losses are other contributors to the uncertainty in solar energy generation assessments (Schnitzer et al. 2012). The accuracy of solar radiation estimations on tilted surfaces using global horizontal radiation data solely, degrades considerably, and mostly depends on the direct and diffuse separation model's accuracy for the study region (Gueymard 2009). The Erbs et al. model, which has been utilized in our research, is extensively employed and recognized as a universal method (Gueymard 2009). Gueymard (2009) compared measured global radiation on tilted plane with estimations from ten transposition models and found that the Perez model, which has been implemented in our research, provides one of the best results, particularly under clear skies.

The measured peak power of PV modules may be about 10% less than the nameplate rating sometimes (Atmaram et al. 2008). Furthermore, PV modules' power decline over time or degradation rate is about 0.3-0.8% annually (Thevenard and Pelland 2013).

PV systems' availability (scheduled and unscheduled maintenance activities) influence their power output (Moore and Post 2008). Moore and Post (2008) investigated a 3.51MW PV system and found that its average overall effective availability for five successive years was about 99.7%.

In adition, on average, soiling can lead to 1.5% to 6.2% of PV energy losses annually (Thevenard and Pelland 2013). Considering the convoluted process of snow accumulation on PV panels and variable nature of snowfall, for various study locations and for fixed-tilt systems, annual PV losses resulting from snow coverage have been measured ranging from 0% to 25% (Ryberg and Freeman 2015).

Using a statistical simulation approach, Thevenard and Pelland (2013) combined uncertainties from various sources to estimate the overall uncertainty in photovoltaic yield predictions. Their estimates of uncertainties in various factors affecting system performance including year-to-year climate variability, average horizontal radiation, radiation calculation in the plane of the array, power rating of PV modules, losses due to dirt and soiling, losses due to snow, and other sources of error were 3.9%, 5%, 3%, 3%, 2%, 1.5%, and 5% respectively. Based on their study, the combined (total) uncertainty (standard deviation) in the system's yield over its lifetime was about 7.9%. The global uncertainty attached to the output of PV systems may differ from one system to another significantly (Thevenard and Pelland 2013). Using the values presented in the literature and the 'rule of squares' described by Thevenard and Pelland (2013), the combined uncertainty for our PV system output was estimated to be about 9.5%.

2.5.4 Uncertainties in wind energy production estimation

The anemometer-based measurements uncertainty (1-2%), the spatial variation uncertainty (1 -2%), the vertical extrapolation uncertainty (0 - 6%), the turbine performance uncertainty (0 - 4%), the electrical losses uncertainty (1- 2%), the environmental effects uncertainty (1%), the curtailment uncertainty (1-4%), the long term wind resource uncertainty (1-6%), and the uncertainty due to inter-annual variability (1-10%) are the main contributors to the wind energy production uncertainty (Clifton et al. 2016). Based on the values presented by literatures, the estimated overall wind energy uncertainty was about 11%.

2.6 Results and discussions

Employing the aforementioned methodology to the University of Lethbridge campus area, the available roof area for photovoltaic equipment and the photovoltaic energy potential was assessed. Based on 2010-2014 electricity usage of the University and evaluated renewable energy potential, this study can help to determine an efficient plan to implement a renewable energy program for clean energy generation on campus.

A total of 1,015,808 m^2 area was found to be suitable for the installment of PV panels in the site (Table 2-5 and Figure 2-3). This total area was reduced to that which would be covered by PV modules. Having this large area, it is possible to install a series of large PV arrays with about 45 MW capacity at the University of Lethbridge campus.

The hourly solar radiation on inclined PV panels was estimated using the Erbs et al. (1982) and Perez et al. (1990) models for years 2010 to 2014. Then, the hourly potential energy outputs from this distribution of area was approximated. Potential electricity output

from the large-scale installation of PV is extremely large, and with more efficient panels it is possible to generate even more electricity. The annual electricity production of this system is shown in Table 2-6.

Table 2-5: Available area for installing PV modules in the study area.

Locations	Suitable area (m^2)
Flat free lands	207,979
Rooftop	32,145
Parking lots	111,474
Coulees	664,210
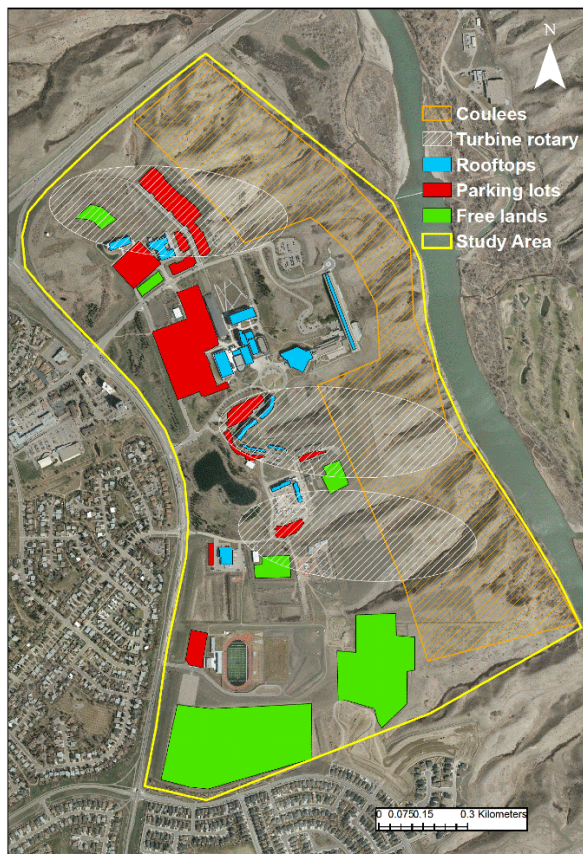
Figure 2-3: Available suitable area for PV and wind turbine installation at the campus.

Table 2-6: Annual solar electricity production in the study area.

Year	Generation (MWh)
2010	71,700
2011	74,700
2012	72,900
2013	73000
2014	72,800

The energy consumption of the University increased between 3-5% annually from 2010 to 2014. It was usually higher during summer (July and August) and autumn (September and October) months with the largest amount in July (Figure 2-4). The total summer electricity consumption was about 10% higher than the total winter electricity consumption on average. On the other hand, the highest potential of solar electricity generation existed during summer months (July and August), spring (March, April, and May), and early autumn (September). The largest amount of solar electricity could be mostly produced in July (Figure 2-4). The electricity consumption decreased from summer to winter, when the solar electricity potential declined as well. In late autumn (November) and winter months (December, January) the solar electricity generation had the lowest potential while the lowest consumption existed in December and February. Therefore, the peak months of electricity consumption and solar electricity generation, and the months with lowest electricity consumption and lowest solar electricity potential, approximately coincide. On average, the annual electricity generation of this solar PV system is about 2.8 times greater than the annual electricity usage of the campus.
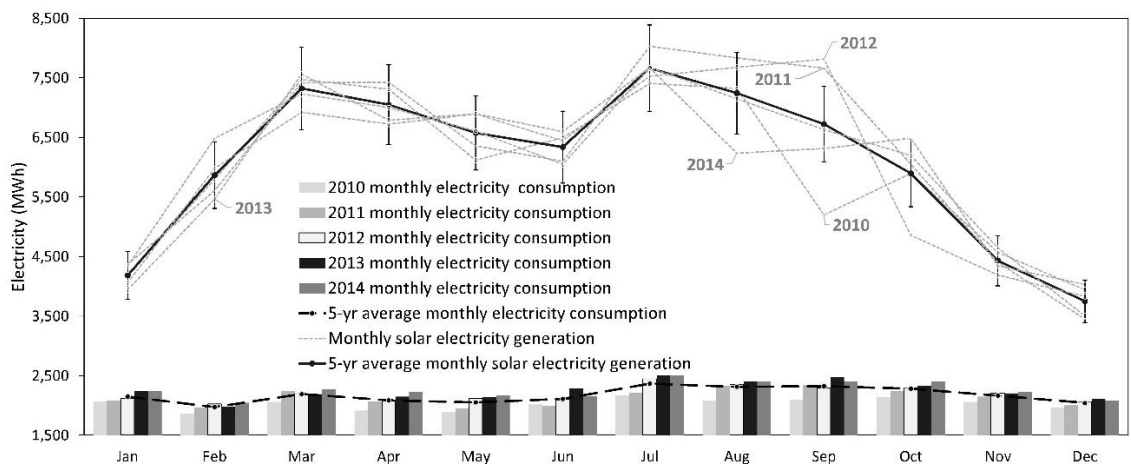
Figure 2-4: Monthly electricity usage and solar PV electricity potential at the campus.

For the five successive years, the average seasonal daily electricity consumption in winter (averaged over three winter months) was about 1.3%, 1.8%, and 1.0% lower than that in summer, autumn (September, October, and November), and spring, respectively (Figure 2-5). The average seasonal daily solar electricity generation (averaged over three months) in spring was about 50% more than that in winter (December, January, and February), 5% more than that in summer, and 31% more than that in autumn. It was about 3.3, 3.1, 2.5, and 2.2 times greater than the average seasonal daily electricity consumption in spring, summer, autumn, and winter, respectively. The average daily solar PV electricity generation over all seasons was about 2.8 times of the average daily solar electricity consumption (Figure 2-5).

Figure 2-5: 5-year average seasonal daily electricity consumption and 5-year average seasonal daily solar PV electricity potential at the campus.

The availability of solar PV electricity during times of high demand of energy is one of the important advantages of this technology, particularly in hot and sunny days (Richardson and Harvey 2015). During daytime, when solar electricity is available, the electricity demand was higher, and as shown in Figure 2-6, the highest amount of solar electricity generation and energy consumption occurred almost simultaneously (Figure 2-6). Between noon and 16:00 pm, the 5-year annual average hourly electricity consumption was higher (with the highest amount at 15:00 pm), while the 5-year annual average hourly PV electricity generation was higher between 11:00 am and 15:00 pm (with the highest amount at 13:00 pm) (Figure 2-6). The maximum 5-year annual average hourly PV electricity generation is approximately 7.7 times greater than the maximum amount of 5-year annual average hourly electricity consumption (Figure 2-6). The peak-shaving ability (the ability of PV systems to match peak load and provide more electricity at times with higher demand) is more important for small PV systems because their contribution to an electric grid is insignificant. Whereas, the energy produced by a large PV system can influence the electric grid significantly (Richardson and Harvey 2015).

Figure 2-6: 5-year annual average hourly electricity consumption and 5-year annual average hourly solar PV electricity potential at the campus.

While solar energy is only available when the Sun is shining, wind energy generation occurs also at night. Wind energy plays an important role in the energy supply. Therefore, the assessment of its technical and economic potential in different regions is crucial (Ritter et al. 2015). A model based on the turbine power curve was used to evaluate the wind electricity potential in the study site employing meteorological data from 2011-2014 on an hourly basis. The wind velocity characteristics at the turbine hub height determines the turbine's potential output, and consequently the economic viability of wind energy production in a region (Ritter et al. 2015). For each hour of day, annual and 5-year mean wind speeds at the hub height were calculated (Figure 2-7). The fluctuations of the 5-year average wind velocity at a specific hour of the day due to the month and season change is shown by the corresponding standard deviations (Quan and Leephakpreeda 2015). From early morning to afternoon, the annual average hourly mean wind speed increases (the highest wind speed appears mostly around 15:00), and then it decreases from evening to night, so the lower amounts occur during night (Figure 2-7).
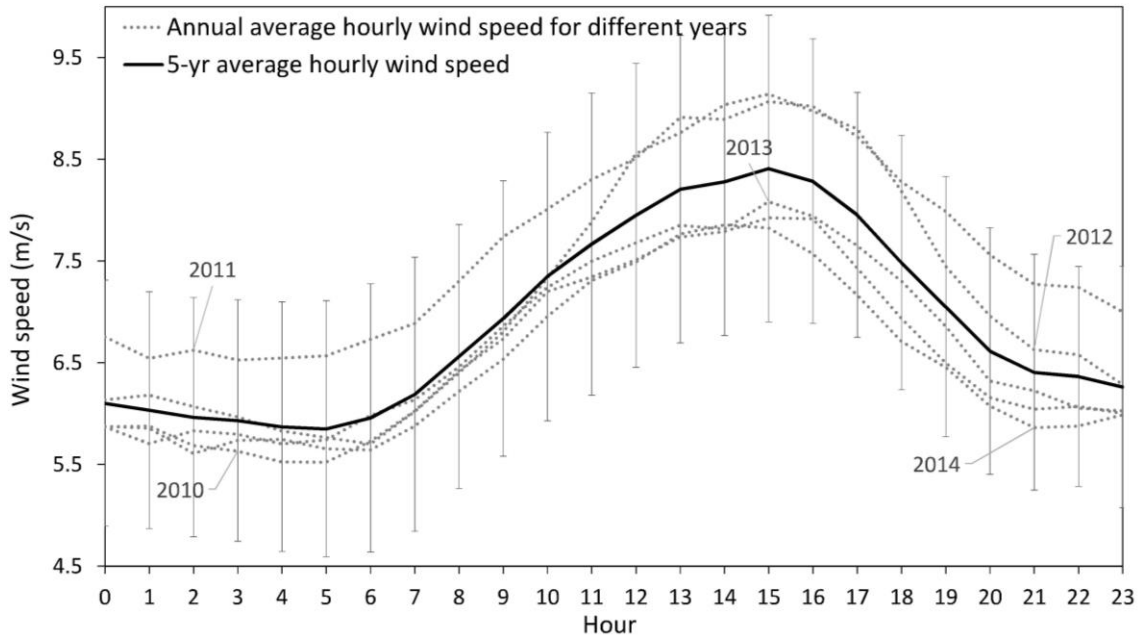
Figure 2-7: The 5-year annual average hourly wind speed at the hub height.

The wind rose diagram of the site at the hub height (Figure 2-8) indicates that the predominant wind blowing direction is between west and southwest. In addition, it illustrates the speed of winds based on their directions (Figure 2-8). For example, in 2014, 35% of all recorded winds had a direction between 220° and 276° and a speed less than 22 m/s (Figure 2-8).
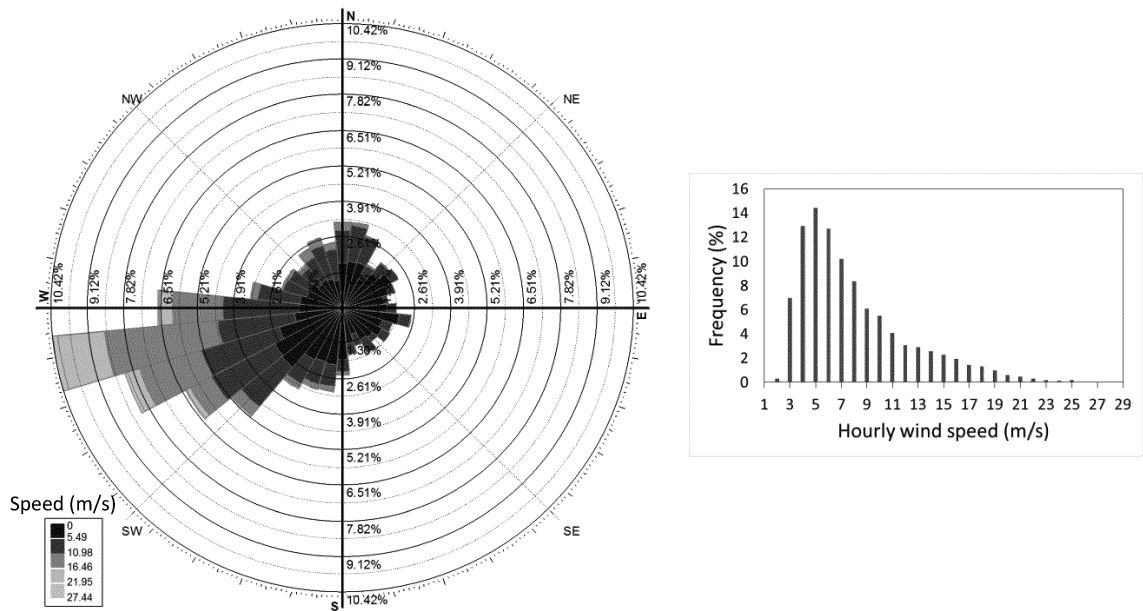
Figure 2-8: Wind rose diagram (left) for the site at the hub height illustrating the wind directions and wind speeds (m/s), and wind speed distribution diagram (right), for 2014.

In any month strong winds can occur, however they often blow in winter (Figure 2-9). The wind energy potential is smaller during summer months when the electricity consumption is higher (Figure 2-9). The 5-year average wind electricity generation in January is about 12% more than the 5-year average electricity consumption in this month, while in July, the 5-year average wind electricity potential is about 44% lower than the 5-year average electricity consumption. Therefore, a combination of both wind and solar electricity, especially for small renewable energy installations, could better match the demand profile. The 5-year annual average electricity potential of the wind system was about 16% smaller than the 5-year annual average electricity consumption of the university.
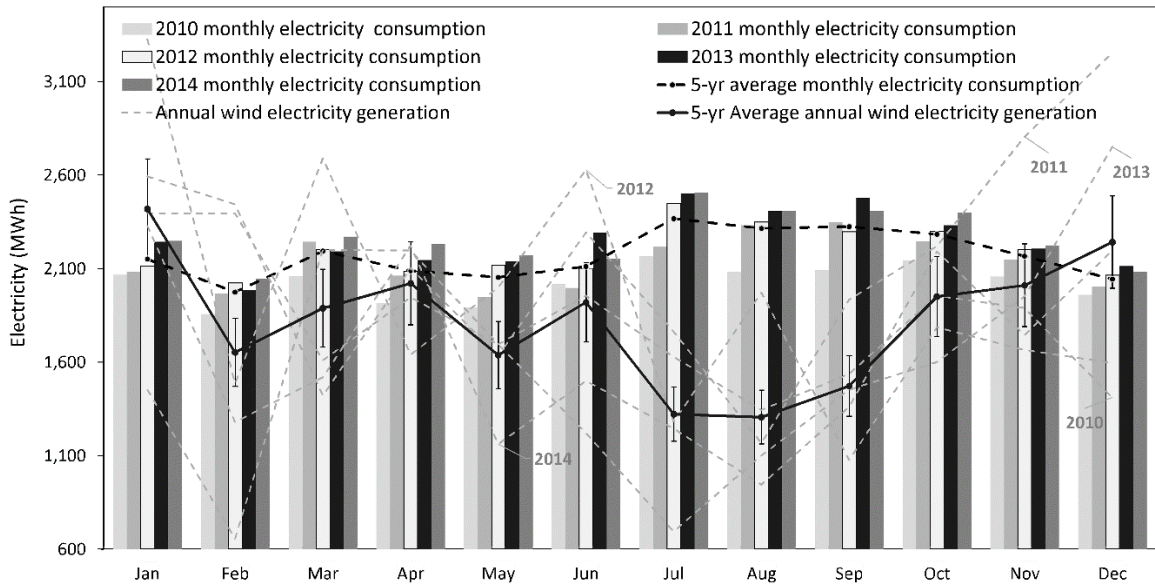
Figure 2-9: Monthly wind electricity potential of the proposed system at the campus.

Wind energy production differs from one day to another day significantly (Figure 2-10). In summer months, the 5-year average daily wind electricity potential is mostly lower than the 5-year average daily electricity demand (Figure 2-10). However, during winter, spring, and autumn, in some days the generation exceeds the daily consumption (Figure 2-10). Among the five years, the maximum electricity consumption occurred on July 2, 2013 (102.16 MWh) which was about 5 times greater than the wind energy potential in this day (20.27 MWh). The highest wind energy potential existed on January 23, 2010 (210.8 MWh) which was 3.7 times larger than the electricity demand in this day (56.96 MWh). The maximum 5-year average daily wind turbine energy potential in winter, spring, summer, and autumn was about 1.54, 1.18, 0.88, and 1.09 of the maximum 5-year average daily electricity usage in these seasons respectively. On average, over all seasons, the 5-year daily wind energy potential was almost always lower than 5-year average electricity demand (Figure 2-10).
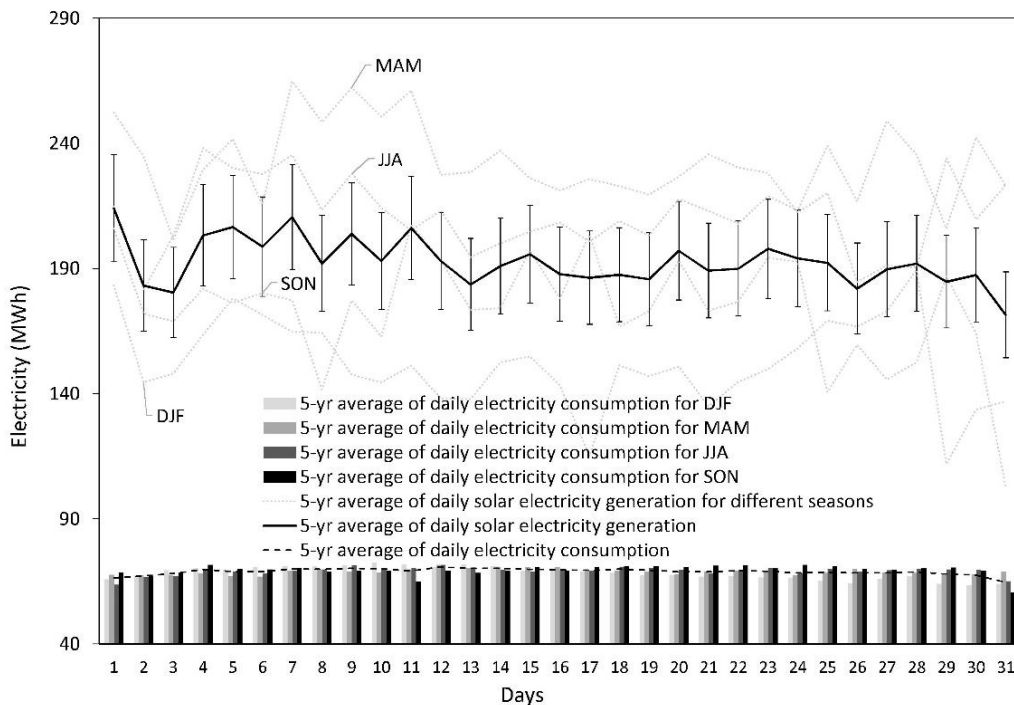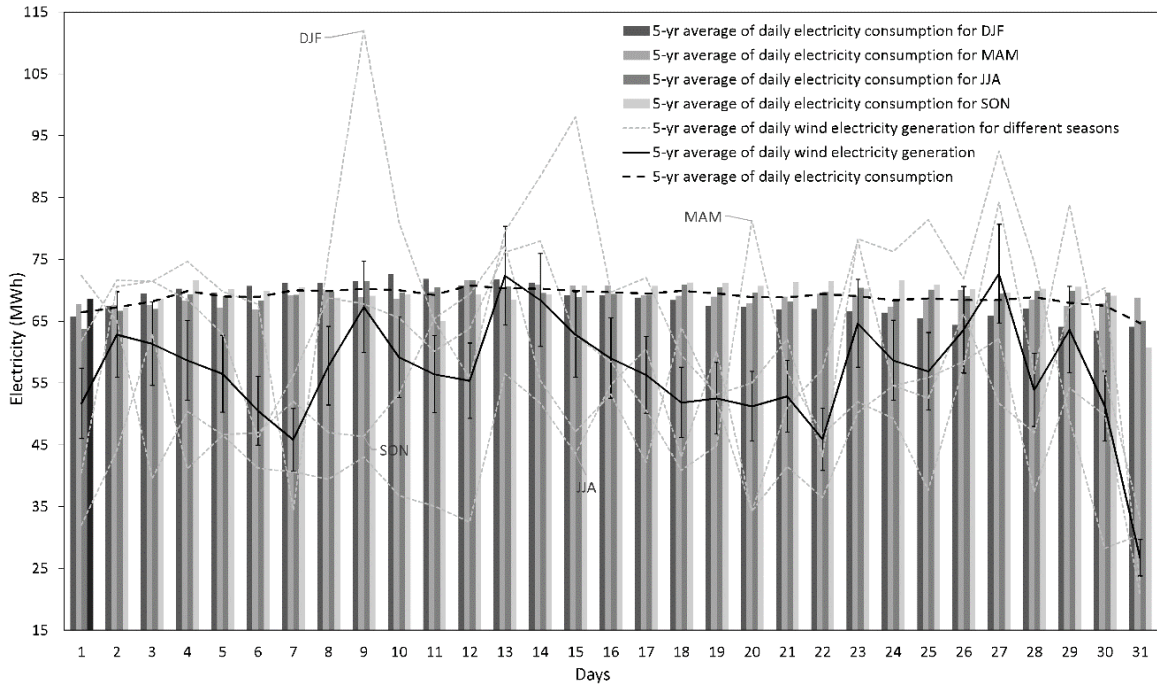
Figure 2-10: 5-year average seasonal daily electricity consumption and 5-year average seasonal wind electricity potential at the campus.

Among the five years, in 2011 and 2012 respectively, the annual average hourly wind energy potential in about 46% and 13% of the 24 hours exceeded the annual average hourly electricity consumption, while in other years, this potential was lower than the usage in all hours (Figure 2-11). The wind energy potential was higher during day hours, whereas the electricity demand was also higher (Figure 2-11). While the maximum annual average hourly wind potential occurred at 15:00 pm or 16:00 pm in each of the 5 years, the highest annual average electricity usage took place at 15:00 pm in these years. The maximum annual average hourly wind energy potential was about 88%, 106%, 102%, 88%, and 83% of the maximum annual average hourly electricity usage in the five successive years respectively (Figure 2-11). In the five years, the lowest annual average hourly electricity consumption took place at 3:00 am or 4:00 am, whereas the minimum annual average hourly wind energy potential existed between 1:00 am and 4:00 am. Therefore, there was

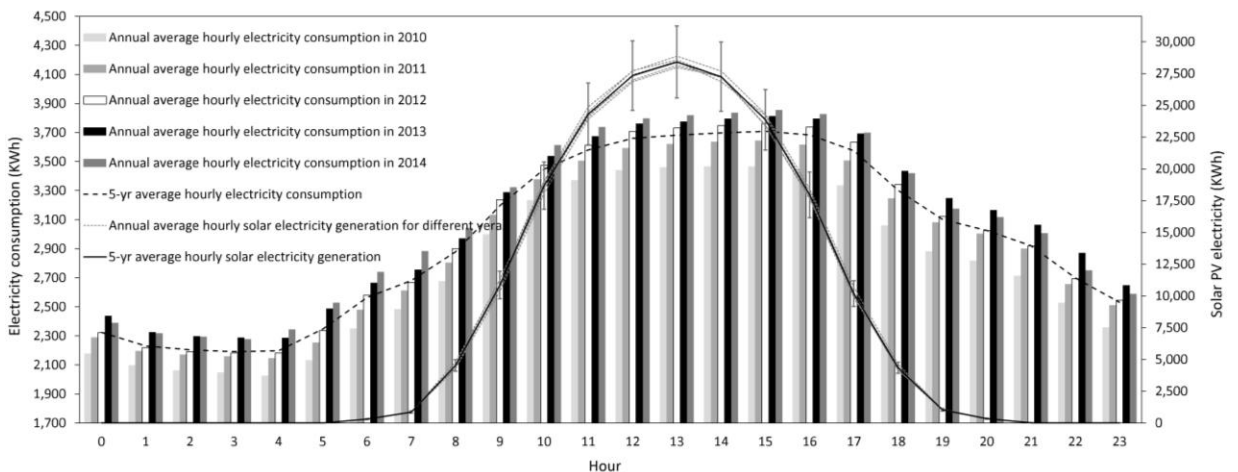a good agreement between hourly wind energy potential and hourly electricity demand (Figure 2-11).
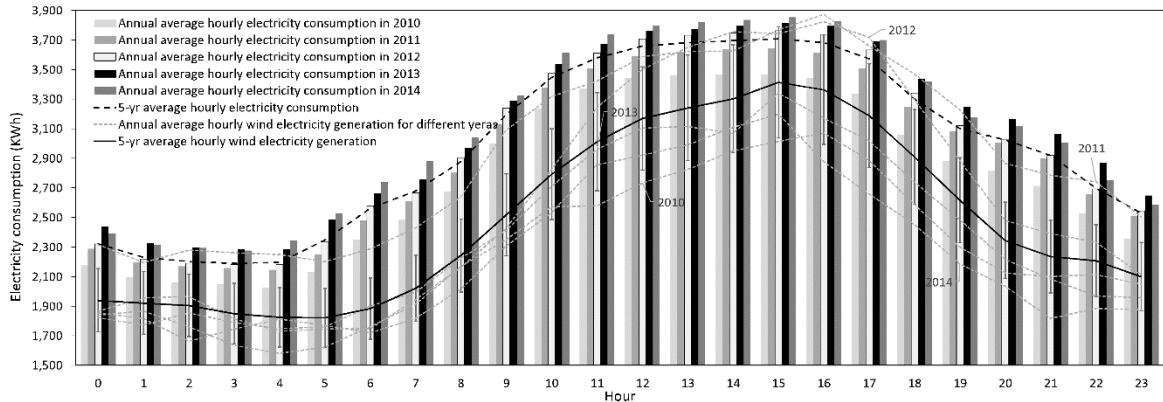
Figure 2-11: 5-year annual average hourly electricity consumption and 5-year annual average wind electricity potential at the campus.

During night-time (between 22:00 pm and 5:00 am), the 5-year average hourly wind electricity potential was about 16% lower than the 5-year average hourly electricity usage. Therefore, the proposed wind energy system could not provide enough energy to meet electricity demand during nights.

Among the selected years, the year 2014 had the smallest potential of wind power generation and the second smallest potential of PV electricity while having the highest electricity consumption. In 2014, for instance, 44% of the total annual wind electricity potential existed in the night-time. In December and January, the night-time wind electricity potential was about 7% and 5% more than the electricity consumption respectively (Figure 2-12). In winter months, the night-time electricity demand was higher than the day-time electricity consumption (Figure 2-12). In other months, the night-time wind potential was on average 36% lower than the night-time electricity consumption (Figure 2-12). In 2014, the total annual day-time and night-time wind electricity potential was about 71% and 74% of the total annual day-time and night-time electricity

consumption, respectively. The total day-time wind energy potential in December, January, and April was about 2.4%, 2%, and 8.7% higher than the total electricity usage in these months respectively (Figure 2-12). In other months, on average, the total monthly wind energy potential was about 66% of the electricity consumption (Figure 2-12).
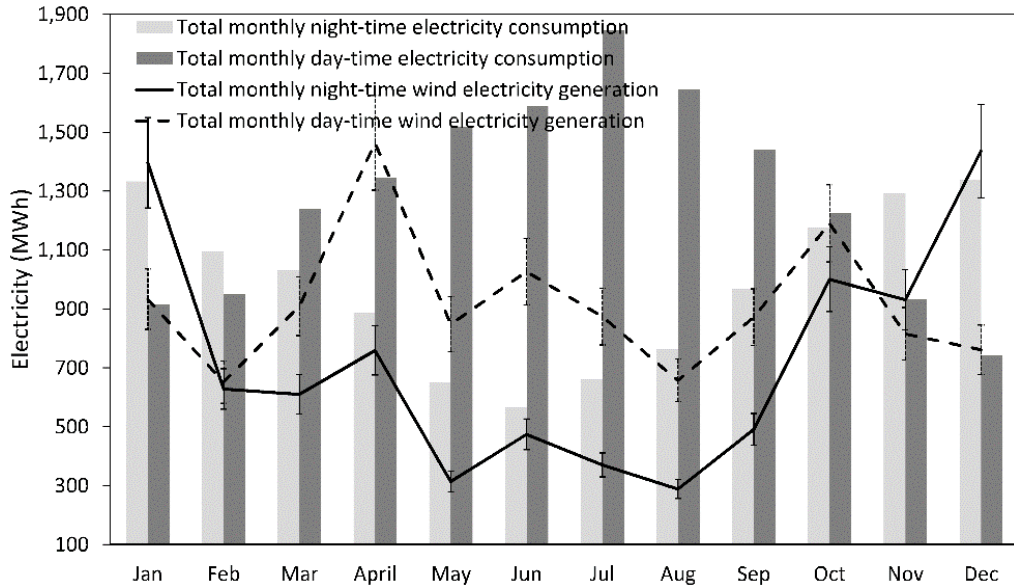
Figure 2-12: Total monthly day-time and night-time wind electricity generation and total monthly day-time and night-time electricity consumption in 2014.

Wind and solar together could generate enormous energy during day-time (Figure 2-13). On average, the 5-year average monthly electricity that could be produced by the combined wind and solar PV system would be 3.6 times greater than the 5-year average monthly electricity consumption (Figure 2-13). The combined system could produce more energy in spring months (March and April) than other months (Figure 2-13).
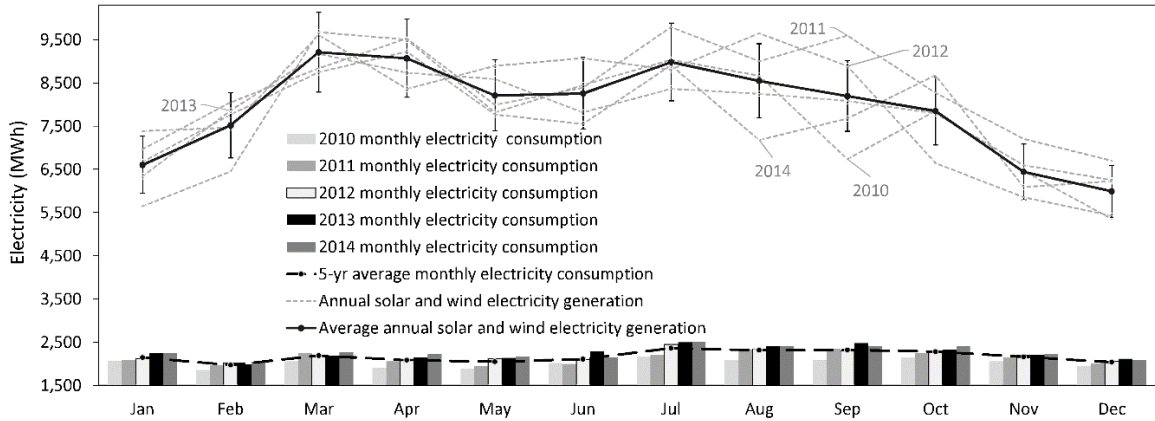
Figure 2-13: Total monthly combined wind and PV electricity potential and total monthly electricity consumption.

The proposed grid-tied PV and wind system can help the university save money. We have assumed that the average purchase price of grid electricity and the average sale price of electricity are 13.5¢/kWh and 6¢/kWh, respectively. The approximate costs for installing a utility scale wind turbine and a utility scale PV system are about 2 $/W and 2 $/W respectively, depending on the choice of products, the size of the system, and the site characteristic (Dodge David and Dylan 2016). The weighted average investment cost for onshore wind decreased about two-thirds between 1983 and 2015 globally, from USD4766/kW to USD1550/kW (Seyboth et al. 2016). The solar PV cost has declined significantly as well, and solar PV electricity is competitive in many energy markets (Seyboth et al. 2016).

In summary, the University of Lethbridge could install renewable energy systems on campus that would cover the university's annual cost of electricity significantly. Herein, we assume the university finances the entire project at rate 4% (constant annual interest rate) over 25 years; the manufacturer's performance warranty. Developments at the federal and provincial level indicate substantial financial support will be available for such

51

institutional development of renewable, clean electrical generation. We assume federal and provincial grants would cover 50% of the cost of these installations. We also assume that the operation and maintenance cost for the solar PV system and the wind turbine system are 10$/kW/year and 11$/kW/year respectively (Wang and Singh 2009, Whaley 2016). Under those assumptions, and using the year 2014 as an example, the annual electricity cost of the university will decline about 90% (Table 2-7).

Table 2-7: Annual cash flow, proposed University of Lethbridge Renewable Electrical system.

Month	Electricity cost ($) with no renewables, 2014	Monthly cost of electricity with the proposed renewable system ($), 2014
Jan	-$303,426	-70,475
Feb	-$276,078	-27,822
Mar	-$306,651	21,092
Apr	-$301,423	73,994
May	-$292,920	-25,217
Jun	-$290,625	-18,938
Jul	-$338,384	26,420
Aug	-$325,056	-85,199
Sep	-$325,161	-55,666
Oct	-$324,167	27,511
Nov	-$300,173	-130,952
Dec	-$280,972	-87,279
Annual	-3,665,037	-352,532

2.7 Conclusion

Environmental and economic concerns promote investments on renewable energy systems. In this study, solar and wind electricity generation potential at the University of Lethbridge campus were investigated. Results showed that there is 1,015,808 m^2 of suitable area available for placing a 46 MW solar PV system in the site which would produce about 2.8 times of the university annual electricity usage on average. The proposed wind system could cover about 84% of the university electricity demand annually on average. Additionally, on average, the 5-year average monthly electricity that could be produced by

the combined wind and solar system would be 3.6 times greater than the 5-year average monthly electricity consumption. Consequently, the university could decrease its electricity cost by 90% approximately. Therefore, the presented hybrid renewable system in this study could help the university to achieve a green energy future target which seems economically viable.

Chapter 3: Evaluating solar energy technical and economic potential on rooftops in an urban setting: the city of Lethbridge, Canada

3.1 Introduction

Extensive energy generation and consumption are the main anthropogenic sources of greenhouse gas emissions and air pollution (two-thirds of all human-induced GHG emissions) (International Energy Agency 2015). Unless sufficient countermeasures are taken in the energy sector, the progressive deterioration of the environment related to these emissions will continue. The rapid and growing global movement toward low-carbon energy sources in response to the imperative of addressing global warming may support a global sustainable energy future, and alleviation of some environmental burdens (International Energy Agency 2015). By introducing new sources of natural capital and exploiting replenishing resources, renewables play a crucial role in efforts to de-carbonise energy supplies and avert negative impacts associated with climate change (Mueller et al. 2016). Renewable energy systems use diverse sources, localise energy generation, decrease transport costs, and reduce long-term price variability (Mueller et al. 2016). Renewables are now well recognised as a main stream source of electricity worldwide and supplied 19.3% of the global final energy usage in 2015 (Sawin et al. 2017). Increasing development of solar PV is mostly due to improving competitiveness and cost parity with other technologies, new government plans, increasing awareness of the potentials of this technology, and rising electricity demand (Sawin et al. 2017). Substantial increases in rooftop solar PV installation resulted in buildings becoming the largest available urban source of space for deployment (International Renewable Energy Agency 2016). In fact, globally, about half of the presently installed PV capacity is composed of distributed PV systems. Although, a large capacity is still untapped (Castellanos et al. 2017).

To supply the increasing needs for energy while reducing climate change and maintaining quality of life, cities require rigorous and holistic sustainable action plans. Cities currently accommodate more than 50% of the global population and are an important contributor to global warming, accounting for 65% of global energy demand and 70% of human-induced (energy-related) CO_2 emissions (International Renewable Energy Agency 2016). Immense renewable energy sources have the largest potential to improve the sustainability of the urban environment, and PV has demonstrated the most potential to contribute in the energy mix, among available micro-generation technologies (International Renewable Energy Agency 2016, Gooding et al. 2013). The number of cities worldwide that have decided to move toward 100% renewable energy and carbon neutrality targets has increased. Some cities have implemented promising policy measures to motivate distributed clean energy development, including rules that oblige utility companies to buy renewable power and building codes that compel the installation of renewable technologies (International Renewable Energy Agency 2016). Some cities and local authorities plan to create a livable, sustainable, and resilient space for their inhabitants (Sawin et al. 2017). However, in general, cities are not well-equipped to cope with many urban growth and sustainability challenges (Kammen and Sunter 2016).

Onsite rooftop PV energy micro-generation could decrease the electricity distribution and transmission costs and losses (Gagnon et al. 2016). The lack of investors' and home-owners' awareness about rooftop PV potential, and the detailed information deficit regarding rooftop spaces suitable for PV installation are important barriers that have impeded the adoption of rooftop PV systems (Castellanos et al. 2017, Strupeit and Palm 2016). Significant research on city-wide distributed renewable energy generators is

required to attain a sustainable urban energy mix (Kammen and Sunter 2016). This research focuses on the technical and economic potential of the roof-mounted photovoltaic (PV) systems in large areas. Estimation of PV potential are challenging, but indispensable for relevant renewable energy policy making (Castellanos et al. 2017). The evaluation of the adequate available roof surfaces is the most crucial stage in implementation of roof-integrated PV applications (Izquierdo et al. 2008). Using light detection and ranging (LiDAR) data, geographic information system (GIS) methods, and PV-performance modeling, the proposed method is an efficient and scalable technique that can be automated and replicated effectively. A new detailed method for calculating solar resource availability using ArcGIS was employed (Mirmasoudi et al. 2018). Solar analyst required inputs which were calculated for the region and the accuracy of the simulated radiation was examined by comparing the results with measured data. Moreover, measured meteorological data were used to define a slope factor that was applied to ArcGIS simulated global radiation estimates on horizontal surfaces. Additionally, the economic potential of rooftop PV systems has been investigated. Considering all building types in the city boundary including commercial and industrial buildings is one of the strengths of the applied methodology. In addition to the quantification of the potential amount of electricity generation, the results reveal which percentage of roof areas are economically viable for PV deployment. The findings can provide an established reference point for rooftop PV in the region and be used by energy and building sectors, and policy makers to assess new development opportunities and guide investments towards clean energy technologies (Izquierdo et al. 2008). To our knowledge, a rigorous comprehensive assessment of rooftop PV technical potential and economic attractiveness in our study region has not been previously published.

3.2 Background

Technical potential quantifies the maximum possible energy production utilizing a specific renewable energy technology in a particular location or region (Gagnon et al. 2016). Rooftops are the best situated parts of buildings to harvest solar energy and generate electricity (Kanters and Davidsson 2014). Calculating the rooftop solar potential is not always simple (Kanters and Davidsson 2014). Rooftop PV potential in urban environments has been estimated in the various regions across globe (Ordóñez et al. 2010). Depending on the size of the study region, the type of available data , and the expected results, different methods of estimation have been used (Gooding et al. 2013). These methods try to assess essential elements such as solar incident intensity, usable roof area availability, and shadows cast by nearby objects (Gooding et al. 2013). Some studies establish a relationship between population density, building densities, and roof areas, especially for large regions (Gooding et al. 2013). The outputs of studies like these are not usually applicable at individual and local scales (Gooding et al. 2013). Based on a representative sample of buildings, Ordóñez et al. (2010) used statistical construction data and digital urban maps to measure the useful roof surface area of the sample, and extrapolated the characterization of the sample to the total study region to estimate the solar energy potential in Andalusia (Spain). Izquierdo et al. (2008) calculated the roof area available for solar applications based on land use, population and building density data using a representative sample of GIS maps of urban areas. They assessed irradiation potential by employing hourly meteorological data from weather stations using Erbs model and Liu–Jordan isotropic model. Establishing a relationship between per capita suitable rooftop area and population density by linear regression on solar rooftop potential data from 1600 cities, IEA (International Energy Agency) Energy Technology Perspectives report (2016) derived the

rooftop solar PV power capacity in other cities. Sometimes the inclination angles of different rooftop surfaces and the spatio-temporal variation of insolation are ignored. The IEA value may be used as a starting point in evaluating PV generation potential, but follow-up evaluation is required.

There are three essential methods for identifying the suitable roof surfaces for PV installation in urban settings: constant-value methods, manual selection methods, and GIS-based methods (Gagnon et al. 2016). Constant-value methods assume that a certain fraction of total roof area is usable for placing PV panels (Gagnon et al. 2016). Presenting several methods for creating rooftop PV supply curves, Denholm and Margolis (2008) translated the total roof area into usable area using an availability factor. They estimated that residential and commercial buildings in their study site have roof area availability factors of 22-27% and 60-65%, respectively. The availability factor of roof area takes into account obstructions and shading from other parts of the roof or neighbouring features (Denholm and Margolis 2008). The constant value method is simple and not computationally intensive because it does not take into account the complexity of rooftops and surrounding objects such as tree canopies (Gagnon et al. 2016). Manual selection method uses sources such as aerial photography and Google Earth to assess the suitability of roof planes of buildings individually (Gagnon et al. 2016, Anderson et al. 2010). Although manual selection can precisely determine the total suitable rooftop area, it is time-consuming and cannot be easily applied to large sites (Gagnon et al. 2016). Anderson et al. (2010) used an IMBY (In My Backyard) solar simulation tool which allows users to draw polygons to estimate the total rooftop area within a city.

GIS-based methods are the most practical and effective techniques for the estimation of usable rooftop area (Gagnon et al. 2016, Verso et al. 2015, Martín et al. 2015, Singh and Banerjee 2015, Jakubiec and Reinhart 2013). These methods are more precise than constant-value methods and can be applied to much larger data sets compared with a manual selection approach (Gagnon et al. 2016). Martin et al. (2015) reviewed different procedures for the solar potential assessment in urban areas. Singh & Banerjee (2015) used land use data and GIS-based satellite image analysis for estimating the building footprint area and the rooftop PV potential for the Indian city of Mumbai. They employed the Liu-Jordan model to calculate the plane-of-array irradiation and determined the optimum PV tilt angle for the study site and inferred that up to 20% of the average daily electricity demand of the city can be met by rooftop PV. Jakubiec & Reinhart (2013) presented a method for estimating city-wide electricity gains from PV panels by creating 3D urban models using LiDAR data and ArcGIS, Daysim–based hourly radiation simulations, and hourly calculated rooftop temperatures. Creating a 3D urban model is crucial when assessing PV rooftop potential in an urban environment (Martín et al. 2015). A comprehensive study of the spatial dimensions of the site is required to gain an accurate knowledge of the PV potential (Martín et al. 2015). The emergence of LiDAR technology has provided a great opportunity for dense urban area mapping (Huang et al. 2015).

Methods using DEMs employ rooftop irradiation or the number of annual daylight hours in determining proper roof areas (Jakubiec and Reinhart 2013). The DEMs are often generated from LiDAR data, and are the most accurate source for measuring the details of an entire urban area (Jakubiec and Reinhart 2013). Gagnon et al. (2016) used LiDAR data, GIS methods, and PV-generation modeling to estimate the suitable rooftops for installing

PV in 128 cities in the United States. Then, they estimated the PV potential of the entire continental United States employing the results from analysis of areas covered by LiDAR data. Jochem et al. (2009) used LiDAR point clouds and a region-growing process to detect potential roof points and perform solar potential analysis for each point. They considered the shadow cast by adjacent objects and the effects of cloud cover by calculating the horizon of each point within the point cloud and employing data from a nearby ground weather station, respectively. Using a GIS-based method and utilizing LiDAR data, Gooding et al. (2013) ranked seven major UK cities according to their capacity to generate electricity from roof-mounted PV systems. They calculated a solar city indicator taking into account the socio-economic factors such as income, education, environmental consciousness, building stock, and ownership. The results revealed that the local buildings' characteristics affect the physical and socio-economic rooftop PV potential of a city significantly and indicated areas that require policy attention to promote maximum PV use (Gooding et al. 2013).

Different procedures for analyzing solar potential in urban environments have various drawbacks, and the existing rooftop PV evaluations inferred from the methods may be imprecise (Castellanos et al. 2017, Jakubiec and Reinhart 2013). In some methods, the shading caused by urban context such as trees and neighboring buildings is not considered, or differentiation among the orientations and slopes of roof segments are not conducted (Jakubiec and Reinhart 2013). Many studies require assumptions about the orientation and slope of rooftops (Boz et al. 2015). Furthermore, few solar potential estimation methods suppose that all rooftops are flat and a constant portion of them is suitable for PV installation (Jakubiec and Reinhart 2013). Rooftop PV studies rarely investigate the economic potential of these systems (Fath et al. 2015). In this chapter, a new detailed

method for calculating solar resource availability using ArcGIS was employed. Additionally, the economic potential of rooftop PV systems was investigated.

3.3 Methods

Modeling the built area, the insolation incident assessment, and the estimation of the suitable roof area are essential in evaluating a building's potential in solar rooftop PV energy generation (Santosa et al. 2014). Urban area modeling is an active research field in Geography (Santosa et al. 2014). Urban areas are dense environments composed of diverse artificial and natural features. This complexity makes building rooftops attractive for solar PV installation (Redweik et al. 2013). Building rooftops provide a large expanse of generally unused area for PV energy production (Gagnon et al. 2016). In the urban context, the existence of various artificial and natural objects including buildings and trees influences the sunlight regime considerably (Huang et al. 2015). Accordingly, an accurate solar insolation simulation model that considers the complexity of the urban form is required to identify relevant aspects of the urban energy landscape (Huang et al. 2015). In an urban environment, representations of three-dimensional form such as elevation, surface slope and aspect, and surrounding obstructing objects determine the accuracy of such simulations (Tooke et al. 2012). Roof surfaces with different slopes and orientations, reflection and shadings from the neighboring objects were modeled separately.

3.3.1 Study area

This study was conducted in Alberta, Canada. Solar electricity can become a mainstream energy source in Canada (Canadian Solar Industries Association 2018). The premium quality renewable resources of Alberta could allow this province to become a leader in solar, wind, and bioenergy. Notwithstanding this potential, much of the province's

renewable resources are untapped (People Power Planet Partnership 2018). The city of Lethbridge (49.7° N, 112.8° W) is in southern Alberta, Canada, a region that receives relatively high rates and extensive hours of solar radiation, with an annual mean daily global horizontal radiation of 3.77 kWh/m^2 and 2,506 hours of bright sunlight (Figure 3-1) (Natural Resources Canada 2017b, City of Lethbridge 2017a). With a moderate continental climate, Lethbridge is characterized by warm summers and mild winters, and has more than 320 days of sunshine per year, which is relatively high among Canadian cities (City of Lethbridge 2017a). This city has a total land area of 124.3 km^2 with a large and growing volume of residential and commercial buildings, which justifies new steps toward building a self-sustainable urban setting (City of Lethbridge 2017a). To our knowledge, an extensive evaluation of rooftop photovoltaic solar potential has not yet been undertaken in this city. Low-height and horizontally dispersed buildings over a large area most likely provide a significant rooftop PV electricity potential. The total number of residential, government, medical, educational, commercial, industrial, cultural buildings in Lethbridge is 55877 (January 2017) (Table 3-1) (City of Lethbridge 2017c). This city had a total population of 96,828 in 2016 (City of Lethbridge 2017b).

Table 3-1: The number of buildings in Lethbridge.

Building type	Number of buildings	Share of sectors (%)
Residential	53,545	95.8
Industrial	1,207	2.16
Commercial	822	1.5
Education	131	0.23
Government	69	0.12
Recreation	68	0.12
Cultural/Heritage	17	0.03
Medical	16	0.03
Transportation	1	0.002
Community Center	1	0.002
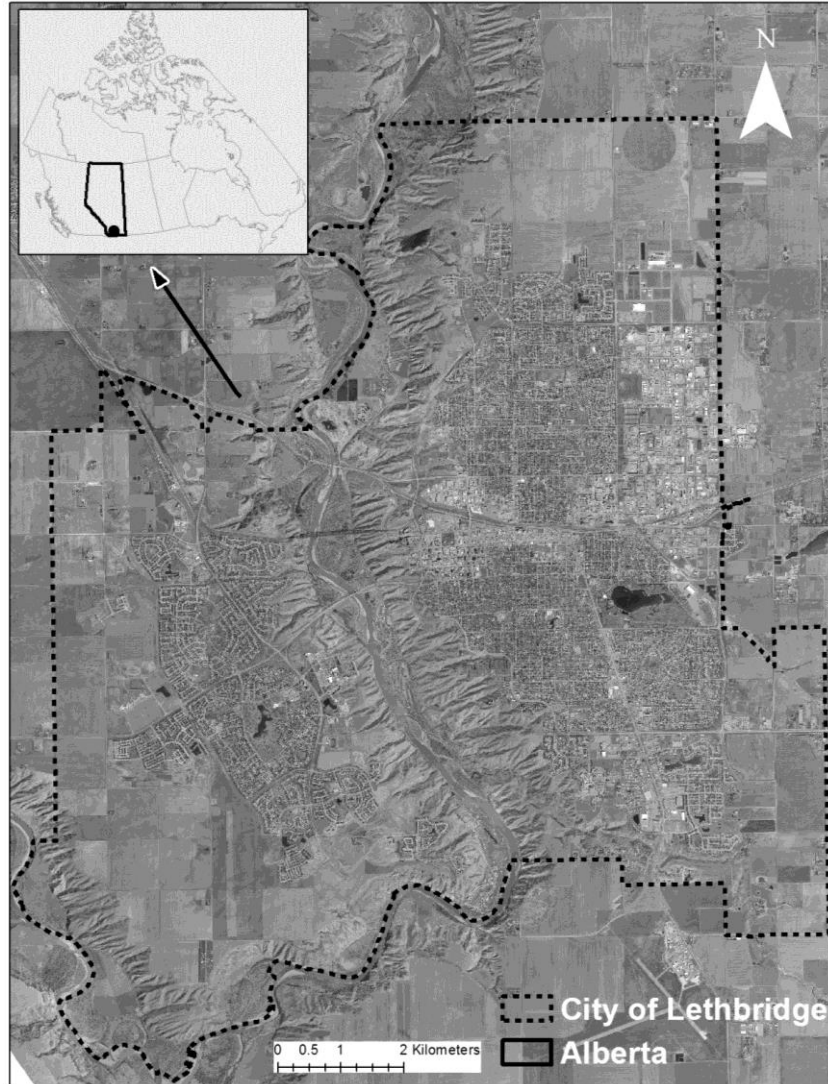
Figure 3-1: Study area, the City of Lethbridge (Esri Canada Ed 2013).

3.3.2 Data

The size of the study area is an important variable in a solar potential analysis (Martín et al. 2015). Vector cartographic maps, digital cadastral services, state geographic information systems, digital elevation and digital surface models (DEM and DSM), and aerial photos are different resources that are widely used in evaluating solar potential. These resources provide required information about building shape, footprint, height, type, location and other urban features (Martín et al. 2015). The need for more detailed city

models has led to increasing use of LiDAR point clouds which contain a wealth of Earth surface information (Martín et al. 2015). Large volumes of LiDAR data collected in July 2015, with vegetation in full leaf-on condition, were provided by the City of Lethbridge through the University of Lethbridge, and used to represent the study area in ArcGIS. The resolution of LiDAR data is 1 m^2. The city boundary data and a polygon shape file of building footprints provided by the City of Lethbridge were used to determine the extent of the study area and to identify rooftops (City of Lethbridge 2017c, d).

3.3.3 Processing LiDAR data to drive suitable rooftop area for PV application

LiDAR data are usually provided in LAS format (a standard format for LiDAR data interchange) and a defined spatial reference is not typically embedded in them (Figure 3-2) (Esri 2013, 2019). The proper spatial reference information of LAS files that was indicated in the LiDAR metadata was defined. Using LiDAR data, two kinds of high-quality elevation models including digital surface model (DSM) and digital elevation model (DEM) can be produced. First return (surface return) or DSM encompasses elevation information for buildings, tree canopies, and bridges, while DEM or ground or bare earth represents the topography (Huang et al. 2015, Esri 2016b, Jochem et al. 2009). To analyze the shading, slope, and azimuth (orientation) of each roof segment at a resolution of 1m^2, LiDAR data was processed. The digital surface model or DSM with a 1×1 meter cell size was created via maximum value interpolation technique to model the high-relief urban area (Figure 3-2) (Esri 2016b). For generating a DSM from LiDAR data, the maximum value is the best technique for biasing the result to higher elevations (Esri 2016b). Because PV panels are placed on top of buildings, the building footprint data was used to clip DSM (Gagnon et al. 2016, Boz et al. 2015). Before intersecting these two files, a 1-m buffer was

applied to building footprint areas (Boz et al. 2015). LiDAR data may contain some noise and may not be precise enough close to the roof edges, and thus may be unable to provide an accurate representation of roof borders (Boz et al. 2015). As a result, there is no explicit or absolute roof boundary discernible from LiDAR data. Applying this 1-m buffer helped to eliminate noise in LiDAR data (Boz et al. 2015). It was assumed that the whole area of rooftops cannot be covered by PV panels and the extent of roof surfaces devoted to the panels is assumed to be bounded by a 1-m-wide perimeter area. This margin area is also required for safety and maintenance purposes (Boz et al. 2015).

Different methods have been used to extract roof footprints from LiDAR data. For instance, Huang et al. (2015) used vegetation information, normalized difference vegetation index (NDVI), from color-infrared image and height information from DSM to recognize building roof surfaces. Chaves and Bahill (2010) used an elevation mask to exclude the locations lower than a specific height. To extract building roof surfaces from the LiDAR data, DSM was clipped by a building footprint polygon shape file. Most of the buildings are single homes with mainly ridged roofs. Topographic characteristics such as hillshade, slope, and aspect were calculated using the extracted DSM from the LiDAR point cloud (Huang et al. 2015).
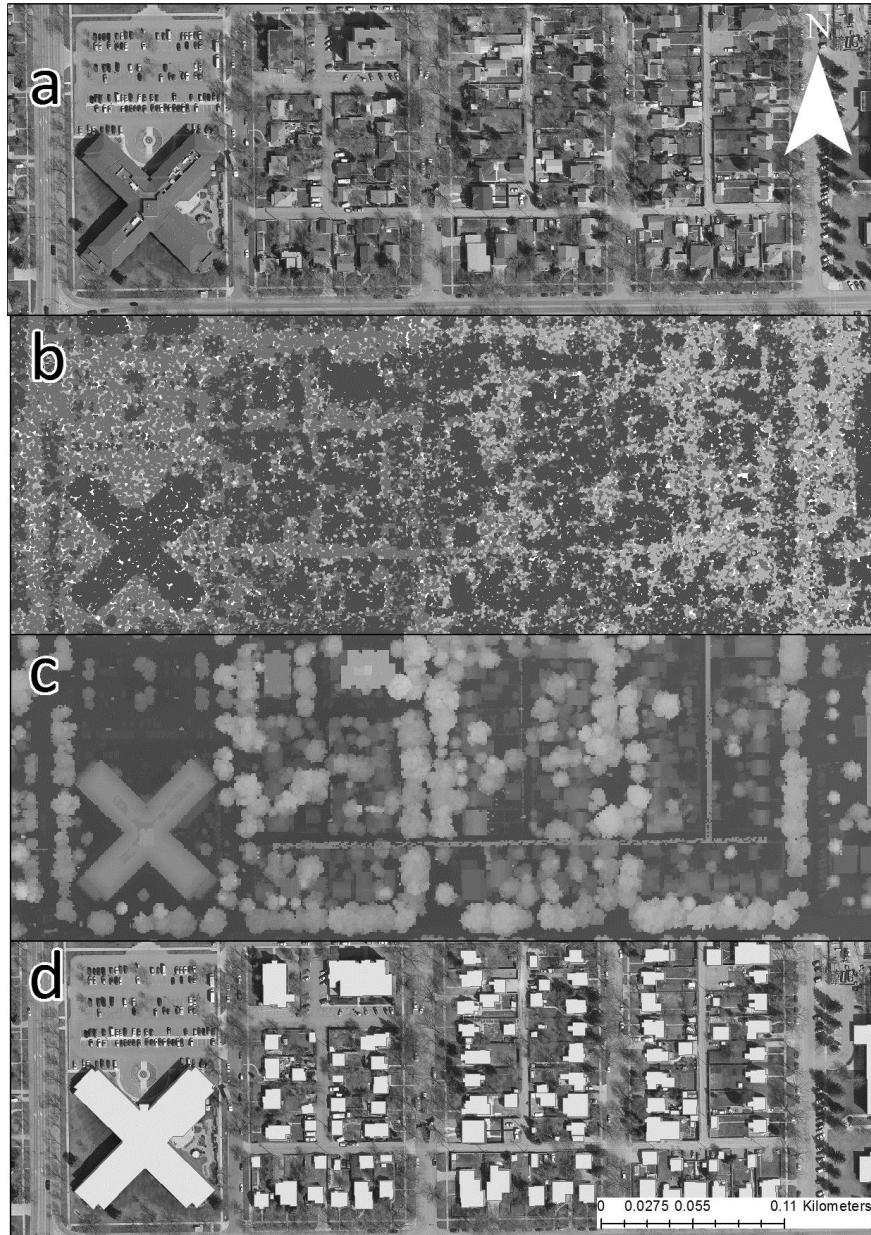
Figure 3-2: Spatial layers: a) aerial imagery, b) LiDAR point clouds, c) DSM, d) building footprint polygons.

3.3.3.1 Rooftop Slope Analysis

The steepest downhill fall from each cell to its eight surrounding cells (the largest elevation change over distance between each cell and its adjacent cells) was calculated in ArcGIS using the average maximum technique (Esri 2014). The slope of each square meter of roof surfaces in the study area was determined. Lower slope values represent flatter

planes (Esri 2014). Surfaces with a tilt less than 10 degrees are usually defined as flat planes (Gagnon et al. 2016, Boz et al. 2015). PV panels installed on pitched roofs usually have an inclination angle equal to the slope of the roof (Verso et al. 2015). On the flat or almost flat roofs, PV panels can be installed with a desired slope (Verso et al. 2015). The optimal PV panel tilt angle varies with latitude. PV systems with tilt angles equal to latitude produce more yearly electricity than others, while those with slopes larger than latitude generate more constant energy but have lower annual production (McKenney et al. 2008). Lower slopes lead to more electricity production in summer, whereas higher tilt angles induce larger energy generation in winter (McKenney et al. 2008). In fact, with higher slopes, the difference between summer and winter energy production decreases, and throughout the year the energy flow is more consistent, while with lower slopes the fluctuation of produced energy during summer and winter is considerably higher, meaning that over the course of a year, generated electricity exhibits a significant seasonal change. Accordingly, a slope classification logic was utilized to organize different rooftop surfaces with various slopes according to their suitability for PV installation (Table 3-2) (Boz et al. 2015).

Slope evaluation with LiDAR data is not always precise or perfectly accurate. The calculated slope might vary throughout a surface with a unique actual slope due to noise in the LiDAR data. Noise is generated when light pulses encounter an object which does not belong to the roof surface (Boz et al. 2015). To reduce noise and obtain the most accurate results, the Majority filter was used. Using this filter, cell slope values were replaced based on the majority of their contiguous neighboring cells (Boz et al. 2015).

Table 3-2: Slope classes for roof areas (Boz et al. 2015).

Slope Value (Degree)	Class
0-10	1
10-20	2
20-30	3
30-40	4
40-50	5
50-60	6
60-90	7

3.3.3.2 Rooftop Azimuth Analysis

Solar panels oriented toward a specific direction exhibit maximum performance (Gagnon et al. 2016). Azimuth (aspect) identifies the compass direction that the surface slope faces at the installed location. The azimuth in positive degrees was derived from the input elevation dataset (the LiDAR-generated DSM) for each square meter of roof area utilizing ArcGIS (Gagnon et al. 2016). Aspect values were measured clockwise, from 0 that defines north to 360 which again indicates north. Flat areas have an aspect value of -1. The azimuth measurements were categorized into nine classes (Figure 3-3) (Gagnon et al. 2016). Next, to eliminate noise, the Majority filter was used (Boz et al. 2015). Azimuth values are used to detect all roof planes. A roof plane is composed of contiguous areas with same azimuth (Gagnon et al. 2016). Roof planes were converted to polygons, thereby individual square meters of roof surfaces were dissolved into homogeneous roof planes. Then, to calculate a single average tilt for each individual roof segment, the Zonal Statistics tool was applied to the slope raster (Gagnon et al. 2016).
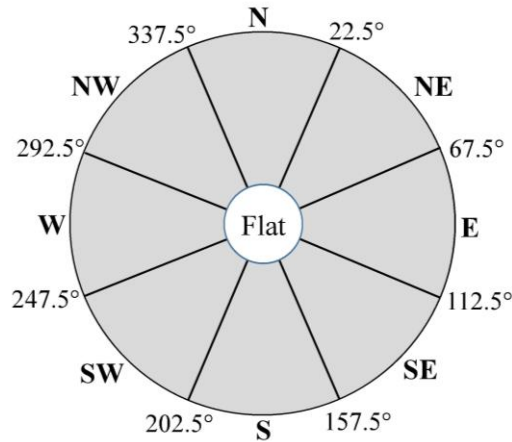
Figure 3-3: Rooftop azimuth classes (Gagnon et al. 2016).

3.3.3.3 Shading Analysis

To model the spatio-temporal variation of insolation on different facets of urban surfaces and to determine the unobscured fractions of each roof plane for most of the time, a shading simulation was applied to the city's DSM to illustrate the spatial and temporal variation of the shadows. The gradual movement of shadows cast by nearby features throughout a day influences the performance of PV systems significantly, and makes it of particular importance to consider the variations in length and direction of shadows in PV installments. By running the shading simulation for each daylight hour for March 21 (vernal equinox), June 21 (summer solstice), September 21 (autumnal equinox), and December 21 (winter solstice) the hourly and seasonal variations of shading were assessed (Gagnon et al. 2016). To investigate the illumination pattern over time and to exclude roof segments that are extremely shaded, ArcGIS hillshade capability was employed to generate a shaded relief based on the local illumination angle (sun's relative position) and shadows (Figure 3-4) (Esri 2017a).
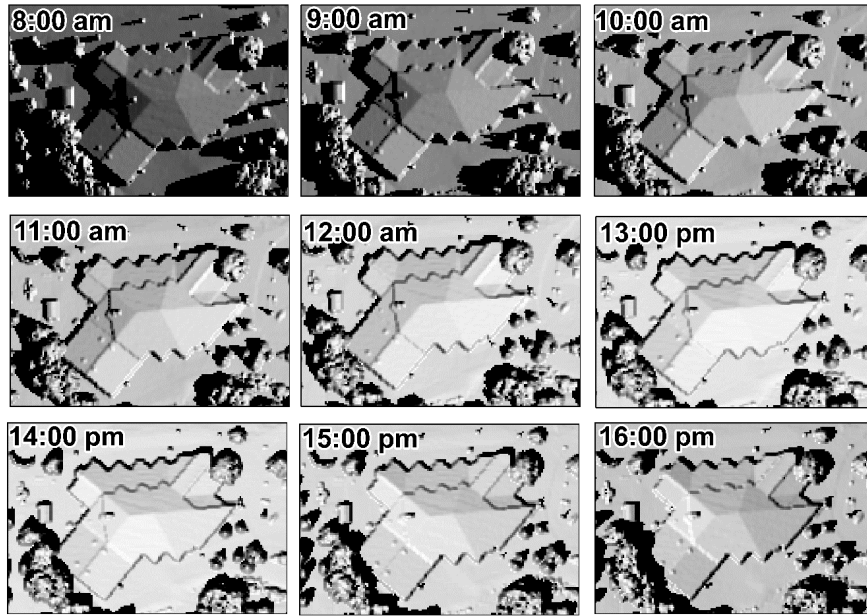
Figure 3-4: Hourly illumination and shading pattern example, June 21.

3.3.4 Suitable Roof Surfaces Selection

Suitable locations for the placement of PV panels possess particular attributes (Chaves and Bahill 2010). Various criteria for selecting suitable roof planes based on their slope (tilt), aspect (azimuth), minimum amount of contiguous area, and received incident solar radiation were applied. Because Lethbridge is located in the northern hemisphere, all roof surfaces oriented toward northwest through northeast (292.5-67.5 degrees) were excluded (Gagnon et al. 2016, Huang et al. 2015). The slope of roof surfaces should be less than 60 degrees, and rooftops larger than 10 m^2 were considered to be suitable for placing PV panels (Gooding et al. 2013, Huang et al. 2015, Boz et al. 2015). The smallest practical residential solar system that can exhibit a tangible energy production is a 1.5-kW system (Gagnon et al. 2016, Solar Choice 2016). Such systems require approximately 10 m^2 of area (Gagnon et al. 2016). This criteria also excludes objects such as chimneys, dormers, and heating, ventilation, and air conditioning (HVAC) apparatus located on roofs (Camargo et al. 2015). In addition, desirable roof surfaces should receive an acceptable

70

number of sunlight hours. In hillshade raster, the illumination status of each square meter of rooftops in each hour is illustrated by an integer value ranging from 0 to 255 (Esri 2017a). At summer solstice, between 9 a.m. and 3 p.m., cells with more than 50% of the full brightness value were considered not shaded and others with lower brightness were filtered out (Boz et al. 2015). By examining a sample of these cells, we found that they have more than 20% of the maximum illumination at winter solstice, between 11 a.m. and 2 p.m. Investigation of the hillshade raster of different months showed that the aforementioned brightness threshold leads to reasonable results, meaning that rooftops with reasonable aspects and exposure to the sun were selected. This multi-criteria strategy eliminates unsuitable rooftop areas that lack appealing characteristics, but it is expected that non-optimally tilted and oriented roof planes will also become economically viable and attractive for placing PV panels in the future due to cost reductions and improved efficiency (Figure 3-5) (Fath et al. 2015).

Figure 3-5: Examples of suitable rooftop area selection (roof applications such as chimneys have been excluded).

The file of roof segments with appropriate slope and aspect was created, and then run through a Dissolve function which merges contiguous polygons with a specific common characteristic to produce continuous suitable areas. Next, the rooftop polygon file was converted to a raster file and reclassified. The reclassified hourly hillshade raster files were combined with the rooftop raster by applying Raster Calculator. Employing Python syntax, Raster Calculator utilizes Map Algebra expressions consisting of various geoprocessing operators on multiple inputs to create a desirable raster (Esri 2017b). To evaluate the actual practicable roof expanse and the PV installed (nameplate or nominal or rated) capacity, the projected roof areas were determined from building footprints and used to calculate the oblique area of each suitable roof segment.

3.3.5 Solar resource evaluation

The solar radiation estimation can be conducted by using different solar models, ground-based meteorological stations or meteorological satellite measurements (Santosa et al. 2014). Solar resource potential was assessed for the entire study area utilizing Solar Analyst. Solar Analyst uses the DSM to produce global, direct, and diffuse insolation maps for a geographic area (Boz et al. 2015). Solar Analyst considers the atmospheric effects, latitude and elevation of the region, steepness (slope) and compass direction (aspect), daily and seasonal variation of the sun position, shadows and topography, while ignoring local weather and temperature (Gooding et al. 2013, Verso et al. 2015). Cloud cover has the largest influence on radiation attenuation in the atmosphere (Tooke et al. 2012). Solar Analyst uses defined default values for the diffuse proportion of global radiation (K_D) and the ratio of the insolation received at the Earth's surface as direct radiation along the shortest atmospheric path at sea level to the insolation at the upper border of the atmosphere

(τ_{sl}, transmittivity), which should be adjusted for local atmospheric conditions (Mirmasoudi et al. 2018, Jakubiec and Reinhart 2013, Esri 2016a). Accordingly, utilizing meteorological measured data over five years from a station (Lethbridge CDA, located at 49° 42' 0" N, 112° 46' 60" W) inside the study region and calculating the actual values of required inputs ($K_D = 0.429$, $\tau_{sl} = 0.589$), the effects of cloud cover and local atmospheric conditions have been included. All meteorological data were obtained from Alberta Agriculture and Forestry, Alberta Climate Information Service (ACIS) (https://agriculture.alberta.ca/acis, 2016). Instead of τ_{sl} in global annual solar radiation calculation, we used $K_{T_{sl}}$ (the ratio of measured global solar radiation on a horizontal surface against the extraterrestrial radiation at sea level) (Mirmasoudi et al. 2018). Between 11:30 and 12:30 hours for each day of the years 2010 to 2014, the hourly K_T was evaluated for the station (Ruiz-Arias et al. 2009). For estimating solar radiation, the annual mean of these K_T values was used. Then, the diffuse fraction of hourly global radiation was estimated utilizing Erbs et al. model (Equation (3-1)) (Duffie and Beckman 2013).

$$K_D = \begin{cases} 1.0 - 0.09K_T & ; K_T \leq 0.22 \\ 0.9511 - 0.1604K_T + 4.388K_T^2 - 16.638K_T^3 + 12.336K_T^4 & ; 0.22 \leq K_T \leq 0.8 \\ 0.165 & ; K_T > 0.80 \end{cases} \quad (3\text{-}1)$$

Solar Analyst algorithm utilizes sea level transmissivity (Fu and Rich 2000). Hence, using Equation 3-2, K_{T_Z} was adjusted for sea level, where z represents elevation (Ruiz-Arias et al. 2009).

$$K_{T_Z} = K_{T_{sl}}^{exp(-0.000118z - 1.638 \times 10^{-9}z^2)} \quad (3\text{-}2)$$

Next, Zonal Statistics was used to average the annual solar radiation values of all individual square meters inside each suitable rooftop segment to identify the roofs' received total solar radiation (Wh/m^2).

In order to assess the accuracy of simulated solar radiation, the results were compared with measured insolation obtained from ACSI for the aforementioned station. The mean bias error (MBE) and the mean absolute bias error ($MABE$) for comparing the monthly average observed and simulated insolation were calculated (Equation 3-3).

$$MBE = \frac{1}{n}\sum_{i=1}^{n}(y_i - x_i) \ , \quad MABE = \frac{1}{n}\sum_{i=1}^{n}|y_i - x_i| \quad , \quad R^2 = 1 - \frac{\sum_{i=1}^{n}(x_i-y_i)^2}{\sum_{i=1}^{n}(x_i-\bar{x})^2} \qquad (3\text{-}3)$$

where x_i, y_i, n, and $\bar{x}$ are the ith measured value, the ith calculated value, the total number of insolation data, and the mean measured global radiation respectively (Besharat et al. 2013). MBE illustrates the model's inclination toward radiation overestimation (positive value) or underestimation (negative value) (Despotovic et al. 2015). The coefficient of determination (R^2) derived from regression analysis was used to interpret how precisely the actual data points are approximated by the model and to determine the extent to which the two data sets are in agreement (Besharat et al. 2013). For 2017 measured radiation, the analysis revealed that the R^2 is 0.98, which means the model predicts the insolation very well and there is a very good fit between the two data sets. In addition, the distribution of residuals did not exhibit a strong non-linear relationship of measured and modeled results. Also, MBE of 5% and $MABE$ of 12% were determined, which are in acceptable ranges (Figure 3-6, Table 3-3). MBE and $MABE$ are normalized by the average of the measured radiation. The monthly measured radiation ranges from 174.2 MJ/m^2 to 928.6 MJ/m^2 with an average equal to 477.8 MJ/m^2.
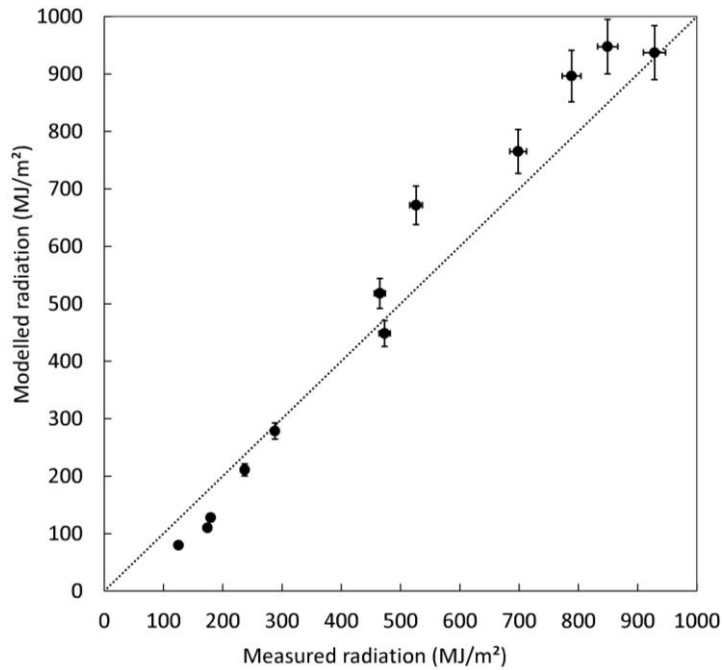
Figure 3-6: Observed versus modelled total monthly solar radiation with calculated annual average diffuse proportion and transmittivity.

Table 3-3: Regression relationships between monthly observed and modelled total solar radiation with calculated annual average diffuse proportion and transmittivity.

$y = a + bx$	$Std.Error_a$	t_a	p	$Std.Error_b$
$y = -61.411 + 1.174x$	30.718	-1.999	<0.001	0.056
t_b	p	R^2	MBE	$MABE$
21.007	<0.001	0.989	0.050	0.120

Using default values of ArcGIS leads to 33% underestimation of radiation (Figure 3-7, Table 3-4), while the employed method induces 5% overestimation considering 2017 measured data.
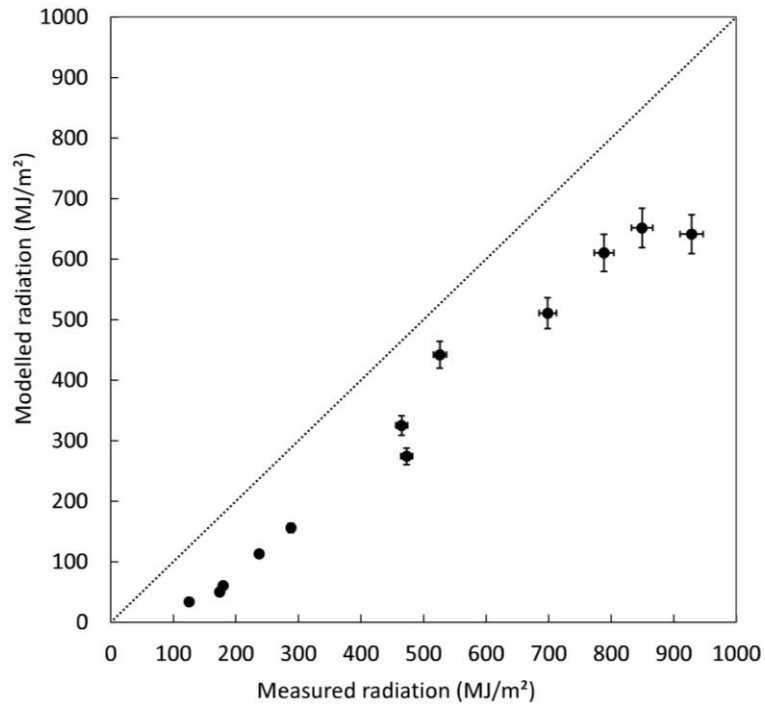
Figure 3-7: Observed versus modelled total monthly solar radiation with solar analyst's default diffuse proportion and transmittivity.

Table 3-4: Regression relationships between monthly observed and modelled total solar radiation with solar analyst default diffuse proportion and transmittivity.

$y = a + bx$	$Std.Error_a$	t_a	p	$Std.Error_b$
$y = -79.842 + 0.842x$	21.466	-3.719	<0.001	0.039
t_b	p	R^2	MBE	$MABE$
21.560	<0.001	0.967	-0.325	0.325

Using monthly averaged values of K_D and τ_{sl} obtained over the years 2010 to 2014 and considering the 2017 measured data, MBE of 1% and $MABE$ of 9.21% were determined which are slightly better than the results of utilizing annual K_D and τ_{sl} (Figure 3-8, Table 3-5). However, for annual rooftop PV electricity potential estimation it seems more practical and sufficiently accurate to use one set of K_D and τ_{sl}. Hence, the annual values of $K_D = 0.429$ and $\tau_{sl} = 0.589$ can be used for solar radiation calculations in the study area. Note also that Solar Analyst does not calculate the reflected component of radiation.
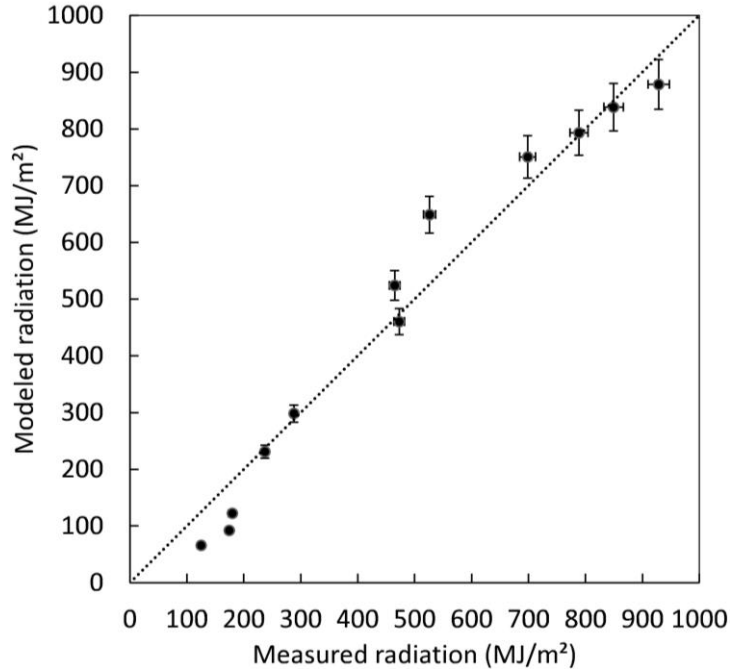
Figure 3-8: Observed versus modelled total monthly solar radiation with calculated monthly averaged diffuse proportion and transmittivity.

Table 3-5: Regression relationships between monthly observed and modelled total solar radiation with calculated monthly averaged diffuse proportion and transmittivity.

$y = a + bx$	$Std. Error_a$	t_a	p	$Std. Error_b$
$y = -31.769 + 1.061x$	34.240	-0.928	<0.001	0.062
t_b	p	R^2	MBE	$MABE$
17.038	<0.001	0.979	-0.010	0.092

PV panels are usually installed with a desirable tilt angle on flat rooftops, hence simulated global solar irradiance on horizontal surfaces was converted to insolation on oblique planes. Hourly measured global solar irradiance data obtained from a station in the study region (Lethbridge CDA) over five years was transferred to tilt planes utilizing transposition and separation models (Perez et al. model (1990), and Erbs et al. model (1982)) considering the reflected component of radiation (Duffie and Beckman 2013). A slope factor was extracted from this transposition and was applied to ArcGIS simulated global horizontal radiation. In this method, roof segments with slopes between 0° and 10° are considered as flat. Based on the Perez et al. model (1990), the radiation on a tilted

77

surface has three components: beam, diffuse and ground reflected. The reflected radiation

is defined as $I\rho(\frac{1-cos\beta}{2})$ where I, ρ, and β are the global radiation on a horizontal surface,

the diffuse reflectance of the surroundings (albedo coefficient), and the tilt angle of the

surface, respectively (Duffie and Beckman 2013). Solar radiation on PV panels increased

by about 7% when the ground reflected component was taken into account, compared with

the case when the ground reflected component was ignored (ρ was set to zero). Figure 3-9

shows different stages of LiDAR data processing for an example building with a complex

roof surface.
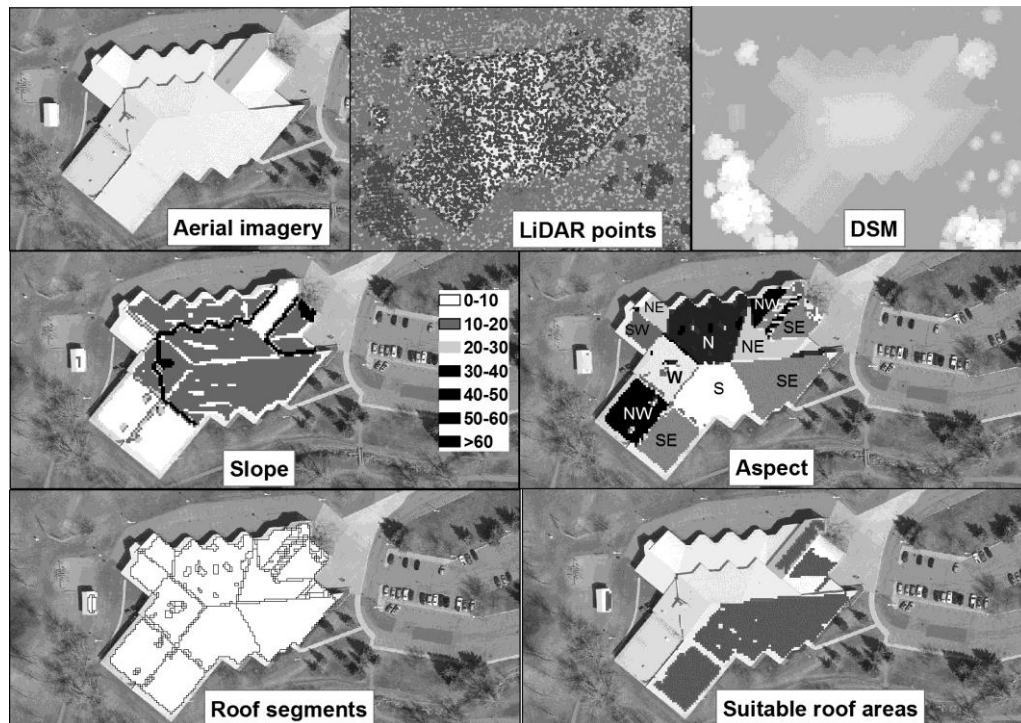
Figure 3-9: Various steps of data processing for an example building.

3.3.6 Rooftop PV electricity production simulation

Electricity output evaluation of a PV system requires the estimation of resource

availability, the physically available area, and the technology's performance (Izquierdo et

al. 2008). The performance capacity of the flat rooftop PV systems is simulated by

78

considering a packing factor which reflects the access space between installed panels required for maintenance purposes and to avoid shading from vicinity panels (row spacing) (Anderson et al. 2010, Wirth and Schneider 2016). Usually solar modules require an installation area about 2.5 times greater than their own surface area which means that about 40% of the suitable flat area is usually covered by solar panels (Wirth and Schneider 2016). The ratio of panel area to roof surface for inclined roofs which accounts for necessary module spacing for racking clamps was taken as 98% (Gagnon et al. 2016). Technical characteristics and assumptions for PV performance modeling are presented in Table 3-6.

Table 3-6: PV system technical characteristics (Gagnon et al. 2016, International Energy Agency 2016, Fath et al. 2015, Philipps and Warmuth 2017).

PV system technical characteristics		
Module efficiency *(η)*	Performance ratio (PR)	Inverter efficiency
15%	80%	95%
Ratio of panel area to suitable rooftop area		**Module tilt angle for flat roofs**
0.4 (Flat roofs)	0.98 (Inclined roofs)	Area latitude angle= 49°
System azimuth		
South facing (Flat roofs)		Azimuth classification

Electricity output E is computed by means of the following equation (International Energy Agency 2016, Fath et al. 2015):

$$E = M_{Irr} * A * \eta * \mathrm{PR} \tag{3-4}$$

where M_{Irr} is the average irradiation of each suitable rooftop, and A is the actual surface area of each suitable rooftop (Fath et al. 2015). Shading simulation being accounted for each rooftop's M_{Irr} by solar analyst. PR is the performance ratio of an implemented system and is defined as below (Schmalensee 2015):

$$PR = \frac{Actual\ AC\ yield\ (kWh/y)}{DC\ power\ rating(KW) \times 8,760(h/y) \times Average\ plane-of-array\ irradiance(W/m^2)/1,000(W/m^2)}$$

$$\tag{3-5}$$

The parameter PR compares the actual annual AC energy yield and the expected DC output of an identical ideal and lossless PV system at the same location and can be used to quantify the overall system losses (Schmalensee 2015). Actual energy yield, and hence PR, is significantly influenced by actual insolation, various losses including shading losses, module efficiency losses, and system losses (Schmalensee 2015). Losses due to accumulation of snow and soil on panels' surface, module parameter mismatch, resistance in the DC circuit, and DC current ripple and algorithm error caused by the switching converter which performs the maximum power point tracking function contribute in the system losses (Table 3-7) (Ropp et al. 1997). PR can be calculated according to Equation (3-6) (Ropp et al. 1997). Furthermore, inverter efficiency (η_{inv}) usually ranges from 92% to 95% (Vignola et al. 2008). Multiplying the PR by the PV module efficiency, the overall system efficiency can be calculated (Pelland et al. 2006).

$$\text{PR} = \eta_{Dust} \cdot \eta_{mismatch} \cdot \eta_{DClass} \cdot \eta_{MPPT} \cdot \eta_{inv} \tag{3-6}$$

Table 3-7: Values representing various losses used in system efficiency calculation (Equation (3-6)) (Ropp et al. 1997).

Parameter	Value
η_{Dust}	96%
$\eta_{mismatch}$	95%
η_{DClass}	98%
η_{MPPT}	95%

Reich et al. (2012) investigated the performance of 100 German PV systems and found that, in part because of Germany's cool climate, the PR of some systems exceed 90%. Given that southern Alberta's solar resources are 30% greater than Germany and considering the latitude similarity between most German cities and southern Alberta, comparable PV system performances are anticipated (McKenney et al. 2008, Pelland and Poissant 2006). In addition, McKenney et al. (2008) developed spatial models of global

insolation and photovoltaic potential for Canada assuming a PR of 0.75. In addition, Pelland and Poissant (2006) evaluated the potential of building integrated photovoltaics (BIPV) in Canada considering a value of 0.75 for the PR of PV systems. With technology advancements, significant improvement in PV systems' performance and module efficiency have occurred over past years, hence, a PR of 80% seems attainable in southern Alberta.

3.3.7 Rooftop PV Economic potential assessment

The economic attractiveness of the rooftop PV systems under current market conditions is investigated to determine whether a specific location is profitable for PV installation or not. Most PV potential studies have not considered the economic feasibility of the PV installations, while, home owners and investors install PV facilities when these systems are economically viable (Fath et al. 2015). Renewables are not currently cost competitive in all places, hence it is important to determine the economically viable fraction of solar PV electricity generation potential.

3.3.7.1 PV Dynamic investment assessment

Net present value (NPV) is used to perform an economic potential analysis and to assess the profitability of the solar rooftop projects (Equation 3-7) (Fath et al. 2015). NPV illustrates the difference between the current value of cash inflows and the present value of cash outflows.

$$NPV = -I_0 + \sum_{t=1}^{T} \frac{CF_t}{(1+r)^t} \ , \tag{3-7}$$

where t is the time of cash flow, T is the total time period or the system life time (25 years), r is the interest rate (2%), and CF_t ($/year) is the net cash flow at time t (Equation 3-8)

(Fath et al. 2015, MacKinnon and Mintz 2017). The parameters i_{deg}, p_{el}, i_{el}, c_{op}, and i_{op} represent the annual degradation rate of generated electricity (0.25 %/year), average electricity price, annual increase in generated electricity price, operating cost, and annual increase in operating cost respectively (Equation 3-8) (Fath et al. 2015).

$$CF_t = E_a \times (1 - i_{deg})^t \times p_{el} \times (1 + i_{el})^t - c_{op} \times (1 + i_{op})^t \qquad (3\text{-}8)$$

In Alberta, from 2013 to 2017, the average increase in the consumer price index of all items such as food, shelter, and transportation was 1.56%, hence i_{op} was set to 1.56% (Statistics Canada 2018). In Lethbridge, the electricity price varies, and with higher electricity prices, solar PV systems become more feasible. While the average power price has been 7.3 ¢/kWh from 2012 to 2018, great changes in regulated electricity rates have been occurring historically (Government of Alberta 2018). Other fees that are charged on electricity bills may increase as well, for instance, average transmission rate in 2027 is forecasted to be about 42 $/MWh which is 33% more than that in 2018 (Statistics Canada 2018, Alberta Electric System Operator 2016, Kuby Renewable Energy Ltd 2018). Solar energy generation can reduce the energy charge, the variable cost of distribution, and the transmission charge on electricity bills (Kuby Renewable Energy Ltd 2018). Estimate of p_{el}, i_{el}, and c_{op} are assumed to be 0.08 $/kWh, 3.5%, and 15 $/kW/year. There is a $36 million rebate program in Alberta, introduced by the provincial government for installing solar PV on residential and commercial buildings aiming to offset up to 30% of residential solar installation costs and up to 25% of solar installation costs for businesses and non-profits (Alberta Government 2017a). We assumed that 25% of the capital costs for all installations would be covered by this program.

Generated solar electricity E_a(kWh/year) provides cash inflows, and in an economically feasible system, the related electricity revenue surpasses all upfront capital costs I_0 and maintenance and operational expenditures over the system's lifetime. A PV system is economically attractive when its NPV is larger than zero (Fath et al. 2015). In 2016, the residential grid-connected rooftop PV systems (up to 10 kW), commercial grid-connected rooftop PV systems (between 10 kW to 250 kW), and industrial grid-connected rooftop PV systems (above 250 kW) cost between 3 to 3.5 CAD$/W, 2.5 to 3 CAD$/W, and 2 to 2.5 CAD$/W respectively (Poissant et al. 2017). Up to a 12.5% decline in PV system prices occurred from 2015 to 2016 (Poissant et al. 2017). Therefore, the upfront investments for 3kW, 10kW, and 250kW PV system sizes have been assumed to be 2,680 ($/kW), 2,200 ($/kW), and 1,760 ($/kW) respectively, applying a 12% reduction to the 2016 system prices (Poissant et al. 2017). Based on these system installment costs, the following relationship between system size P(kW) and investment I_0($/kW) was created to calculate the specific investment for other rooftop PV system sizes:

$$I_0 = 2877.2 \times P^{-0.064} \tag{3-9}$$

Using Equation (3-9), the initial investment cost for the midpoint of each system size class presented in Table 3-8 has been calculated (Fath et al. 2015). For systems larger than 50 kW and smaller than 5 kW the midpoints were set to 60 kW and 3 kW.

Table 3-8: Initial investment cost of PV system classes derived from Equation (3-9).

System size (kW)	Install cost ($/kW)
$P \leq 5$	2,640
$5 < P \leq 10$	2,600
$10 < P \leq 20$	2,400
$20 < P \leq 50$	2,300
$P > 50$	2,200

3.4 Results and discussion

Applying the preceding method to the City of Lethbridge, 38,496 suitable rooftop segments with a total actual area of about 2,372,000 m^2 were identified which cover approximately 30% of the total roof area. The accuracy of the rooftop segment selection has been examined by analyzing and investigating several buildings' rooftop areas using the region's aerial image. The individual suitable segments belong mostly to residential (about 83%) and commercial (about 9%) buildings, providing about 48% and 20% of the suitable area respectively (Figure 3-10, Table 3-9). Most of the segments are flat or have a slope less than 20° (about 91% of them or 84% of the suitable area). Low slope and flat roofs allow us to install PV panels with the most effective tilt angle (Boz et al. 2015).
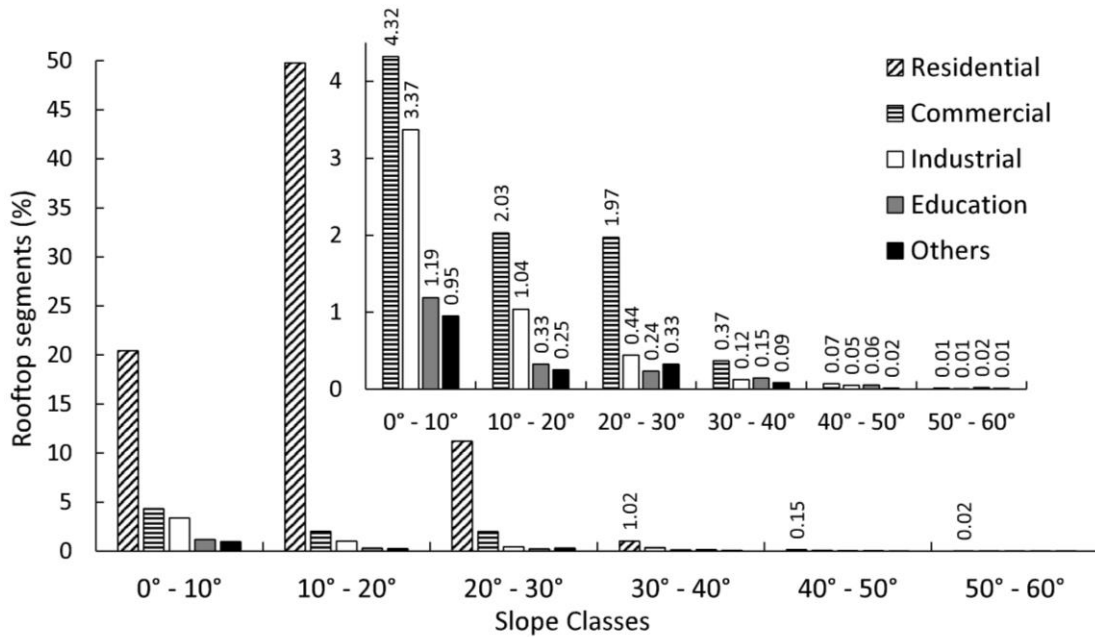
Figure 3-10: Percentage of rooftop segments in different slope classes.

While industrial and commercial buildings account for just about 3% and 4% of the flat individual segments, they constitute the largest portion of the suitable flat area (m^2), about 22% and 18% of the available flat area respectively, demonstrating the importance

of these sectors' engagement in developing a successful solar PV industry in cities (Table 3-9). Furthermore, rooftop PV installation by homeowners can boost the urban solar electricity generation significantly because residential buildings with roof pitch between 10° and 20° account for more than 25% of the total suitable roof area (about half of the segments), which is the highest share among various building types and slope classes (Table 3-9).

Table 3-9: Suitable rooftop segment area (m^2) and its percentage by building type and slope classes.

| Building type | Slope Classes | | | | | |
| | 0° - 10° | | 10° - 20° | | 20° - 30° | |
	m^2	%	m^2	%	m^2	%
Residential	368,544	15.54	598,017	25.21	163,377	6.89
Commercial	414,781	17.49	26,845	1.13	16,614	0.7
Industrial	513,397	21.64	22,403	0.94	4,000	0.17
Education	109,708	4.62	9,595	0.40	2,306	0.10
Others	94,299	3.98	4,489	0.19	4,496	0.19
Total area	1,500,729	63.26	661,349	27.88	190,794	8.04

| Building type | Slope Classes | | | | | | | |
| | 30° - 40° | | 40° - 50° | | 50° - 60° | | Total Area | |
	m^2	%	m^2	%	m^2	%	m^2	%
Residential	9,155	0.39	1,066	0.04	125	0.01	1,140,285	48.07
Commercial	2,825	0.12	508	0.02	99	0.00	461,673	19.46
Industrial	1,130	0.05	470	0.02	132	0.01	541,531	22.83
Education	1,390	0.06	451	0.02	294	0.01	123,745	5.22
Others	1,340	0.06	185	0.01	121	0.01	104,932	4.42
Total area	15,840	0.67	1,066	0.11	772	0.03	2,372,165	

Some building rooftops have more than one suitable segment, especially those with complex structure. After combining multiple suitable segments of individual buildings' rooftops, it was found that about 48% of the all buildings possess a suitable roof plane which could host PV systems (26,959 buildings). About 94% of these buildings are residential (Figure 3-11).
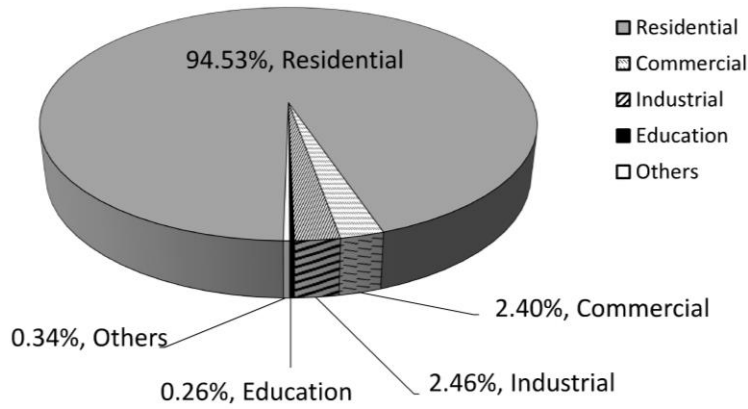
Figure 3-11: Percentage (%) of the different building sectors with suitable roof surface for PV installment.

The majority of the suitable rooftop planes of residential buildings (45% of them) have an area between 20 m^2 and 50 m^2, while most of the commercial and industrial building's suitable rooftops fall between 500 m^2 and 1000 m^2 (Figure 3-12). Around 13%, 22%, 49%, and 32% of the commercial, industrial, education, and other buildings with suitable rooftops have a PV appropriate roof surface larger than 1000 m^2 and smaller than 22,000 m^2, respectively (Figure 3-12). Suitable rooftops larger than 22000 m^2 exist in education and commercial sectors (Figure 3-12).
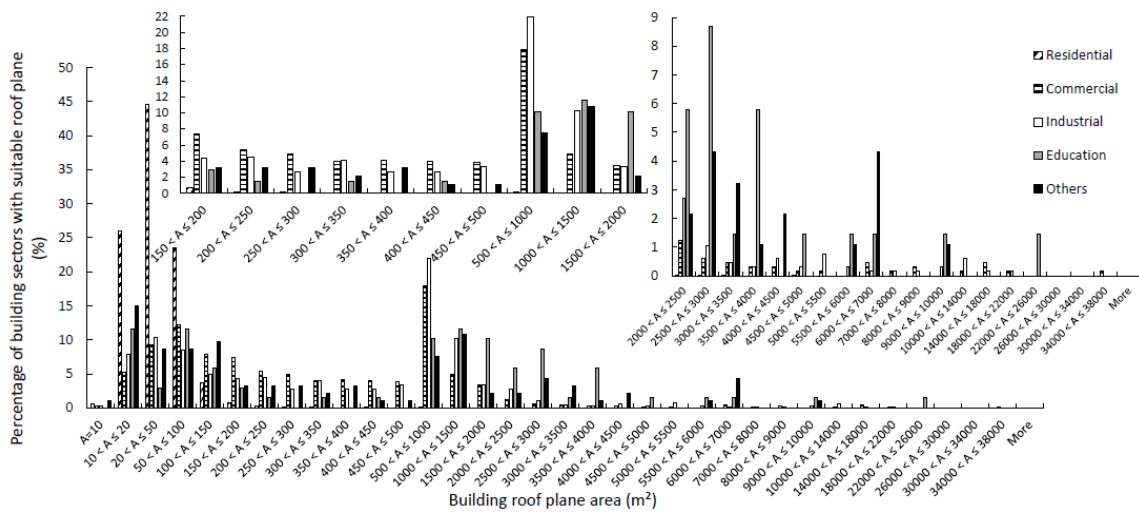
Figure 3-12: Area histogram of buildings' suitable roof plane for PV installment.

Residential buildings with suitable rooftops mostly (about 90%) can accommodate PV systems with a size less than 10 kW, while suitable rooftops of commercial, industrial, education, and other building types demonstrate larger system capacity (Figure 3-13). For instance, while just 0.09% of the suitable residential rooftops can host PV systems larger than 100 kW, around 45% of the education buildings with suitable rooftops can provide sufficient space for rooftop PV systems larger than 100 kW (Figure 3-13).
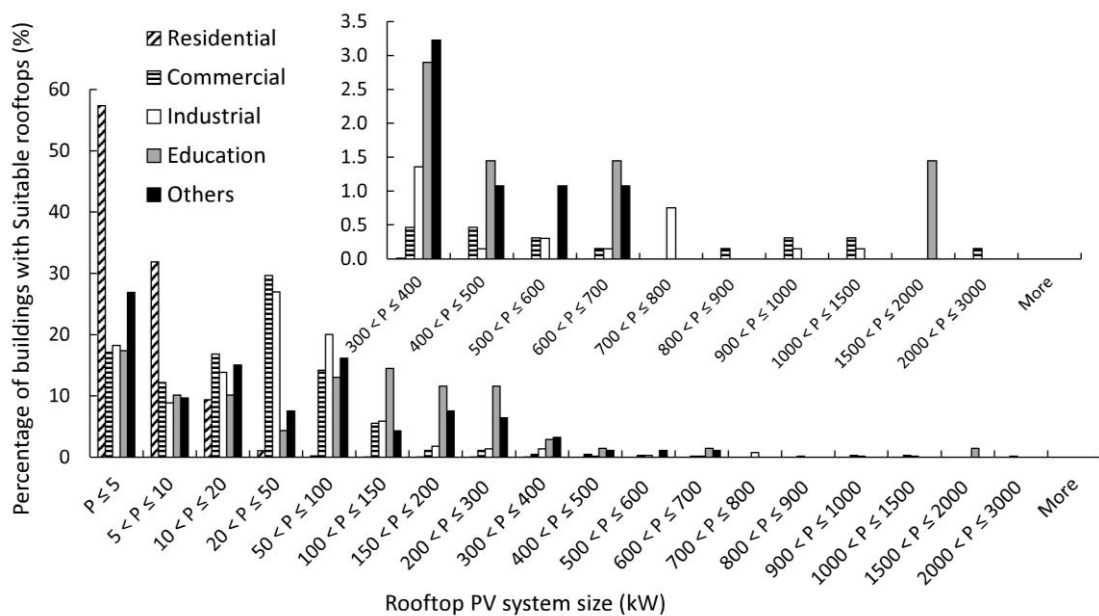
Figure 3-13: PV system size histogram of rooftops for different building types.

The identified suitable surfaces provide enough area for installing approximately 218 MW of rooftop PV systems, with residential buildings accounting for about half of the installed capacity. Based on the computed solar radiation, this installment could generate around 301 ± 29 (SD (standard deviation)) GWh of solar electricity annually (Figure 3-14). More than half of this electricity would be produced by residential buildings' rooftop (about 57%) (Figure 3-14). Industrial and commercial buildings are the second and third largest potential contributors to rooftop PV energy production (Figure 3-14). Combining all

uncertainties in various stages of the system yield evaluation, a total of 9.5% uncertainty in solar PV energy output calculation is estimated (Thevenard and Pelland 2013). In 2015, in Lethbridge, electricity usage per person (for all sectors) was 8.2 MWh (Environment Lethbridge 2017). This consumption is lower than provincial and national average electricity consumption and recently has not changed significantly from year to year (Environment Lethbridge 2017). Considering the city's population in 2016, the estimated rooftop PV electricity would enable the city to offset almost 38% of its annual electricity consumption.
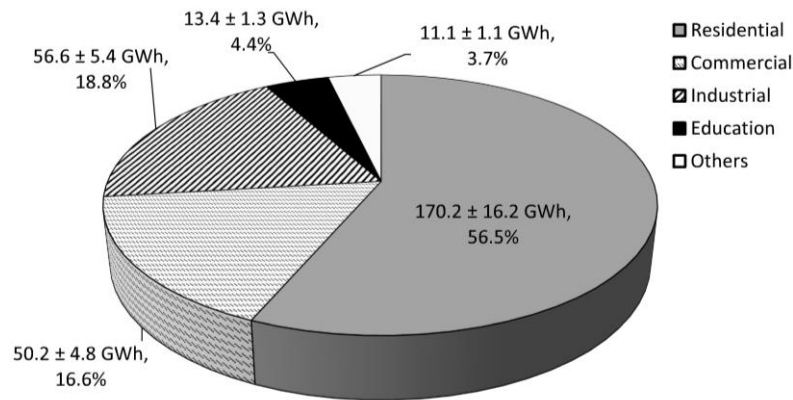
Figure 3-14: Rooftop PV electricity potential generation by different building sectors.

Capacity factor (CF), which shows the difference between the actual performance of a PV system and the energy output of an ideal and lossless PV system with alike rated capacity receiving constant irradiance (1000 W/m^2), is used to compare different power systems' potential in producing energy (Schmalensee 2015). For instance, typical yearly capacity factors for hydropower plants, natural gas combined cycle plants, coal power plants and wind plants are about 40%, 44%, 64%, and 31% respectively. System energy yield is proportional to the capacity factor, where capacity factor is defined as (Schmalensee 2015):

$$CF = \frac{Actual\ AC\ yield\ (kWh/year)}{DC\ peak\ power\ rating(kW) \times 8{,}760(hour/year)} \qquad (3\text{-}10)$$

The average capacity factor of the determined rooftop PV systems is about $16 \pm 1.5\%$, which is very promising for this urban region.

The NPV graphs for system size classes presented in Table 3-8 and various electricity output level are delineated in Figure 3-15 to indicate annual electricity threshold for profitable systems.
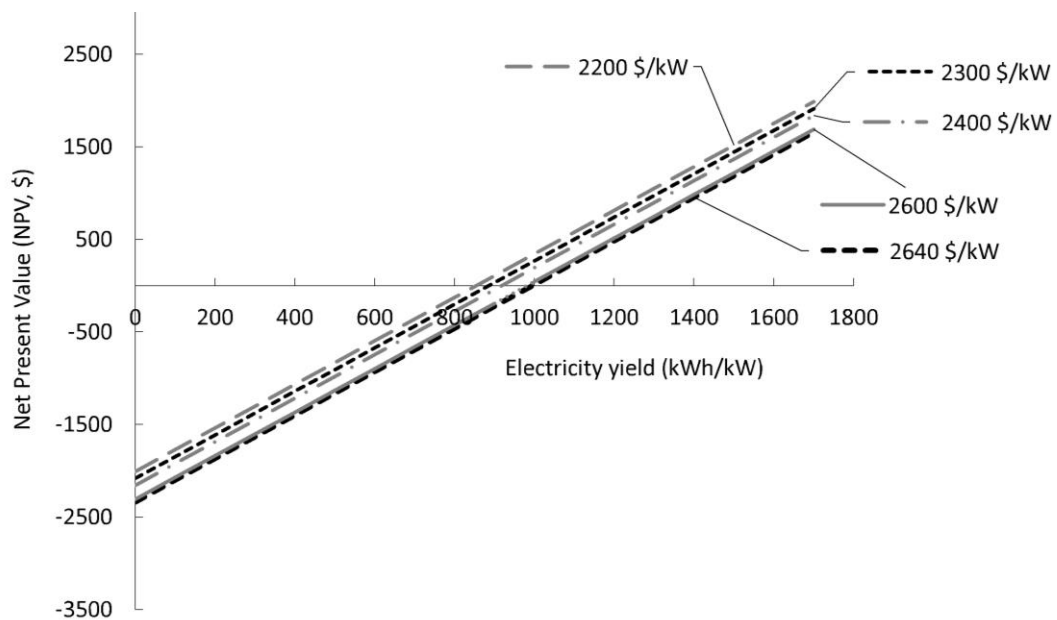
Figure 3-15: NPV graphs for different system size classes versus annual electricity yield.

Systems with an initial investment of 2,640 $/kW need to generate about 994 kWh/kW/year to become economically viable (Figure 3-15, Table 3-10). The initial cost of systems with 2,200 $/kW investment will be compensated over their lifetime if they produce at least 854 kWh/kW/year (Figure 3-15, Table 3-10). Based on NPV graphs, about 96% of the identified suitable rooftop systems are profitable. Small systems occupying small areas are the most likely to fail to be economically justified. However, with more

decline in PV costs and improved efficiencies, small areas can achieve a higher packing factor, produce more energy and become economically attractive.

Table 3-10: Minimum (kWh/kW/year) solar energy production for a NPV= 0.

System capital cost	Minimum(kWh/kW/year) solar energy production for a NPV= 0
2,640	994
2,600	981
2,400	917
2,300	886
2,200	854

Recently, the Climate Leadership Plan was introduced by the provincial government, with a goal of ending the use of coal for electricity production by 2030 and utilizing more renewable sources (Government of Alberta 2017). According to this plan, 5,000 MW of new renewable energy capacity will be built by 2030, with renewables to supply 30% of the electricity demand which can lead to a significant growth in clean energy investment (Government of Alberta 2017).

3.5 Conclusion

Rising climate change risks and global sustainability challenges along with the significant decreases in costs of renewables have led to recognition of solar electricity systems as major parts of mitigation strategies (Castellanos et al. 2017). Providing end users with a self-managed, usable energy source with minimal operation and maintenance costs, rooftop PV is distinct among low-carbon technologies (Strupeit and Palm 2016). Here, an exhaustive rooftop PV potential assessment in an urban area has been conducted in order to fill a gap in the available public information about the potential of such systems. Alberta's electricity generation sector currently relies heavily on fossil fuels, and coal in particular, producing approximately 17% of the province's annual GHG emissions in 2015 (Government of Alberta 2017). To achieve the goal of zero emissions from coal-based

electricity production of the Alberta climate plan by 2030, some supporting programs such as the "Residential and Commercial Solar Program" and "Alberta Municipal Solar Program" have been established to stimulate the PV system installation on buildings and municipal facilities (Government of Alberta 2017). In response to this great movement towards more renewable energy sources, this study tries to present an effective and scalable methodology for simulating the insolation resource and rooftop solar PV energy and economic potential in an urban area in Southern Alberta. LiDAR data and ArcGIS was employed to identify suitable rooftops for PV installation and the Solar Analyst simulation engine was applied and adjusted based on data characterizing the local environment to accurately assess the region's insolation resource. Precise solar radiation resources assessment in a large area like an urban area is always challenging, hence a new method was developed to calculate solar radiation using ArcGIS. In addition, the slope of PV modules installed on flat roofs, and the reflected radiation component have been taken into account. Finally, utilizing market prices and dynamic investment methods, the economic potential of rooftop PV systems were investigated. Results illustrated that rooftop PV has a great potential to offset the city's energy demand. The study described in this thesis chapter was undertaken in part to increase the awareness about the characteristics and economics of rooftop PV, which is vital to more renewable energy deployment. The results of this research can assist investors in energy and building sectors and accelerate an informed transition towards a more sustainable future.

Chapter 4: Multi-Criteria PSO-based optimal design of grid-connected hybrid renewable energy systems

4.1 Introduction

The global economy relies heavily and increasingly on fossil fuels. Currently fossil fuels supply about 85% of human energy demands (Mitchell 2015, Bhandari et al. 2015, Akram et al. 2017). The side effects of combustion and inefficient use of energy are the main causes of emerging climate change, which is one of the primary global challenges we face today (Mitchell 2015). The risks of climate change cannot be diminished without a considerable reduction in fossil fuel usage and a transformation in global energy production (Mitchell 2015). Massive renewable energy deployment and energy-saving improvements in efficiency of energy use are the two prime paths towards limiting global climate change (Wang and Singh 2008). Furthermore, the deployment of renewable energy sources will result in increased energy independence and security (Wang and Singh 2008). Using current technology, it is feasible to meet 100% of global energy demand reliably by renewable resources (wind, water, and the sun) by 2050 without imposing excessive costs (Delucchi and Jacobson 2011).

Renewable energy generation from wind and solar sources depends on weather conditions, which vary and often can not be accurately predicted (Bhandari et al. 2015). Hence, renewable energy sources are considered to be unreliable and often unavailable. They also require relatively high capital investments (Wang and Singh 2008, Bhandari et al. 2015). Integrating different renewable power sources can help to alleviate their individual unreliability (Nafeh 2011). Hybrid systems provide a practical path to achieving a balance among cost, emissions, and load availability (Wang and Singh 2008, Bhandari et

al. 2015). Precise planning of HRESs components is essential in attaining the most cost-effective hybrid system with the most reliable energy output (Wang and Singh 2008, Bhandari et al. 2015). Connecting HRESs to the grid can also mitigate the unpredictable nature of electricity production from renewable resources (Khare et al. 2016).

Solar and wind resources are ample in our study region. In this research, they are employed simultaneously to mitigate their respective variations and instabilities. By incorporating storage batteries into such hybrid systems (PV and wind turbine), fluctuations in each intermittent resource's energy production can be smoothed out, making the three components complementary to one another (Wang and Singh 2008). Excess solar and wind energy production (production higher than demand) can be stored for times when energy production is too little to meet the demand (Wang and Singh 2008). By minimizing the waste and curtailments of renewable energy systems, batteries can increase energy availability, match supply and demand, and decrease the operational costs (Wang and Singh 2008). The amount of renewable energy production, load demand, and the site characteristics will determine the appropriate size of the battery (Jahanbani and Riahy 2011).

Consumer's greenhouse gas emission footprint can be reduced by limiting the amount of the purchased electricity from the grid below a specific threshold. To design and size different components of a HRES, particle swarm optimization has proven to be an outstanding metaheuristic method (Del Valle et al. 2008). This method can find nearly optimal solutions to highly nonlinear, multi-criteria design problems. Multi-criteria design is a promising approach to aggregate various design objectives (Wang and Singh 2009).

4.2 Background

The optimal design of renewable energy systems is receiving increasing attention and becoming an active field of research (Erdinc and Uzunoglu 2012, Maleki et al. 2017). The primary goal of reducing the system cost (lifetime cost including the fixed costs (capital and maintenance costs) and operational expenditures) is achieved by employing economic-environment (emission) or techno-economic optimization approaches (Erdinc and Uzunoglu 2012, Alsayed et al. 2013). Various optimization algorithms including genetic algorithm (GA) (Bilal et al. 2010), simulated annealing (SA) (Ekren and Ekren 2010), particle swarm optimization (PSO) (Maleki et al. 2017), linear programming (Ter-Gazarian and Kagan 1992), neural networks (Mellit and Benghanem 2007), simplex algorithm (Lagorse et al. 2009), dynamic programming (Margeta and Glasnovic 2010), stochastic approache (Cabral et al. 2010), iterative and probabilistic approaches (Prasad and Natarajan 2006, Tina et al. 2006), response surface methodology (Ekren and Ekren 2008), design space based approach (Arun et al. 2009), quasi-Newton algorithm (Ashok 2007), and energy hub concept (Alejandro et al. 2009) have been used. Various storage and backup strategies have been sugested; including battery storage, pumped hydro storage (PHS), internal combustion engines (ICE), and connection to the conventional grid, to reduce the impact of the random nature of renewable energy sources (RES) (González et al. 2015). Many evaluation indices have been used to model power supply reliability (Xu et al. 2013). Loss of load expected (LOLE)[1], Loss of power supply probability (LPSP) , the levelised cost of energy (LCOE)[2] (the net value of the unit cost of electricity over the lifetime of the

---

[1] Considering the daily peak load fluctuations, LOLE calculates the number of days that the peak load surpasses the installed system capacity (Okinda and Odero 2015).

[2] LCOE $= \frac{TPV \times CRF}{E_L}$; E_L(kWh), CRF, and TPV are, respectively, the annual output, capital recovery factor, and the total present value of all system components costs (Rouhani et al. 2013, Okinda and Odero 2015)

generation), and the annual net balance are some of the reliability indexes utilized in hybrid optimization studies (Jahanbani and Riahy 2011, Mohammed et al. 2016, Okinda and Odero 2015). Erdinc and Uzunoglu (2012) and Bhandari et al. (2015) reviewed hybrid renewable power systems optimization and sizing techniques presented in the literature.

To minimize the gap between renewable energy production and electricity demand over a 24-hour time span, Kellogg et al. (1996) used an iterative optimization to propose several viable combination of PV, wind, and storage for a stand-alone residential home system, ultimately selecting the combination with the minimum total annual cost. Gavanidous and Bakirtzis (1992) designed an autonomous wind-PV-battery bank system to supply electricity to a building, using a trade-off method that systematically selects the size of various system components by minimizing the "loss of load probability" (LOLP)[3] as well as the initial investment. Nafeh (2011) utilized a Genetic Algorithm to optimize the design of a residential PV-wind hybrid energy system with battery storage. Simulating the proposed hybrid system in MATLAB, they aimed to minimize the hybrid system's total cost while meeting a specific reliability target through satisfying an LPSP constraint. Utilizing two iterative search algorithms for designing renewable sources and battery capacity separately, Akram et al. (2017) proposed a methodology for optimal sizing of a grid-linked PV-wind-battery system based on maximum reliability and minimum cost constraints. Minimizing the levelised cost of energy while achieving high energy reliability, Mahesh and Sandhu (2017) employed a Genetic Algorithm to optimally design a grid-linked PV-wind-battery system utilizing an energy filter algorithm for regulating the energy

---

[3] LOLP $= \frac{\sum_0^t Shortage\ Load\ Time}{8760} \times 100\%$, (LOLP is the fraction of hours at which there is an electricity deficit) (Garcia and Weisser 2006, Mohamed et al. 2016).

injected into the grid. Minimizing the net present value (NPV) (the difference between the present value of cash inflow and the present value of costs over time) objective function, González et al. (2015) utilized a Genetic Algorithm and the net annual balance index to design an optimal wind-PV grid-linked system for a rural township with 1271 residential dwellings. Maleki et al. (2017) presented an economic model for a grid-linked residential PV-wind turbine-fuel cell-solar thermal collector hybrid system. They used a modified heuristic particle swarm optimization method over a 24-hour period to determine the conditions for optimal operation of the system.

This research extends the attempts to optimize HRESs by integrating solar, wind, and battery with conventional grid for a university, providing a detailed plan based on the results. Cost, reliability, and emissions were modeled and different scenarios were investigated. These types of assessments will be required frequently in the future as engineers, planners, and managers develop policies that lead institutions to transition from conventional grid-based power to local and regional solar PV and wind turbine sources of electricity. The methodology outlined in this research is based on a combination of the loss of power supply probability, the annualized system cost, and quantities of greenhouse gas emission avoided by adoption of the HRES design. Considering the required (allowable) LPSP, the optimal configuration of the system was determined first, and then, among all the possible choices, the system with the lowest annual cost was found. The potential of the systems to reduce the resulting overall carbon intensity was also considered as a constraint. The goal of the project was to find a balance between LPSP, the total annual cost of the system, and the GHG emission footprint. A key feature of this research is the use of real on-time data for a university with large electricity consumption to investigate the behaviour

of the proposed methodology and the structure of the required systems. A great deal of additional research in this area is needed to plan for replacement of conventional electrical grids and accelerate the movement towards renewable energy and sustainability (Wang and Singh 2008).

4.3 Methods

4.3.1 Multi-objective optimal design of hybrid renewable energy generation systems

Grid-connected or stand-alone hybrid generation systems are composed of various parallel connected energy resources such as photovoltaic cells, wind turbines, and storage batteries (Wang and Singh 2008, Bhandari et al. 2015, Nafeh 2011, Jayachandran and Ravi 2017, Wang and Singh 2009). When demand exceeds the renewable generation plus battery capacity, energy must be drawn from the conventional utility grid, which can usually be assumed to be fossil fuel based (Kellogg et al. 1996, Akram et al. 2017). When the renewable generated electricity exceeds the demand and the storage batteries are fully charged, extra power is diverted to the grid, balancing the demand load and generated power (Owayjan et al. 2013, Wang and Singh 2008, Kellogg et al. 1996). In effect, the utility grid plays a backup role here (Akram et al. 2017). Each of these electricity sources possesses specific economic, technical, and environmental characteristics which can be improved by incorporating individual sources into a hybrid generation system (Wang and Singh 2008). The aim of this incorporation and the attempt to determine the optimum design for it is to balance multiple conflicting objectives in order to meet the energy demand, while simultaneously optimizing a set of desirable economic, environmental, and operational-reliability measures (Wang and Singh 2008, 2009). In addition, the integration of PV and wind decreases the required battery storage capacity compared with the single

utilisation of renewables (Bhandari et al. 2015). The reliability of the energy generated by the hybrid system considering the weather condition variability together with the overall system cost are two crucial design concerns (Bhandari et al. 2015, Akram et al. 2017). The main objective here is to ascertain the optimal size of the hybrid system components while satisfying the preceding criteria. To determine the optimum wind turbine, PV, and battery size, the hybrid system may be considered as an autonomous (off-grid) system (Akram et al. 2017, Xu et al. 2013). In this context, producing extra energy and selling it to the grid is not considered to be desirable (Alsayed et al. 2013). The environmental advantages of renewable hybrid systems are compromised by purchasing power from the utility grid; henc minimizing the amount of power purchased is considered as an optimization objective (Xu et al. 2013).

4.3.2 Photovoltaic performance simulation

Operation simulation of different system elements is the first stage in HRESs sizing (Bhandari et al. 2015, Nafeh 2011). Receiving insolation of G_T (W/m^2) (the total solar radiation on the tilted PV plane), PV modules with an efficiency of η_c and an area of A_{PV} (m^2) exhibit a power output of P_{PV} given by (Gavanidous and Bakirtzis 1992, Mahesh and Sandhu 2017, Diaf et al. 2007):

$$P_{PV} = \eta_c . A_{PV} . G_T . PR \tag{4-1}$$

Performance ratio (PR) that represents the overall system losses was set to 80% (Schmalensee 2015). Using transformation and separation models, measured hourly global horizontal insolation data obtained from a nearby station is converted to insolation on the tilted plane of PV array. The beam and diffuse fractions of total horizontal hourly radiation were separated and evaluated using the Erbs et al. (1982) model (Duffie and Beckman

2013). Utilizing the Perez et al. (1990) model, the diffuse radiation on the tilted surface was estimated (Duffie and Beckman 2013, Yang et al. 2007). The Perez et al. model renders the diffuse radiation on the tilted surface using Equation (4-2).

$$I_{d,T} = I_d[(1 - F_1)\left(\frac{1+cos\beta}{2}\right) + F_1\frac{a}{b} + F_2 sin\beta] \qquad (4\text{-}2)$$

where F_1 and F_2 are circumsolar and horizon brightness coefficients. I_d (Wh/m^2) and β (degrees) are diffuse components of the hourly radiation on a horizontal plane and the slope angle of the surface, i.e. the array surface tilt angle from horizontal, and a and b are given by Equation (4-3) (Duffie and Beckman 2013).

$$a = \max(0, cos\theta), \qquad b = \max(cos(85°), cos\theta_z) \qquad (4\text{-}3)$$

θ and θ_z are angle of incidence (the angle between the beam radiation on a surface and the normal to that surface) and zenith angle (the angle between the vertical and the line from the surface to the sun), respectively. $I_b R_b$ (Wh/m^2) and $I\rho_g(\frac{1-cos\beta}{2})$ (Wh/m^2) are the beam and ground reflected components of insolation on a tilted surface respectively. R_b is the ratio of beam radiation on the oblique surface to that on a horizontal surface, I (Wh/m^2) denotes hourly total radiation on a horizontal surface, I_b (Wh/m^2) is beam radiation on a horizontal surface, and ρ_g is the ground reflectance (the albedo) (Duffie and Beckman 2013).

In addition, the effect of temperature and various losses on efficiency were considered. The operating temperature of PV cells was evaluated employing the Skoplaki model (Equation (4-5)) (Skoplaki et al. 2008).

$$\eta_c = \eta_{T_{ref}}[1 - \beta_{ref}(T_c - T_{ref})] \qquad (4\text{-}4)$$

$$T_c = T_a + \left(\frac{0.32}{8.91+2.0V_f}\right)G_T \quad ; \qquad V_f > 0 \tag{4-5}$$

where $\eta_{T_{ref}}$ and β_{ref} ($°C^{-1}$) are the efficiency of PV module and the efficiency correction

coefficient at temperature $T_{ref} = 25°C$ and at solar radiation of 1000 W/m², respectively.

T_c, T_a, V_f, G_T are the PV cell operating temperature (°C), the ambient air temperature (°C),

the wind velocity in the windward side of the PV array (m/s), and irradiance on module

surface (W/m²) (Skoplaki et al. 2008). The equation $V_f = V_w/0.67$ relates near the PV

array wind speed (V_w) to the free stream wind speed (V_f) (undisturbed natural air flow

speed (International Electrotechnical Commission 2018)).

4.3.3 Wind turbine performance simulation

The underlying equation that illustrates the wind turbine's mechanical power yield is

(Bhandari et al. 2015, Duffie and Beckman 2013):

$$P = \frac{1}{2}\rho A_{WT,SA}C_P v^3 \tag{4-6}$$

where ρ, $A_{WT,SA}$, C_P, and v are, respectively, the air density (kg/m³), the area swept by the

turbine blades (m²), the turbine power coefficient (Betz's coefficient with a theoretical

maximum of 0.593) which illustrates the ratio of the turbine output to the total energy

contained in the wind, and the wind speed (m/s) (Bhandari et al. 2015). For a good design,

the power coefficient can reach a value of 0.50 (Hemami 2012). The combined efficiency

of the drive train and generator (the system's efficiency in generating electricity), η, is

assumed to be 0.9 (Duffie and Beckman 2013). Using the power curve method, wind

turbine electrical power output can be evaluated by means of the following piecewise model

(Mathew 2006):

$$P_W = \begin{cases} 0 & ; v < v_i \\ av^n + b = P_R \left(\frac{v^n - v_i^n}{v_r^n - v_i^n} \right) & ; v_i \leq v \leq v_r \\ P_R & ; v_r < v \leq v_o \\ 0 & ; v > v_o \end{cases} \quad (4\text{-}7)$$

where $\quad P_W = \frac{1}{2}\rho . A_{WT,SA} . \eta_{WT} . C_P . v_r^3$ $\quad\quad\quad\quad$ (4-8)

where v_i, v_r, v_o, P_R, n are cut-in velocity (m/s), rated velocity (m/s), cut-out velocity (m/s), turbine's rated power (W), and the velocity-power proportionality, respectively (Figure 4-1) (Duffie and Beckman 2013, Mathew 2006). The velocity power proportionality was assumed to be three (Jahanbani and Riahy 2011, Mathew 2006). Table 4-2 demonstrates the wind turbine typical technical parameters utilized in the simulations.

Table 4-1: Wind turbine technical parameters.

P_R	2.0 MW
v_i	2.0 m/s
v_r	12.0 m/s
v_o	25.0 m/s
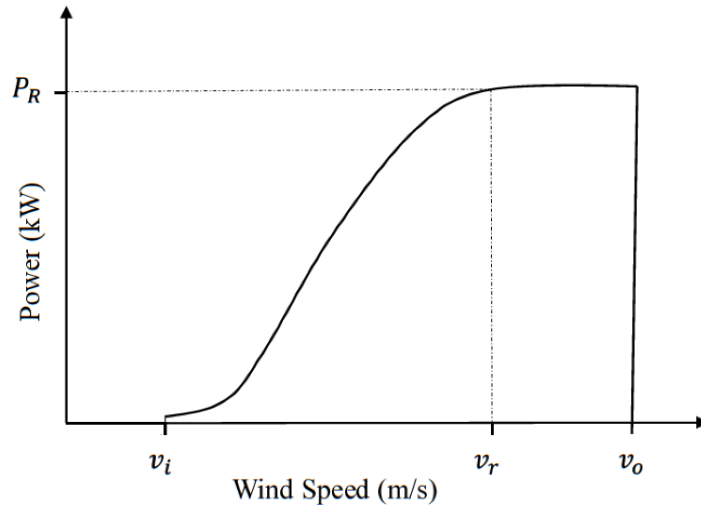
Figure 4-1: Wind turbine typical power curve and essential wind turbine characteristic velocities.

4.3.4 Battery storage modelling

By improving the availability and stability of grid-connected and off-grid renewable energy systems, energy storage elevates the value of renewable energy (Divya and Østergaard 2009). The maximum depth of discharge (the discharge extension, as batteries are not usually discharged fully), rated battery capacity, battery longevity, and self-discharge rate (the discharge rate when battery is not used) are fundamental battery characteristics utilized in battery design and sizing (Bhandari et al. 2015, Divya and Østergaard 2009). Battery types include Lead acid, sodium sulphur (NaS), lithium ion (Li ion), metal air, and flow batteries (Divya and Østergaard 2009). Divya and Østergaard (2009) reviewed battery energy storage technology employed in the power sector and its influence on power systems, and investigated different methods for evaluating economic benefits of battery design and configuration. Lead-acid battery is the most technically mature (Divya and Østergaard 2009). The majority of battery models employed in reliability and stability analysis of power systems are not based on a specific battery technology type (Divya and Østergaard 2009).

Battery capacity (C_{Bat}) is usually the key design variable in system sizing (Nafeh 2011). The state of charge of a battery at time $t, SOC(t),$ is a function of the battery's state of charge at time $(t - 1)$ combined with the energy generation and consumption conditions in time interval from $(t - 1)$ to t (Diaf et al. 2007). The time variable t is generally measured in hours. When the wind and solar PV output exceeds the energy demand, the battery is charging and the available battery capacity at hour t [$C_{Bat}(t)$ (kWh)] is (Ai et al. 2003, Diaf et al. 2007, Jahanbani and Riahy 2011):

$$C_{Bat}(t) = C_{Bat}(t-1)(1-\sigma) + \left(E_{PV}(t) + E_{WT}(t) - \frac{E_L(t)}{\eta_{inv}}\right)\eta_{Bat} \qquad (4\text{-}9)$$

where $C_{bat}(t-1)$, $\sigma, E_{PV}(t), E_{WT}(t), E_{L(t)}, \eta_{inv}$, η_{bat} are, respectively, the available battery capacity at hour $(t-1)$ (kWh), battery hourly self-discharge rate (0.01), energy generated by PV at time t (kWh), energy generated by wind turbine at time t (kWh), load demand at time t (kWh), inverter efficiency (it is assumed that η_{inv} is constant and about 95%), and the battery bank charge efficiency (Ai et al. 2003, Vignola et al. 2008, Mahesh and Sandhu 2017). When the renewable generated electricity is smaller than the load demand, the battery is discharging, and the available battery capacity is (Ai et al. 2003, Diaf et al. 2007, Gavanidous and Bakirtzis 1992, Jahanbani and Riahy 2011, Mahesh and Sandhu 2017):

$$C_{Bat}(t) = C_{Bat}(t-1)(1-\sigma) - \left(\frac{E_L(t)}{\eta_{inv}} - (E_{PV}(t) + E_{WT}(t))\right)\eta_{bat-dis} \qquad (4\text{-}10)$$

The battery's discharging efficiency ($\eta_{bat-dis}$) is assumed to be 1, while the charge efficiency varies with charging current, ranging between 65% and 85% (Nafeh 2011, Diaf et al. 2007, Ai et al. 2003). Battery efficiency during charging was taken into account (Gavanidous and Bakirtzis 1992). Over-charging or over-discharging reduces battery lifetime (Nafeh 2011). To prolong life span, the battery's capacity must be kept within the following range at any hour t (Diaf et al. 2007, Gavanidous and Bakirtzis 1992):

$$(C_{Bat})_{min} \leq C_{Bat}(t) \leq (C_{Bat})_{max} \qquad (4\text{-}11)$$

The maximum admissible battery capacity, $(C_{Bat})_{max}$, can be considered as the battery's nominal or rated capacity, $(C_{Bat})_n$, and the depth of discharge (DOD) may be used to define the minimum acceptable battery capacity (Diaf et al. 2007, Ai et al. 2003):

$$(C_{Bat})_{min} = DOD \times (C_{Bat})_n \ , \ (C_{Bat})_{max} = (C_{Bat})_n \qquad (4\text{-}12)$$

The DOD is usually about 30-50%; in this research, DOD was assumed to be 30% (Ai et al. 2003).

4.3.5 Objective function

Achieving a rational trade-off between a system's technically appealing characteristics and the associated costs requires an inclusive system cost estimate which includes many factors, such as the equipment cost, system longevity, and the interest rate (Wang and Singh 2008). The system's initial cost or capital investment (I_C), present worth of equipment replacement cost ($C(Rep)$), present worth of the system's maintenance and operation cost ($C(O\&M)$), and the annual costs of purchased electricity from the grid (C_{GPur}) constitute the main expenditures. Selling electricity to the grid (R_{GSel}) and selling obsolete equipment at the end of the system's operation time (present worth of elements salvage value ($R(Sal)$)) can create some revenue (González et al. 2015, Maleki et al. 2017, Nafeh 2011). The present worth of the total annual system cost ($/year) is presented by the following objective (fitness) function (F_C) (Nafeh 2011, Maleki et al. 2017, González et al. 2015, Wang and Singh 2009)

$$F_C = Minimize(\sum_i Cost_i - \sum_k Income_k) \tag{4-13}$$

$$F_C = \frac{\sum_{i=WT,PV,Bat}(I_{Ci}+C(O\&M)_i+C(Rep)_i-R(Sal)_i)}{N} + C_{GPur} - R_{GSel} = f(A_{PV}, A_{WT,SA}, C_{Bat}) \tag{4-14}$$

The total system cost is assumed to be a function of the total PV panel area (A_{PV}), the total wind turbine rotor swept area ($A_{WT,SA}$), and the battery storage capacity (C_{Bat}) (González et al. 2015, Nafeh 2011). A_{PV} could be limited to the maximum available area for PV installment and $A_{WT,SA}$ may be constrained according to the maximum number and

size of wind turbines that can be installed in the study area (Nafeh 2011). In addition, the allocated budget can be another restricting factor (Nafeh 2011). Instead of dividing the total cost by N (system lifetime) to evaluate the annualized cost, total cost may be multiplied by recovery factor (CRF) which is defined by Equation (4-15) (Maleki et al. 2015).

$$CRF = \frac{Annualized\ cost}{Total\ cost} = \frac{r(1+r)^N}{(1+r)^N-1} \tag{4-15}$$

r is the interest rate (Mohamed et al. 2016). The capital cost can be expressed by the following equation (González et al. 2015):

$$I_C = I_{C,PV} + I_{C,WT} + I_{C,Bat} = N_{PV} \cdot I_{PV} \cdot P_{PV,rat} + N_{WT} \cdot I_{WT} \cdot P_{WT,rat} + I_{Bat} \cdot C_{Bat} \tag{4-16}$$

where N_{PV} and N_{WT} are the number of PV modules, and the number of wind turbines (González et al. 2015). I_{PV}, I_{WT}, and I_{Bat} are the capital cost of PV panels in \$/kW, the capital cost of wind turbine in \$/kW, and the capital cost of battery storage in \$/kWh (González et al. 2015). $P_{PV,rat}$, $P_{WT,rat}$, and C_{BAT} are each panel's rated (nominal) power, each wind turbine's rated power, and the battery's capacity (González et al. 2015). The number of PV panels (N_{PV}) can be calculated by dividing the total PV area (A_{PV}) by one panel's area (A_{Panel}) (González et al. 2015):

$$N_{PV} = A_{PV}/A_{Panel} \tag{4-17}$$

Also, the number of wind turbines (N_{WT}) can be calculated by dividing the total swept area ($A_{WT,SA}$) by a single turbine's swept area (A_{SW1}) (González et al. 2015) :

$$N_{WT} = A_{WT,SA}/ A_{SW1} \tag{4-18}$$

It was assumed that the module's nominal maximum power under standard test conditions (STC) and the PV module's dimensions are 270W and 1658 × 992 mm,

respectively. Since 2014, the cost of battery storage has decreased approximately 50%, and is anticipated to be reduced by 11.4% annually until 2020 due to continued technology improvement and increased competition (Power Advisory LLC 2017). Average battery costs were less than US$230/kWh in 2016, a significant decrease from about US $1,000/kWh in 2010 (Stevens and Chung 2017). The present worth (discounted value) of each component's operation and maintenance cost after i years is calculated as (González et al. 2015, Nafeh 2011):

$$NPV_{O\&M} = \sum_{i=1}^{N} C_{(O\&M)k} \cdot \frac{(1+j)^i}{(1+r)^i} \tag{4-19}$$

where $C_{(O\&M)k}, j, r$ are, respectively, each component's current operation and maintenance cost value (\$/year), the annual (general) inflation rate, and the interest rate. k and N represent different system components and the system lifetime respectively (Nafeh 2011, González et al. 2015). The annual maintenance and operation cost is taken to be 0.5% of the wind turbine capital cost, 0.5% of PV system capital cost, and 0% of battery storage capital cost for these three components. PV systems require minimum maintenance to function (Wang and Singh 2009). It is assumed that the lifetime of PV panels and wind turbines is equal to the lifespan of the system (25 years), therefore they do not need to be refurbished or replaced over the operational lifetime of the system (Lantz et al. 2013, Nafeh 2011); thus only batteries need to be replaced. The total present worth of the capital and replacement costs of batteries is given by (Nafeh 2011, González et al. 2015, Wang and Singh 2009):

$$I_{C,Bat} + NPV_{Rep,Bat} = I_{Bat} \cdot C_{Bat} \cdot \sum_{x=1}^{X_{Bat}} \left(\frac{1+j_R}{1+r}\right)^{(x-1)\cdot L_{Bat}} \tag{4-20}$$

where X_{Bat}, j_R, and L_{Bat} are, respectively, the total number of batteries' replacement during system's lifespan, the inflation rate of the equipment acquisition cost which is not necessarily equal to the general inflation rate, and the battery lifetime (González et al. 2015, Nafeh 2011). X_{Bat} can be expressed as (Nafeh 2011):

$$X_{Bat} = int[N/L_{Bat}] \tag{4-21}$$

The present worth of PV panel's salvage value, NPV_{Sal-PV}, and the present worth of wind turbine salvage value, NPV_{Sal-WT}, are given by (Nafeh 2011):

$$NPV_{Sal-PV} = S_{PV} \cdot A_{PV} \cdot \frac{(1+j)^N}{(1+r)^N} \tag{4-22}$$

$$NPV_{Sal-WT} = S_{WT} \cdot A_{WT,SA} \cdot \frac{(1+j)^N}{(1+r)^N} \tag{4-23}$$

where S_{PV} and A_{PV} are the panels' salvage value per square meter ($/m^2) at present and total panel area, respectively (Nafeh 2011). S_{WT} and $A_{WT,SA}$ are turbine current salvage value ($/m^2) and the total wind turbine rotor swept area. The battery storage salvage value is estimated to be very low, and hence can be disregarded (Nafeh 2011, Wang and Singh 2009). It was presumed that the salvage price of a PV module is about 3% of its capital cost. Sometimes, decommissioning a wind farm at the end of its useful lifetime and reclamation may result in some of the investment not having economic worth due to the high costs of reclamation. The salvage price of a wind turbine was taken as 1% of its original capital cost. The cost of the inverter is ignored because it was not intended to optimize this component (Sharafi and ElMekkawy 2014).

4.3.6 Energy management and control strategy

When renewable energy generation is not sufficient to satisfy the load, the energy deficit will be provided by battery storage. If the demand is still not fully met, the remaining

deficit will be purchased from the grid (Ardakani et al. 2010). The power purchased from

the utility grid at time t, $P_{GPur}(t)$, can be expressed as (Xu et al. 2013):

$$P_{GPur}(t) = P_L(t) - [P_{WT}(t) + P_{PV}(t) + P_{Bat-dch}(t)] \tag{4-24}$$

When the renewable energy generation exceeds load demand, the excess energy is

first used to charge the battery storage up to the maximum permissible level, with the

remainder being fed directly into the utility grid (Xu et al. 2013). Thus the highest priority

for meeting the load demand is assigned to renewable electricity, while purchasing power

from the utility grid has the lowest priority in supplying power (Ardakani et al. 2010). The

power fed into the grid at any hour t, $P_{GSel}(t)$, can be expressed as (Xu et al. 2013):

$$P_{GSel}(t) = [P_{WT}(t) + P_{PV}(t)] - [P_L(t) + P_{Bat-ch}(t)] \tag{4-25}$$

where P_{WT}, P_{PV}, P_L, $P_{Bat-dch}$, and P_{Bat-ch} are, respectively, power generated by wind

turbine, power generated by PV, demand load, power taken from battery (discharge), and

power used to charge the battery. The annual cost of purchased electricity from the grid,

C_{GPur}, and the annual revenues from selling electricity to the grid, R_{GSel}, can be expressed

as (González et al. 2015, Wang and Singh 2009):

$$C_{GPur} = \sum_{t=1}^{T} P_{G,Pur}(t) \cdot \varphi(t) \tag{4-26}$$

$$R_{GSel} = \sum_{t=1}^{T} P_{G,sold}(t) \cdot \xi(t) \tag{4-27}$$

where φ (\$/kW), ξ (\$/kW), and T are the grid power price, the sale price of power supplied

to the grid, and the operation time interval (8760 hours = 1 year) (González et al. 2015).

The power purchased from the utility grid may be damped by the following constraints:

$$\sum_{t=1}^{T} P_{GPur}(t) \leq P_{GPur,max} \tag{4-28}$$

The maximum allowable power purchase from the utility grid is shown by $P_{GPur,max}$ (Ardakani et al. 2010).

Sometimes it is assumed that the total annual renewable electricity generated by a HRES should be equal to the total annual electricity demand (the design criterion is net annual balance) (González et al. 2015). Producing extra renewable energy and selling it to the grid may be undesirable due to additional cost and social unacceptability of installing more HRES equipment. Alsayed et al. used the total energy lost (TEL) indicator to minimize the extra renewable energy generation (Alsayed et al. 2013).

4.3.7 Renewable hybrid system reliability simulation

Reliability measures the system's ability to perform as intended during its life span, and evaluates the quality of the provided service in fluctuating load and weather conditions. Reliability analysis approximates the physical features of the system and utilizes mathematical modeling or simulation to manipulate the reliability factors (Wang and Singh 2008). Reliability analysis is an attempt to lessen the uncertainties and risks in power generation, and is taking a center stage in system planning. Uncertainty and intermittency of renewable sources of energy, in conjunction with unknown fluctuations of load and random system collapses, make reliability analysis complicated (Wang and Singh 2008).

Along with minimizing the total annual system cost, the system's reliability adequacy is evaluated by means of the "loss of power supply probability" (LPSP) concept which demonstrates the long-term average unserved load fragment for the energy supplier (hybrid system) (Nafeh 2011, Diaf et al. 2007). A zero LPSP indicates that the demand will always be met, while a LPSP equal to unity means that the demand will never be satisfied (Nafeh

2011, Xu et al. 2013). The LPSP_{max} (reliability threshold) is defined based on the energy prices and reliability desired to find a system with the lowest LPSP (Nafeh 2011). The system LPSP over the course of time span T is given by Equation (4-29) (Nafeh 2011, Xu et al. 2013, Mahesh and Sandhu 2017).

$$LPSP = \frac{\sum_{t=1}^{T} LPS(t)}{\sum_{t=1}^{T} E_L(t)} = \sum_{t=1}^{T} \frac{E_L(t) - E_{supplied}(t)}{\sum_{t=1}^{T} E_L(t)} = \frac{\sum_{t=1}^{T}[E_L(t) - (E_{PV}(t) + E_{WG}(t) + C_{Bat}(t))]}{\sum_{t=1}^{T} E_L(t)} \qquad (4\text{-}29)$$

where $E_{supplied}(t)$ is the total energy provided by the system at any time t. $\text{LPSP} \leq \lambda_L$ where λ_L is the load's permissible LPSP or the tolerance limit of the system reliability (LPSP_{max}) (Xu et al. 2013, Mahesh and Sandhu 2017, Nafeh 2011). The "loss of power supply" for hour t is illustrated by $\text{LPS}(t)$ which represents the insufficiency in renewable energy generated by the hybrid system and available stored energy in batteries to meet the load in hour t, $E_L(t)$ (Nafeh 2011). T is the system's operating time (8760 hours) (Xu et al. 2013). Several possible operational situations for a hybrid grid-connected renewable energy system were examined to explore the behaviour of the proposed optimization method.

4.3.8 Optimization strategy and design constraints

The optimum size of the system's components will be selected from among a set of finite samples by an iterative approach through minimizing the total annual cost (Xu et al. 2013, Maleki et al. 2017). In a multi-objective problem solving procedure, a specific objective is defined as the main objective and others are considered as constraints and conditions to solve the problem and achieve the main objective (Mahesh and Sandhu 2017). Here, minimizing the total annual cost of the hybrid system is the main objective, while the minimization of the amount of purchased electricity and unmet demand, and maximization of the amount of avoided CO_2 emissions are considered as necessary complementary

conditions. Hence, to solve the optimization problem, all the aforementioned constraints listed below should be satisfied:

$$\text{LPSP} \leq \lambda_L, \ (C_{bat})_{min} \leq C_{bat}(t) \leq (C_{bat})_{max}, \ \sum_{t=1}^{T} P_{GP}(t) \leq P_{GP,max}$$

$$A_{PV,min} \leq A_{PV} \leq A_{PV,max}, \quad A_{WT,SA,min} \leq A_{WT,SA} \leq A_{WT,SA,max} \tag{4-30}$$

4.3.8.1 Particle swarm metaheuristic optimization (PSO) method

The particle swarm optimization technique was adopted for this non-linear, multidimensional objective function optimization. Kennedy and Eberhart devised particle swarm optimization in 1995 (Eberhart and Kennedy 1995). Showing astonishing promise in a variety of applications including power systems and solving large-scale nonlinear optimization problems, this evolutionary stochastic population-based heuristic optimization method operates so as to imitate animals' social behaviour and movements, for example bird flocks seeking grain (forage) or schools of fish (Maleki et al. 2017, Poli et al. 2007, Del Valle et al. 2008). Unlike other methods that utilize the gradient of an objective function, direct operation in a continuous real number search space is the main feature of PSO (Khare and Rangnekar 2013). In light of the flexibility of PSO in managing numerous qualitative restrictions, in power system economic dispatch (ED) studies, the performance of PSO's surpasses that of the majority of heuristic and mathematical approaches (Del Valle et al. 2008). For instance, designing a residential photovoltaic-wind turbine-fuel cell-solar thermal collector system, Maleki et al. (2017) demonstrated that PSO outperforms the genetic algorithm. Methaheuristic methods including PSO are recommended for designing HRESs owing to their provision of a rigorous search of probable solutions space (Mohammed et al. 2016).

In PSO, a random search space for the defined function is created and several particles (simple entities, population members, or possible solutions) are placed in it, and which can move inside the space with given velocities (random particles with random positions and random velocities) (Poli et al. 2007, Del Valle et al. 2008, Khare and Rangnekar 2013). The objective function is evaluated for each of the particles at the particles' present position, while in each iteration, each particle's position is updated based on its own and its neighbours' previous values (Poli et al. 2007, Del Valle et al. 2008). In this approach the particles possess memory, exchange information, and move around their neighbours' and their own best found positions randomly (Poli et al. 2007). Essentially, a potential solution is a point (particle) that flies in the search space while having access and responding to information from other particles (Khare and Rangnekar 2013).

The position of each particle in multidimensional search space, $x_i \in R^n$, and its velocity, $v_i \in R^n$, are determined by Equations (4-31) and (4-32) (Del Valle et al. 2008, Maleki et al. 2017). The position of each particle changes based on randomly generated velocities.

$$v_i^{k+1} = \omega . v_i^k + \varphi_1 . r_1 . \left(p_{best,i}^k - x_i^k \right) + \varphi_2 . r_2 \left(g_{best}^k - x_i^k \right) \tag{4-31}$$

$$x_i^{k+1} = x_i^k + v_i^{k+1} \tag{4-32}$$

where $x_i = [x_{i1}, x_{i2}, x_{i3}, \dots, x_{id}]$, $v_i = [v_{i1}, v_{i2}, v_{i3}, \dots, v_{id}]$, and 1, 2, 3, …, d illustrate the possible dimensions for $i = 1, 2, 3, \dots, i$ particles having position x and velocity v (Khare and Rangnekar 2013). φ_1 and φ_2 are acceleration constants or learning factors (positive numbers representing cognitive and social parameters) and r_1 and r_2 are two uniformly distributed random numbers between 0 and 1 (Del Valle et al. 2008, Maleki et al. 2017). The parameters $p_{best,i}$ and g_{best} are the best individual particle position and the best global

swarm position respectively (Maleki et al. 2017). The parameter k represents the present iteration and ω is the inertia weight that can be either a fixed value or a dynamically changing value (Khare and Rangnekar 2013, Del Valle et al. 2008).

The first component of the velocity update equation, Equation (4-31), demonstrates the particle's inclination to move in its current direction and denotes inertia momentum or habit. The second component of v_i^{k+1} denotes memory or self-knowledge and shows the tendency of each particle towards the best position achieved by the particle so far. Finally, the third component of v_i^{k+1} illustrates the particles' urge towards the best position achieved by all particles (Del Valle et al. 2008). Based on this stochastic mechanism, each particle searches new areas to find the best position while it tries to avoid being trapped in any local optima (Jahanbani and Riahy 2011). Particles that pass the boundaries of the search space are returned to their previous position.

Here, each particle has three dimensions which express the capacity of the components. The viability of each particle is examined by simultaneous simulation of fitness function and constraints. The operation of each particle (each configuration of HRESs) is modeled over one year using hourly climate data. The annual LPSP and CO_2 emissions are evaluated for the particle; subsequently, the objective function will be assessed for particles with desirable LPSP and CO_2 emissions in the optimization process. If the cessation criteria are not satisfied, particles are updated and their performance and adequacy reevaluated. The cycle is stopped when tolerance criteria is fulfilled (Figure 4-2).

The following alternative modified version of PSO that proposes a constriction coefficient (χ) can also be used in order to improve the performance of the algorithm (Del Valle et al. 2008, Shi 2001):

$$v_i^{k+1} = \chi . [v_i^k + \varphi_1 . r_1 . \left(p_{best,i}^k - x_i^k\right) + \varphi_2 . r_2\left(g_{best}^k - x_i^k\right)] \tag{4-33}$$

$$\chi = \frac{2}{\left|2-\varphi-\sqrt{\varphi^2-4\varphi}\right|} \qquad \varphi_1 + \varphi_2 = \varphi > 4.0 \tag{4-34}$$

The typical value of φ is 4.1 which leads to a constant χ of 0.729 (Shi 2001).
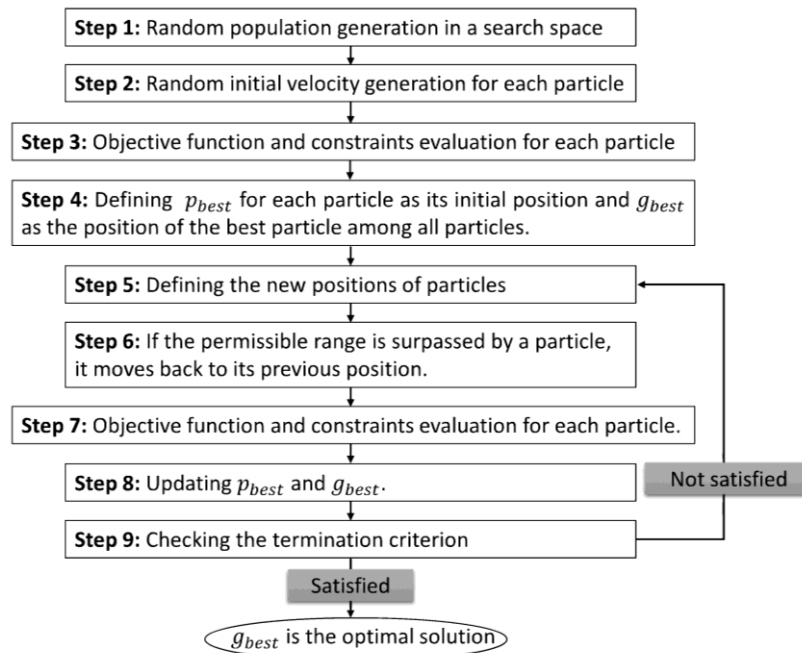
Figure 4-2: Executed steps in PSO algorithm (Maleki et al. 2017).

The size of population and the iteration numbers for each particle influence the method's performance (Maleki et al. 2017). The population size is usually determined empirically, and generally lies between 20 and 50 particles (Poli et al. 2007, Khare and Rangnekar 2013).

4.4 Results and discussion

HRES systems are designed based on the historical University of Lethbridge electricity consumption. This medium-sized institution is located on the west side of the City of Lethbridge, southern Alberta, Canada (49° 40' 38" N, 112° 51' 51" W). Long-term hourly solar radiation, wind speed, and air temperature data for a nearby station, Lethbridge CDA (49° 42' 0" N, 112° 46' 60" W) was obtained from the Alberta Climate Information Service (ACIS) (http://agriculture.alberta.ca/acis, 2016). The university utility service supplied the university electricity consumption data. The simulations are carried out utilizing the meteorological data and load profile over the course of one year (year 2014) illustrated in Figure 4-3, Figure 4-4, and Figure 4-5. The utilization of hourly time-series data over one year assists us to capture the daily and seasonal variations of the weather data and demand and also, to consider the stochastic nature and intermittency of the renewable sources. The smallest potential of wind and the second smallest potential of PV electricity, but the highest electricity consumption during 2010 to 2014 occurred in 2014.
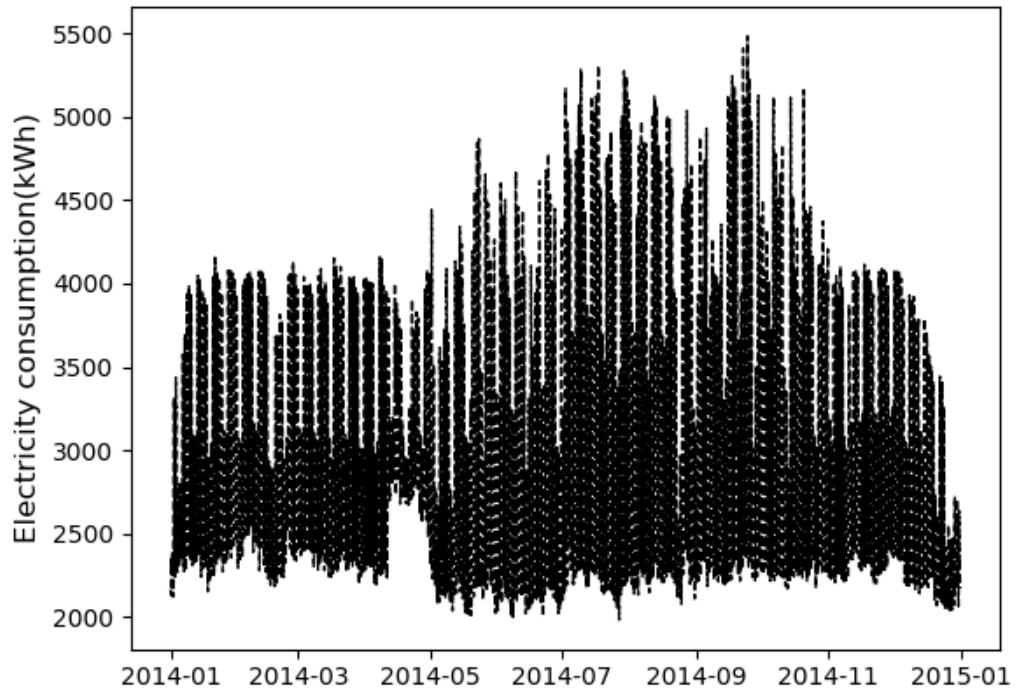
Figure 4-3: Hourly electricity load over one year.

The average wind speed at 10m elevation is 15.2 kph and the max wind speed is 63.6 kph. The maximum load is 5484 kWh/h which happened in September 24 (2014) at 3:00 pm (Figure 4-6). In all months, the maximum electricity consumption occurred at noon or in the afternoon (12:00 pm to 16:00 pm). The total annual electricity consumption was about 27,148 MWh.
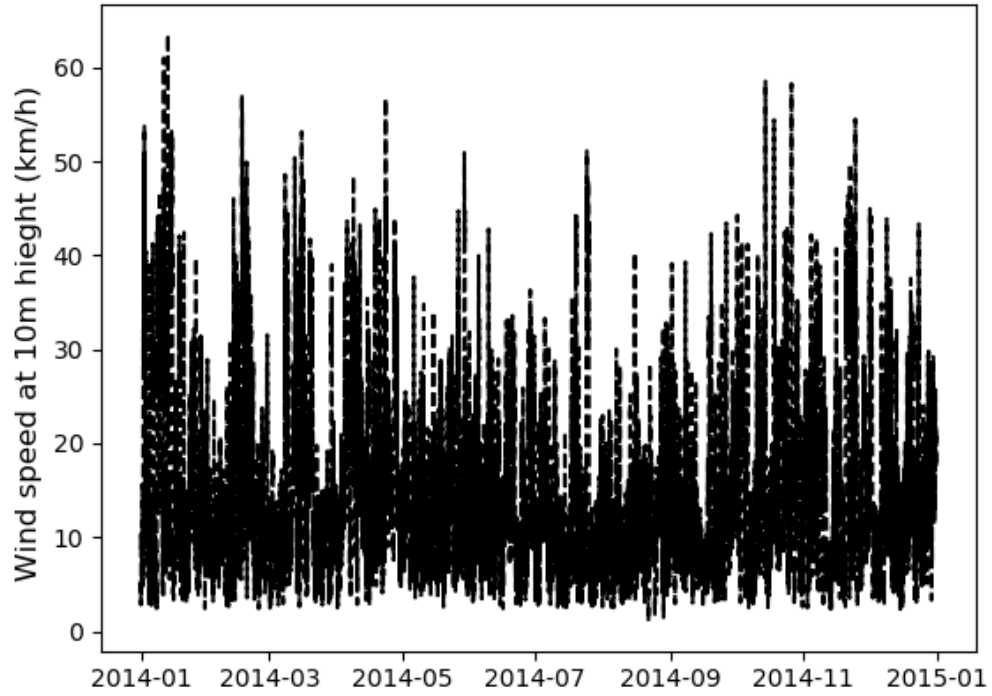
Figure 4-4: Hourly wind speed data over one year.
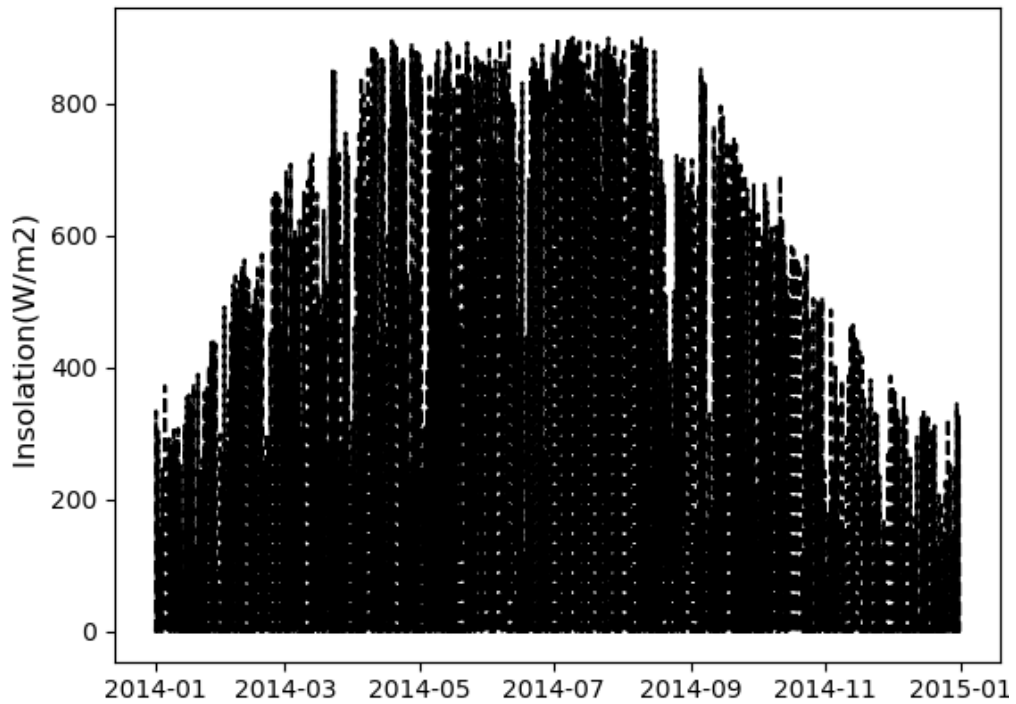
Figure 4-5: Hourly solar radiation data over one year.

The electricity consumption pattern for some weekdays and weekends during November, April, and July are illustrated in Figure 4-7, Figure 4-8, and Figure 4-9. The

load profile of both weekdays and weekends are sharply peaked during afternoon and evening time. In November (Figure 4-7), the electricity consumption during 24 hour weekdays was about 23% more on average than that over 24 hour weekends, while in July, this difference was about 25% on average (Figure 4-9). Moreover, in November, the electricity demand during weekday daytime (8:00 am to 5:00 pm) was 33% higher on average than that over weekday nighttime (6:00 pm to 7:00 am) (Figure 4-7). However, during weekend daytime in November, the demand was on average 18% more than that over nighttime (Figure 4-7). In July, the electricity usage during weekday daytime (6:00 am to 10:00 pm) was about 420% larger than that over weekday nighttime (23:00 pm to 5:00 am) on average, while for weekends this number was about 320%. The proposed HRES should satisfy this high fluctuating electricity usage in a reliable way. Moreover, fluctuations of solar and wind energy make it more critical to design a satisfactory HRES that fulfils the demand. Generally, wind speed, solar insolation, load profile, and cost of the backup energy supplier and unit cost of grid electricity govern a hybrid system design (Ekren and Ekren 2009).
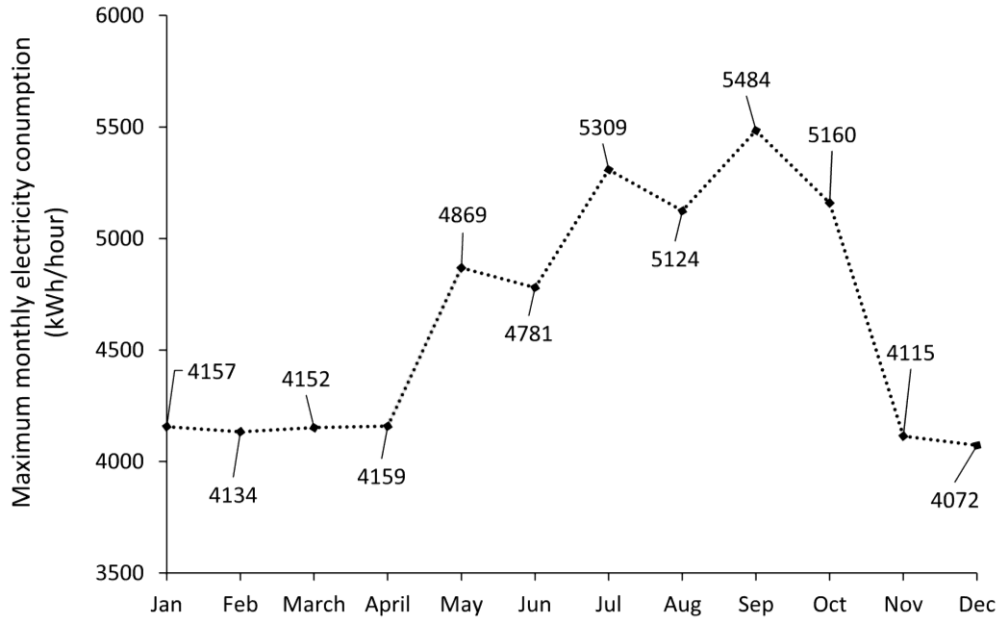
Figure 4-6: Maximum monthly hourly electricity consumption (kWh/hour).
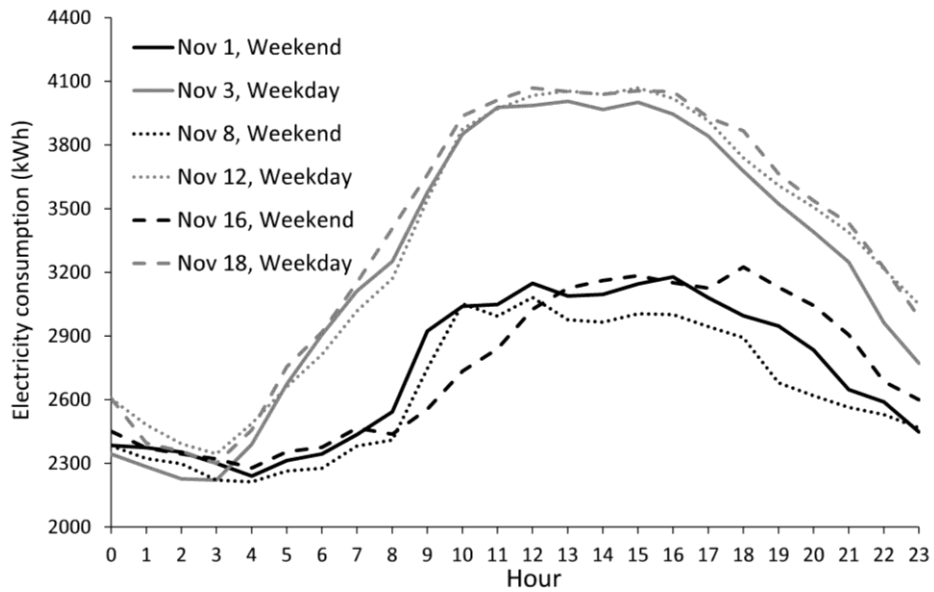
Figure 4-7: Electricity consumption pattern during some weekdays and weekends in November.
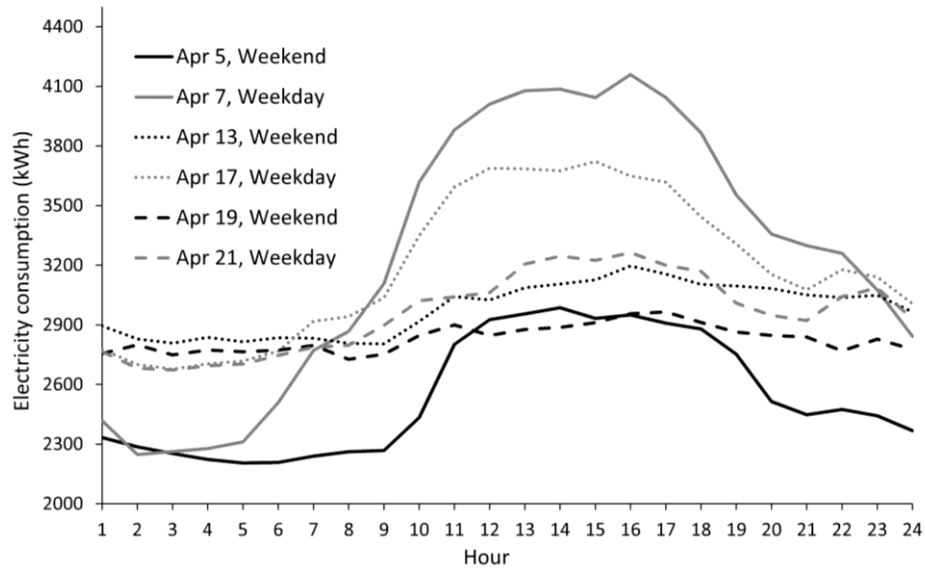
Figure 4-8: Electricity consumption pattern during some weekdays and weekends in April.
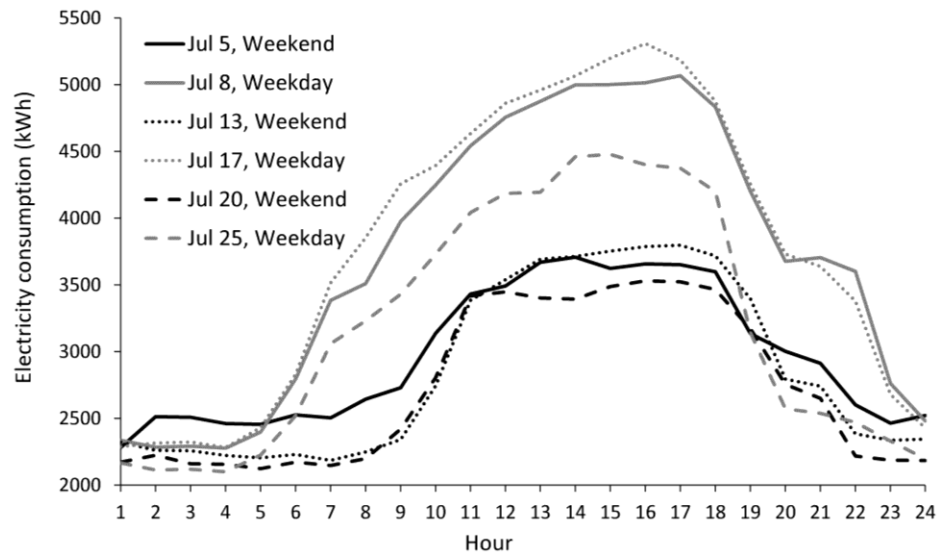
Figure 4-9: Electricity consumption pattern during some weekdays and weekends in July.

4.4.1 PSO factors

Resolving large-scale multi-objective complex nonlinear optimization problems usually encompasses consideration of incompatible, contradictory, and conflicting design objectives (Ranjithan et al. 2001). The proposed PSO optimization methodology that can

reasonably simulate and integrate the nonlinear characteristics of the renewable technologies, the variable nature of renewable energy sources, and the dynamic and complex interaction between load and stochastic variations in generated renewable energy, is implemented in Python. In multi-objective optimization, a set of compromised and satisfactory solutions known as non-dominant or non-inferior solutions can be discovered by examining objectives which conflict in the sense that improving performance with respect to one may worsen another (Sharafi and ElMekkawy 2014, Khalkhali et al. 2010). Hence, a single optimum solution that can maximally satisfy all objectives may not be found in these problems (Khalkhali et al. 2010). Exploring a set of solutions is a viable empirical way of resolving such multiple-objective optimization problems (Fadaee and Radzi 2012). In the proposed multi-objective method, the annualized cost of systems is to be minimized while carbon footprint and reliability indicator of the systems are concurrently considered as restriction limits. Changing these constraints can reveal various non-inferior solutions; this method is known as an ε-constraint method, in which one objective is selected to be optimized while the others are treated as bound constraints (Sharafi and ElMekkawy 2014).

The population of particles in PSO was set to 100 and each particle was characterized by three dimensions: the swept area of wind turbines, the PV area, and the battery capacity. Based on the extent of our search space, ω, φ_1, and φ_2 were set to 0.03, 0.05, and 0.5. These values confine the movement of the particles while allowing them to search a larger area so as not to miss best solutions. These values were determined by a trial-and-error approach in setting initial conditions in multiple runs of the code. Appropriate selection of PSO parameters reduces the convergence time of the particles. Moreover, an allowable

convergence tolerance can be defined, based on the application, to shorten the running time (the minimal thresholds change during iteration). The standard deviation, an indicator of the spread (variability) of a distribution, for the PV, wind, and battery elements was used to terminate the optimization process (SciPy.org 2018). Figure 4-10 illustrates the overall simulation and optimization methodology.
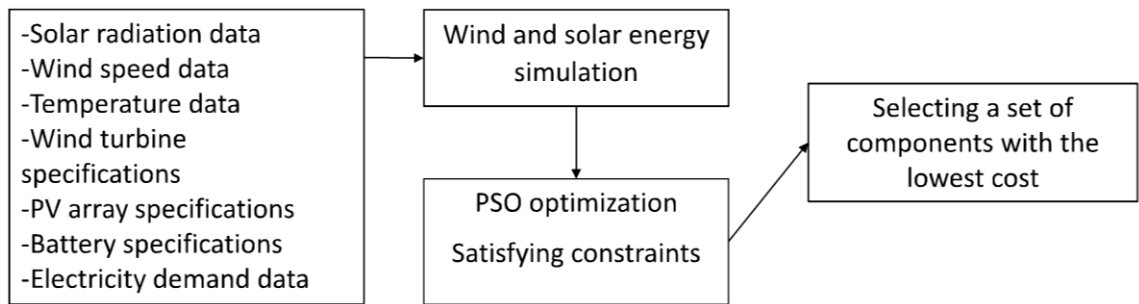
Figure 4-10: Overall simulation and optimization procedure flowchart.

4.4.2 System factors

The data utilized in the modeling is illustrated in Table 4-2.

Table 4-2: Data used in the proposed simulation and optimization.

Variable	Index	Value	Source
System lifetime	N	25 years	(González et al. 2015, Sharafi and ElMekkawy 2014)
Battery lifetime	n_{Bat}	10	(Wang and Singh 2009, Jahanbani and Riahy 2011)
Wind turbine lifetime	n_{WT}	25	
Interest rate	r	2%	(MacKinnon and Mintz 2017)
PV module lifetime	n_{PV}	25	
Inflation rate	j	1.5%	
Capital cost of large-scale wind turbine installation		2.0 \$/W (505.6 \$/m^2)	(Doluweera et al. 2018)
Capital cost of large-scale PV installation		2.0 \$/W (328.3 \$/m^2)	(Doluweera et al. 2018)
Capital cost of battery	I_{Bat}	350 \$/kWh	
O&M cost of wind turbine		11 \$/kW/year (2.8 \$/m^2/year)	(Wang and Singh 2009)
O&M cost of fixed mount PV		10 \$/kW/year (1.64 \$/m^2/year)	
O&M cost of battery		0	

Variable	Index	Value	Source
Salvage value of PV		10 $/m^2 (0.03 capital cost)	(Wang and Singh 2009)
Salvage value of wind turbine		5.1 $/m^2 (0.01 capital cost)	
Salvage value of battery		0	
Electricity purchase price	φ ($/kW)	0.135	
Electricity sell price	ξ ($/kW)	0.065	
Wind turbine efficiency	η_{WT}	90%	(Duffie and Beckman 2013)
Wind turbine power coefficient	C_p	0.42	
PV efficiency	$\eta_{T_{ref}}$	15%	
Battery efficiency	η_{Bat}	82%	(Wang and Singh 2009)
Battery self-discharge rate	σ	1%	(Mahesh and Sandhu 2017)

4.4.3 Simulation and optimization results

4.4.3.1 PV-wind turbine-battery system

Various renewable energy reliability levels were explored and the overall optimization method and HRES design algorithm behaviour were scrutinized. Proper design of generation and storage components aims to reliably supply the annual demand and decrease a consumer's total yearly cost. LPSP is a statistical indicator and a fundamental index for adequacy assessment of generating systems that incorporates the intermittent nature of the renewable energy resources and the electricity load (Mohammed et al. 2016, Wang and Singh 2009). Determining a mix of components that provide a desired LPSP is one of the important targets of the optimization (Abbes et al. 2014). Employing the explained method and the defined parameters, the HRES is designed for different LPSP values (Table 4-3, Figure 4-11). Results demonstrate the trade off and correlations among system reliability values and system component sizes in conjunction with annual costs and avoided GHG emissions. Given the random nature of the system generation in search space, there is a slight difference among results of different optimization runs. The size of the system components are limited by the available area (and

may be available budget). The goal of this optimization is to find a reliable system that satisfies all constraints including the size limitations. LPSP is selected based on these limitations and reliability concerns. Various thresholds for LPSP have been considered in different studies, including 5%, 7%, 8%, and 9% (Abbes et al. 2014, Borhanazad et al. 2014). An acceptable LPSP for an on-grid system may be 2% (Athari and Ardehali 2016). The capital investment required for constructing a HRES is governed by the chosen LPSP. A set of non-inferior solutions are presented in Table 4-3. These solutions illustrate various systems with minimum annualized cost for different LPSP values.

Capacity factors are common measures for comparing power systems (Schmalensee 2015). Capacity factor illustrates the percentage of installed capacity that is utilized to produce electricity and serve a load profile, and for a wind turbine is the ratio of average energy yield to its rated capacity[4] (Abed and El-Mallah 1997, Alberta Electric System Operator 2018). The capacity factor of a PV system compares the energy production of the system with an ideal system's output with same rated capacity under constant peak irradiance (1,000 W/m^2) (Schmalensee 2015). In sum, capacity factor demonstrates, over the course of a year, how much energy a power generating plant has produced on average relative to its rated capacity (Weis et al. 2010). Average wind capacity factor in southern Alberta over 2017 was 35%, however it can be as high as 40% (Doluweera et al. 2018, Alberta Electric System Operator 2018). Capacity factor of fixed mounted PV systems ranges from 10-20% in different provinces, and in Alberta, average capacity factor for fixed PV systems is about 15% (Doluweera et al. 2018). Hence, wind turbines are more efficient

---

[4] Rated capacity or nominal capacity is the capacity provided by manufacturers at nominal (standard) operating conditions ((Sauer et al. 1999).

in generating energy. The optimization algorithm tends to use the wind and battery resources more than the solar resource especially for higher LPSP values when the renewable energy contribution is lower illustrating that the optimization algorithm has prioritized the wind resource (Table 4-3). The cost of the energy produced by the PV and wind turbine and the availability of renewable sources are other important factors here.

By decreasing LPSP from 30% to 0.1%, A_{PV} surged about 3 times while $A_{WT,SA}$ increased only 1.2 times (Table 4-3). Results illustrate that systems with lower LPSP are larger and need larger available areas. Systems with lower LPSP values consist of nearly the maximal admissible amount of wind turbine swept area ($A_{WT,SA,max}$= 24,000 m^2) and battery capacity (1,500 kWh) due to the absence of the sun during night, the turbines higher capacity factor, and battery's low capital cost (Table 4-3). In addition, the ratio of sold power to purchase power rises when the dimension of the system increases or LPSP decreases (Figure 4-11). This ratio for a HRES with an LPSP equal to 0.1% is about 30% more than that of a HRES with a LPSP of 30%, notwithstanding that the first system must serve more load. Avoided GHG emissions for each case was calculated based on the net purchased electricity, which is the difference between purchased electricity and sold electricity. The amount of electricity that is not purchased (because of renewable energy production and compared with the base case) is calculated and the ratio of this value against the base case (no renewables) purchased electricity is used as the avoided GHG emissions. By decreasing LPSP, the amount of purchased electricity decreases and the amount of sold electricity increases.

Table 4-3: Designed HRES with different LPSP values.

	LPSP	A_{PV}(m²)	$A_{WT,SA}$(m²)	C_{BAT}(kWh)	Purchased power (MWh)	Sold power (MWh)	Avoided grid electricity [a] (MWh)	Avoided GHG emissions [c] (%)
1	30%	8,619	18,297	1,015	16,289	2,712	13,751	50
2	25%	13,981	18,248	1,015	15,387	3,049	14,811	55
3	20%	12,849	19,370	1,223	15,287	3,462	15,323	57
4	15%	14,242	20,247	1,290	14,856	3,980	16,272	60
5	10%	17,275	21,295	1,250	14,166	4,757	17,740	65
6	5%	18,783	22,243	1,298	13,745	5,364	18,768	69
7	1%	19,213	23,238	1,346	13,490	5,914	19,572	72
8	0.1%	25,065	22,066	1,257	12,884	5,873	20,138	75

a: Avoided grid electricity = (total consumption [b] - (purchased power - sold power)).

b: Total electricity consumption = 27,148 MWh.

c: Avoided GHG emissions compared with base case (no renewables) = Avoided grid electricity / total electricity consumption.
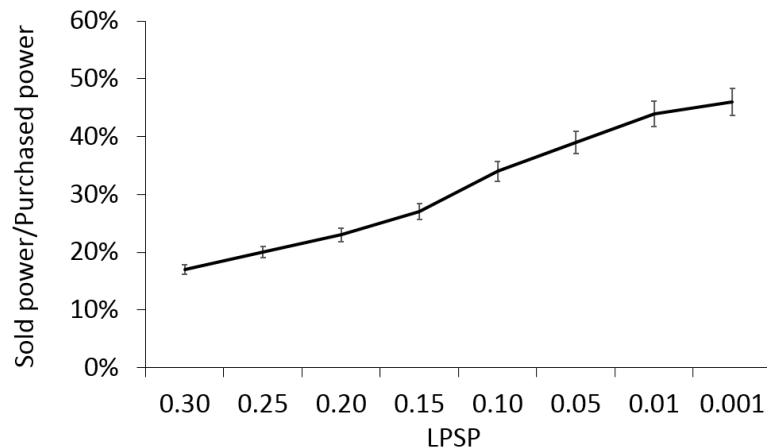
Figure 4-11: Ratio of sold renewable energy power to purchased utility grid power for systems presented in Table 4-3.

The annual cost (2014) for purchasing grid electricity when there is no HRES (base case) was about $3,665,000. All the optimum systems (Table 4-3) have an annualized cost less than the base case since they compensate a significant part of the demand and are able to sell a considerable amount of energy. Energy generated by a HRES creates a revenue stream over the system's lifespan. It is worth mentioning that the renewable electricity sold price is assumed to be less than half of the grid electricity purchase price (Table 4-2). The

annualized and capital cost of systems presented in Table 4-3 are depicted in Figure 4-12. A system with a LPSP of 5% has about 34% lower annual cost than the base case, which is a significant cost reduction (Figure 4-12). This yearly cost reduction for a HRES with a LPSP of 0.1% is about 36%.
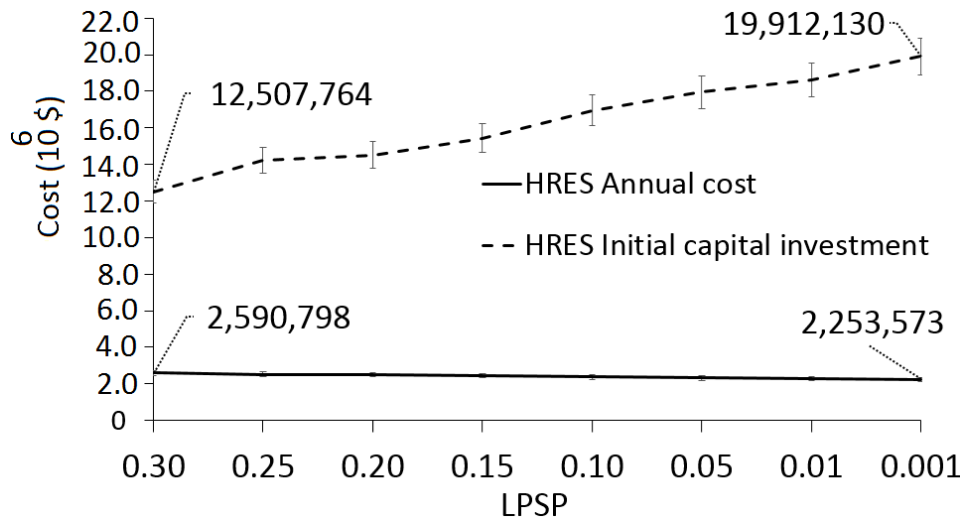
Figure 4-12: Capital cast and annual cost of HRES with different LPSP values and different avoided GHG emissions.

Appreciable cost abatement occurs when we increase the system's ability to supply demand, thus reducing the amount of purchased power. By decreasing LPSP from 30% to 0.1%, the annual cost of HRES declines by 13% taking into account the difference in the sold power to purchased power ratio (Figure 4-12). The designed systems possess a PV panel area not larger than 30,000 m^2, a wind turbine swept area of less than 24,000 m^2, and a battery storage capacity smaller than 1,500 kWh (Table 4-3). Finding solutions with small sizes could be a desirable target for the optimization due to their lower capital cost, however, larger systems with higher initial investments could have lower annualized costs. Based on the identified wind turbine swept area and PV panel area, the number of a specific turbine and number of PV panels can be determined (Nafeh 2011). According to these

results, a grid-tied HRES can be economically favourable; however, the capital investment may be significant. The initial investment of a HRES with an LPSP of 0.1% is 60% greater than that of a system with a LPSP of 30%, taking into account their different sold to purchase power ratio (Figure 4-12, Figure 4-11).

The amount of power purchased from the utility grid which is presumed to be fossil fuel-based may fall inside a determined range (Wang and Singh 2009). The dynamic and multi-dimensional interaction among the renewable energy resources, their cost, the cost of grid power, the efficiency of various energy sources, and the availability of energy sources makes it hard to find the best solution. Therefore, in grid-linked systems, imposing a limitation on the amount of purchased electricity may help the algorithm to find systems that produce more renewable energy, buy less conventional electricity, and probably have less annualized cost. However, the high capital investment of these systems may be limited by the available budget, while their required area is limited by the available area restrictions. Furthermore, there is a trade-off between LPSP and the amount of purchased electricity, meaning that decreasing LPSP reduces the amount of purchased electricity. Optimization is a process of reconciling conflicting goals. Solving the problem for different situations and targets may assist the algorithm to find the most desirable solution. Moreover, restricting the amount of purchased electricity may be used as a tool to design more carbon-neutral systems. Generally, systems with lower LPSP have lower annual cost, consist of larger components, and produce and sell a greater amount of energy (Table 4-3). Hence, lower LPSP means greater reduction in carbon footprint, which is a favourable outcome.

Avoided GHG emissions for each case was calculated based on the net purchased electricity, which is the difference between purchased electricity and sold electricity (Table 4-3). By replacing fossil fuel based grid electricity, the designed systems can reduce the carbon footprint more than 75%, which is a desirable environmental achievement. The main goal of renewable energy development is to reduce GHG emissions. Moreover, the overall consumers' electricity costs over the long term will also significantly decline with the help of renewable energy systems. In the proposed optimisation technique, a limitation on purchased electricity along with other constraints can also be used to confine the systems' carbon footprint and attain reliability targets concurrently. For instance, limiting the purchased power to 45% of the total demand, different systems can be designed with different amounts of avoided CO_2 emissions. Imposing this limitation could reduce CO_2 footprint by about 79% for an LPSP equal to 4% compared with the base case, while this index for a system with an LPSP of 1% and purchased power to demand ratio of about 50% is 7% lower (Table 4-3, Table 4-4). With this limitation, the capital investment of a system with an LPSP of 4% (Table 4-4) is 17% greater than that of a system with an LPSP of 1% and a purchased power to demand ratio of about 50%, however the annualized cost of the second system is about 3% more (Table 4-3, Figure 4-12). For more reduction in CO_2 emissions, larger systems are required. Results presented in Table 4-3 and Table 4-4 illustrate that systems with larger reduction in CO_2 emissions have lower LPSP values and higher capital investments. The GHG emission reduction goal leads the algorithm to arrive at systems with larger wind and solar elements, lower battery capacity, and therefore, higher initial investments (Table 4-4).

Table 4-4: Designed HRES with a ratio of power purchased to total demand of 45%.

LPSP	$A_{PV}(\mathrm{m^2})$	$A_{WT,SA}(\mathrm{m^2})$	$C_{BAT}(\mathrm{kWh})$	Capital investment ($)	Avoided GHG emissions (%)
7%	34,758	20,196	583	21,905,055	78
4%	32,490	21,386	688	21,803,585	79
2.5%	33,558	20,480	868	21,755,492	78
0.6%	32,187	21,223	942	21,709,873	78

The scattergrams of generated 3-dimensional particles for an optimization run are depicted in Figure 4-13. After moving around, the particles will converge to the best found solution without getting trapped in a local minima (Figure 4-14). The standard deviation of PV area dimension (STD) of the particles that illustrates how particles gradually discover the optimum or near optimum solution is demonstrated in Figure 4-15. The behaviour of the proposed optimization procedure has been examined for many different LPSP and CO_2 emission targets.
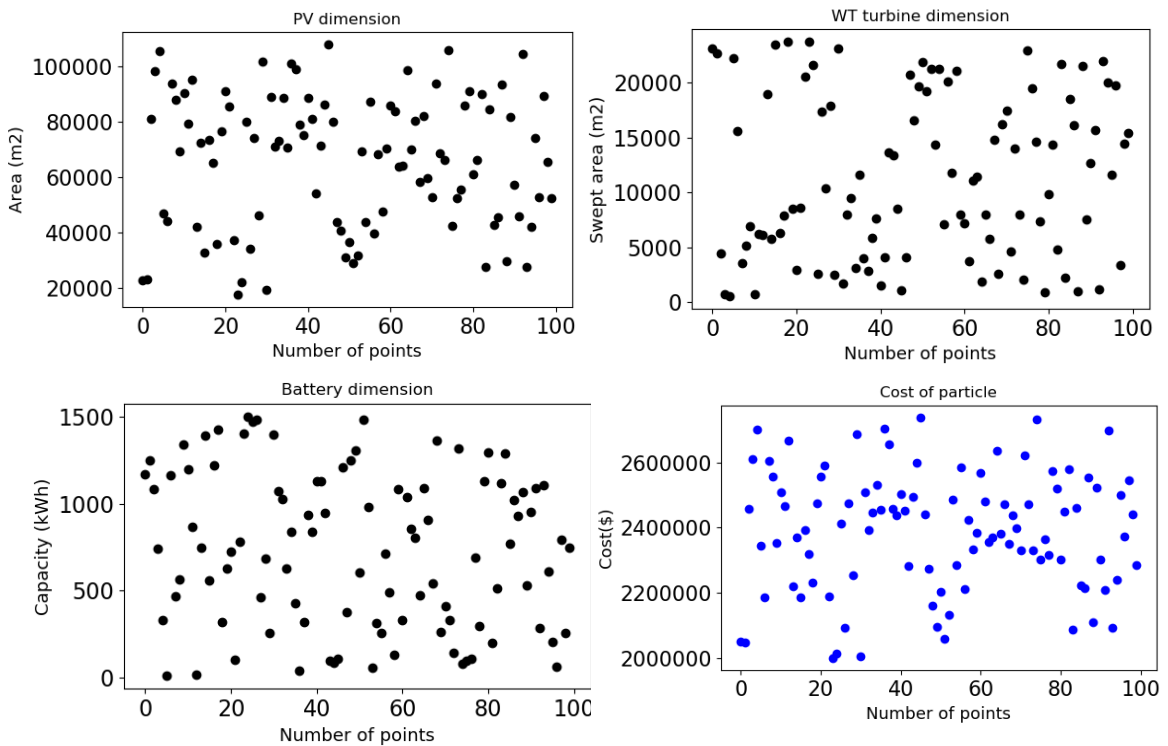
Figure 4-13: The initial population generated in search area in an optimization process.
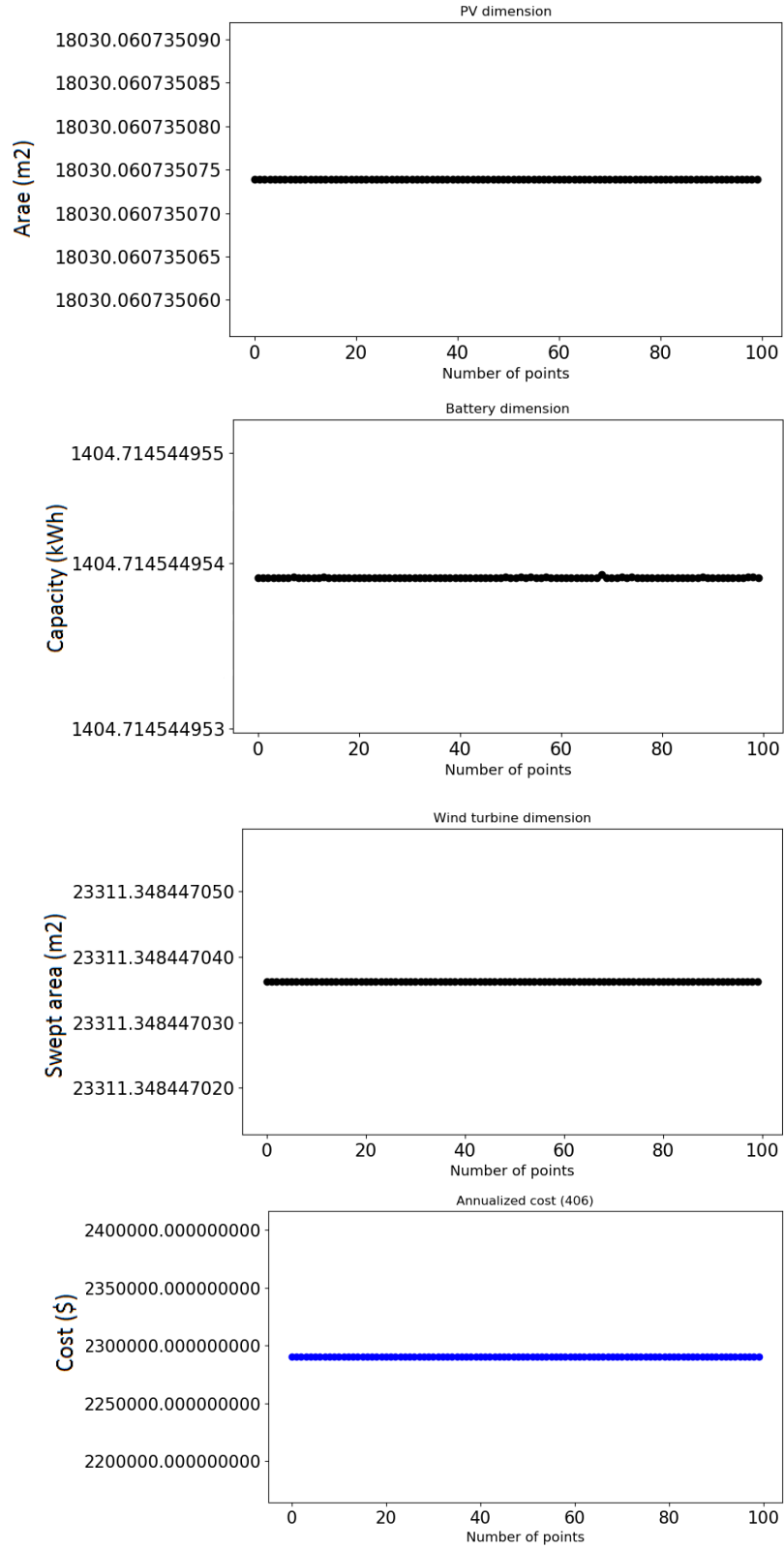
Figure 4-14: Convergence of generated particles.
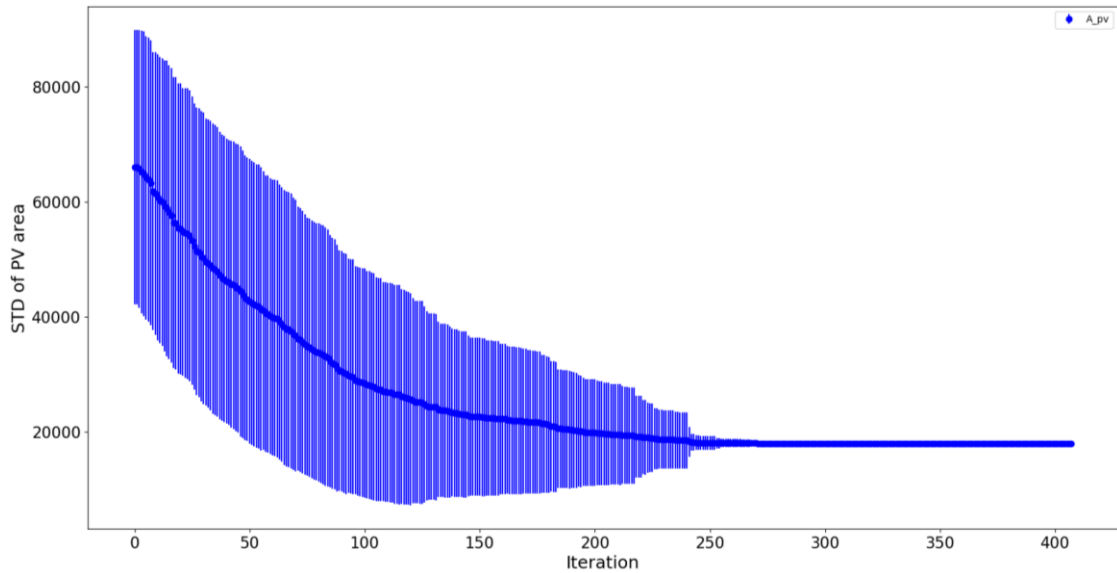
Figure 4-15: Standard deviation of PV area dimension of the particles.

The operation and maintenance cost of the renewable systems is an essential factor that is reflected in the annualized cost. Figure 4-16 illustrates the total operation and maintenance cost variation of the presented solutions in Table 4-3. The operation and maintenance cost of systems has a reverse relationship with the LPSP value, and by decreasing LPSP from 30% to 0.1%, the cost increases by about 58%.
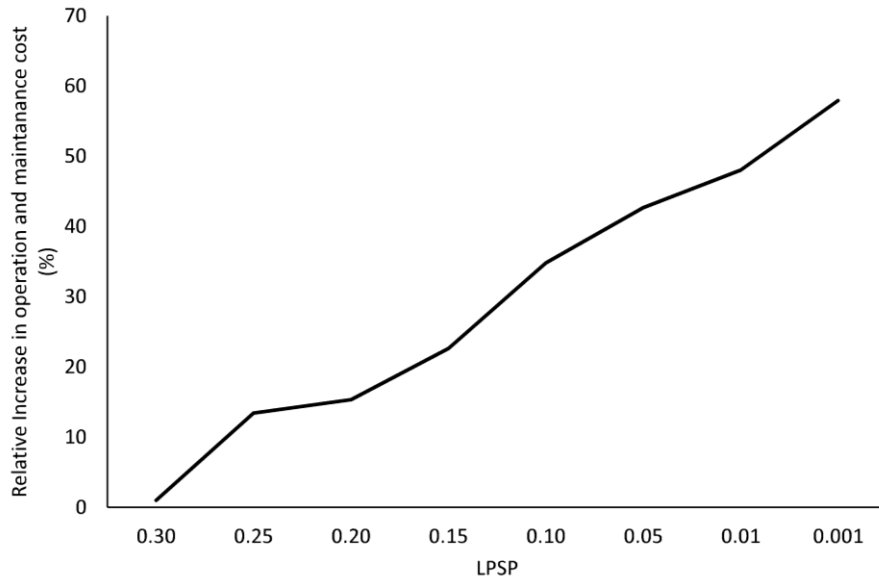
Figure 4-16: Relative increase in operation and maintenance cost of systems with various LPSP values.

4.4.3.2 PV-battery system

Utilizing a single renewable technology, especially when the energy demand is high, leads to an excessive system cost with a low reliability (Chauhan and Saini 2014). Some non-dominated solutions are presented in Table 4-5. Compared with PV-wind turbine-battery options (Table 4-3), obtaining an LPSP of about 5% means that the annual cost will increase by 30% approximately, however, the capital investment surges by about 60% (Figure 4-12, Table 4-5, and Figure 4-17) . The ratio of the purchased grid electricity to the total demand for the sized systems illustrated in Table 4-5 ranges from 61% to 66%. As we can see, utilizing the PV technology solely is not as efficient and economically viable as employing wind turbine and PV concurrently. However, the annual costs of the proposed PV-battery options are lower than that of the base case.

Table 4-5: Designed PV, battery systems with various LPSP values.

LPSP	A_{PV}(m²)	$A_{WT,SA}$(m²)	C_{BAT}(kWh)	Annual cost ($)
30%	58,001	0	1,438	3,085,776
20%	66,463	0	1,496	3,042,781
17%	70,578	0	1,411	3,022,157
10%	78,182	0	1,446	2,990,629
5%	84,990	0	1,347	2,962,752
1%	86,966	0	1,485	2,958,100
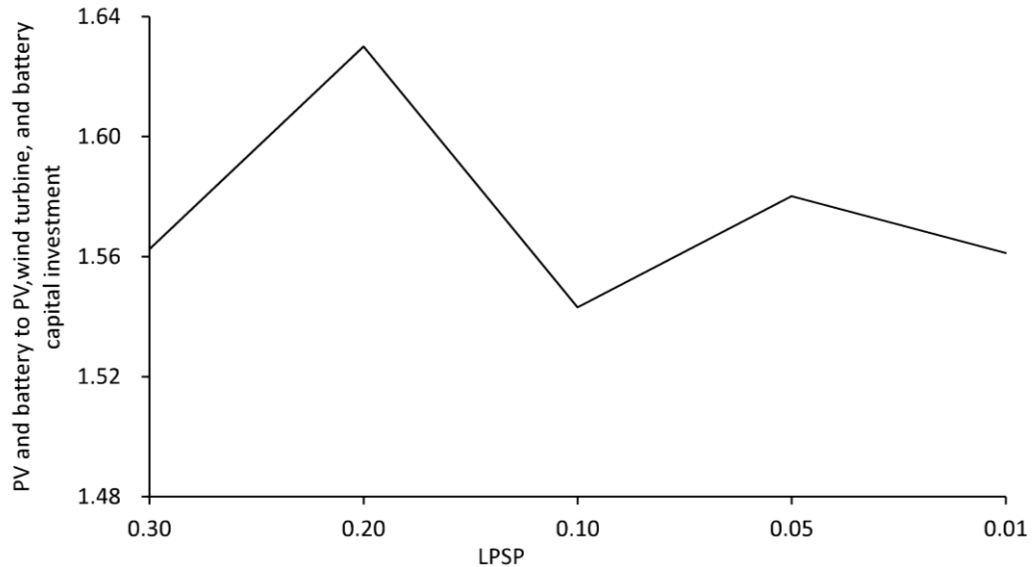
Figure 4-17: Ratio of PV-battery system capital investment to the PV-wind turbine-battery system capital investment, for systems presented in Table 4-3 and Table 4-5.

The selection of the optimum system may be based on the minimum annualized cost together with other objectives including reliability and GHG emission targets. A proposed system with the lowest annualized cost may be ignored because of its lower potential to reduce GHG emission. A system with higher GHG emission reduction potential may be refused due to its higher capital costs. Therefore, considering the conflicting targets, among the non-dominated options, based on a decision maker's interests, one system may take precedence. There is some uncertainty, ambiguity, and variability attached to this selection owing to the intermittent nature of renewable resources and loads, uncertainties related to

the costs of the HRES components, and uncertainties pertaining to the renewable energy generation calculations.

4.5 Conclusion

Hybrid renewable energy systems have attracted great attention in recent years due to increasing concerns about climate change and energy security. Optimization of renewable energy systems and sizing can lead to a significant increase in renewable energy penetration because it reduces some of the economic hurdles (Erdinc and Uzunoglu 2012). To minimize electricity cost while reliably meeting annual electricity demand, the optimum combination of solar PV and wind generators coupled with battery banks for an energy intensive consumer was investigated. The large energy demand, significant daily and seasonal variability of demand, and fluctuations of wind and solar resources make arriving at an optimum design a critical task. It is not easy to mathematically model this nonlinear, multiple objective problem with traditional techniques (Khare and Rangnekar 2013). A particle swarm optimization (PSO) algorithm was developed to solve this non-linear and constrained optimization problem dealing with multiple conflicting goals. Different aspects of HRESs optimization were investigated and the performance of the proposed methodology was examined. The main contribution of this research is to propose a multi-objective optimization method for planning a large-scale HRES that integrates the intermittent renewable sources with dispatchable grid power to satisfy a large demand with high reliability. The sensitivity and flexibility of the proposed method to different objectives were explored and a set of optimal options composed of PV and battery components and also PV, wind turbine, and battery components with different characteristics were presented.

135

Chapter 5: Summary and conclusions

The potential of solar and wind energy resources in producing electricity at the University of Lethbridge campus to meet electricity demand, and the rooftop PV electricity potential of the City of Lethbridge, was investigated and evaluated in this research. In addition, using the University of Lethbridge electricity consumption data, a multi-criteria PSO-based optimal design of grid-connected hybrid renewable energy systems was developed to determine the optimum number and configuration of photovoltaic (PV) modules, wind turbines and battery units by minimizing the annual system cost while maximizing the reliability of the hybrid system in matching the electricity supply and demand.

The following four objectives were presented in this thesis and addressed in Chapters 2, 3, and 4:

1- Quantify the full potential of solar and wind energy sources in generating electricity to meet the electrical demands of the University of Lethbridge (a feasibility assessment for campus solar PV and wind turbine installations).

2- Estimate rooftop photovoltaic electricity potential of buildings in an urban environment, the City of Lethbridge, employing a multi-criteria approach using geographic information systems and LiDAR.

3- Conduct an economic assessment utilizing present market prices to determine economically attractive rooftop PV systems in the City of Lethbridge.

4- Develop an optimal sizing and design strategy based on a heuristic particle swarm optimization (PSO) technique to determine the near optimum number and configuration of photovoltaic (PV) modules, wind turbines and battery units minimizing the annual system cost while maximizing the reliability of the hybrid system in matching the electricity supply and demand.

In Chapter 2, which presented the results of employing Light Detection And Ranging (LiDAR) data and aerial photography to assess the solar photovoltaic electricity potential and wind turbine power curve method to estimate the wind electricity potential, a feasibility assessment for campus solar PV and wind installations was conducted. Measured weather data including hourly solar radiation data, hourly wind speed data, and hourly temperature data were used to simulate solar PV and wind turbine performance, and evaluate energy production. Separation and transposition models including Erbs et al. (1982) model and Perez et al. (1990) model were used to estimate the incident solar radiation received by the sloped PV surfaces utilizing measured global radiation on horizontal planes. The operating temperature of photovoltaic cells was assessed utilizing the Skoplaki model (Skoplaki et al. 2008) . The "Area Solar Radiation" tool was used to calculate the amount of radiant energy for the coulee area and then, areas receiving above a defined annual insolation were selected as suitable locations (coulee areas) for installing PV modules. Suitable rooftops, open spaces and parking lots were selected using aerial imagery in GIS. Wind turbine energy production was calculated using measured wind speed data and the power curve method.

A comparison of the resulting solar PV and wind turbine generation over five years with the university electrical demand revealed that wind turbine and solar PV systems

together could generate more than 3.7 times of the annual electricity consumption of the university on average. There is 1,015,808 m^2 of suitable area available for placing a 46 MW solar PV system on the campus, which would produce at least 2.8 times of the university annual electricity usage. In addition, the proposed wind system could cover about 84% of the university electricity demand annually on average. Employing this system, the annual electricity cost of the university could decrease about 90% (Table 2-7). By installing renewable systems, the University can achieve a sustainable energy future and demonstrate its commitment to environmental responsibilities.

In Chapter 3, a multi-criteria approach based on geographic information systems (GIS) and light detection and ranging (LiDAR) data was used to estimate rooftop photovoltaic electricity potential of buildings in an urban environment, the City of Lethbridge. Unlike energy generation from fossil fuels, renewable energy sources have relatively low geographic density and are spread unevenly over large areas. Therefore, especially in cities where space has greater value and opportunity costs, finding suitable spaces for implementing solar PV systems is essential to promote the use of solar PV technologies. Using remote sensing data, the intricate topography of the city was modeled, and employing a new methodology, solar insolation incident at each location was estimated. An economic assessment was conducted utilizing present market prices to determine economically attractive rooftop PV systems. The total rooftop photovoltaic (PV) electricity potential was evaluated and compared with the local electricity demand. Effective expansion of rooftop solar PV power systems in the city was achieved by determining the geographic distribution of the best locations for installing the systems.

Chapter 3 results revealed that the rooftop PV electricity generation potential of the City of Lethbridge is approximately 301 ± 29 (SD) GWh annually (almost 38% of its annual electricity consumption in 2016), and about 96% of the recognized potential rooftop PV systems are economically feasible. The identified suitable rooftop surfaces provide enough area for installing approximately 218 MW of rooftop PV systems, with residential buildings accounting for about half of the installed capacity. The 38,496 suitable rooftop segments with a total actual area of about 2,372,000 m^2 identified were approximately 30% of the total roof area. Results illustrated that the individual suitable rooftop segments belong mostly to residential (about 83%) and commercial (about 9%) buildings, providing about 48% and 20% of the suitable area respectively. Most of the roof segments are flat or have a slope less than 20° (about 91% of them or 84% of the suitable area). While industrial and commercial buildings account for just about 3% and 4% of the flat individual segments, they constitute the largest portion of the suitable flat area (m^2), about 22%, and 18% of the available flat area respectively. Residential buildings with roof pitch between 10° and 20° account for more than 25% of the total suitable roof area (about half of the segments), which is the highest share among various building types and slope classes. It was found that about 48% of the all buildings possess a suitable roof plane which could host PV systems (26,959 buildings). About 94% of these buildings are residential. Residential buildings with suitable rooftops most often (about 90%) can accommodate PV systems with a size less than 10 kW. This study demonstrated that the average capacity factor of the determined rooftop systems is about $16 \pm 1.5\%$, which is very promising for this urban region. The results can assist in making informed policy decisions about investment in deployment of renewable energy generation.

In Chapter 4, optimum designs of hybrid renewable energy systems including PV modules, wind turbines, and battery storages was investigated. The unreliable nature of renewable resources are impediments to developing renewable projects. More reliable, effective, and economically feasible renewable energy systems can be designed and established by consolidating renewable energy sources such as wind and solar into hybrid systems supported by batteries and back-up power distribution units, such as conventional energy generators or grids (Erdinc and Uzunoglu 2012, Bhandari et al. 2015). A hybrid renewable energy system (HRES) offers a promising engineering solution to the intrinsic stochastic and intermittent nature of most renewables by enhancing the economic and technical performance of power plants (Erdinc and Uzunoglu 2012, Alsayed et al. 2013). In fact, in a well-designed HRES, multiple renewable energy sources complement each other (González et al. 2015). The precise design of such systems is a critical step towards their effective deployment. An optimal sizing and design strategy was developed based on a heuristic particle swarm optimization (PSO) technique to determine the optimum number and configuration of photovoltaic (PV) modules, wind turbines, and battery units, minimizing the annual system cost while maximizing the reliability of the hybrid system in matching the electricity supply and demand. In addition, by constraining the amount of conventional electricity purchased from the grid, environmental concerns were also considered in the presented method. Employing current time-series weather data and electricity demand profile, the proposed method was applied to a case study of power generation at the University of Lethbridge. Various systems with different reliabilities and potential of reducing consumer CO_2 emissions were designed and the behaviour of the proposed method was comprehensively investigated.

Chapter 4 results illustrated how the capital investment required for constructing a HRES is governed by the chosen LPSP *(Loss of power supply probability)*. Results indicated that systems with lower LPSP are larger and need more available area. It was found that the optimization algorithm tends to use wind and battery resources more than the solar resource. By decreasing LPSP from 30% to 0.1%, A_{PV} (total PV panel area) surged about 3 times while $A_{WT,SA}$ (total wind turbine rotor swept area) increased only 1.2 times. In addition, the ratio of sold power to purchase power rises when the dimension of the system increases or LPSP decreases. This ratio for a HRES with an LPSP equal to 0.1% was about 30% more than that of a HRES with an LPSP of 30%, notwithstanding that the first system must also serve more load. All the optimum systems have an annualized cost less than the base case (when there is no HRES) since they compensate a significant part of the demand and are able to sell a considerable amount of energy. A system with an LPSP of 5% has about 34% lower annual cost than the base case which is a significant cost reduction. By decreasing LPSP from 30% to 0.1%, the annual cost of HRES declines by 13% taking into account their different sold power to purchased power ratio. In addition, results demonstrates that the initial investment of an HRES with an LPSP of 0.1% is 60% greater than that of a system with an LPSP of 30% taking into account their different sold to purchase power ratio. By replacing fossil fuel based grid electricity, the designed systems can reduce the carbon footprint more than 75%, which is a desirable environmental achievement. Results showed that systems with larger reduction in CO_2 emissions have lower LPSP values and higher capital investments. Furthermore, the operation and maintenance cost of systems has a inverse relationship with the LPSP value, and by decreasing LPSP from 30% to 0.1%, operation and maintenance cost increases by about 58%. For hybrid PV-battery systems, compared with PV-wind turbine-battery systems,

obtaining an LPSP of about 5% means that the annual cost will increase by 30% approximately, however, the capital investment surges by about 60%. Overall, reaching a certain reliability level with a HRES composed only of PV and batteries requires about 1.6 times larger investment compared with a PV-wind turbine-battery combination. This study explored and illustrated that how utilizing hybrid renewable energy systems can assist reaching a balance among cost, emissions, and reliability.

5.1 Recommendations for future research

This thesis evaluated the potential of solar PV and wind turbine electricity generation at the University of Lethbridge campus and also the solar PV rooftop electricity potential at the City of Lethbridge. In addition, a multi-criteria PSO-based optimal design for grid-linked hybrid renewable energy systems was presented. The following recommendations for future research and developments are determined:

- The proposed method for evaluating solar and wind energy potential can be expanded by including the PV electricity potential of buildings' façade in an urban setting. Building facades usually provide larger surfaces than rooftops, are free from other building apparatus including chimneys and ventilators, and accommodate PV panels in better maintenance conditions because often they do not gather snow and dust (Redweik et al. 2013).

- A more rigorous and meticulous economic assessment may be conducted considering detailed engineering characteristics of the renewable energy facility.

- Environmental impacts of renewable energy facilities may be investigated, for example, a glare assessment may be conducted in the study areas to explore the glare produced by the solar PV facilities.

• Renewable energy employment evaluation may be expanded by investigating technical, economic, social or public, and cultural barriers to penetration in the energy mix. For instance, people sometimes do not support development of wind and solar facilities since they do not recognise why these technologies are advantageous (Sovacool 2009). Increasing development of renewable energy systems has confronted public opposition due to, for example, landscape change and its resultant changes and interruptions in adjacent residents' routine life (Pasqualetti 2011). Therefore, multi-dimensional assessments of the potential constraints on renewable energy development are essential for increased investment in transition to renewables (Richards et al. 2012) .

• The proposed optimization methodology used real electricity usage of the consumer over the course of one year. It may be more realistic to consider the variation of electricity consumption for a longer period of time and design a HRES that meets consumers' long-term electricity need.

References

Abbes, Dhaker, André Martinez, and Gérard Champenois. 2014. "Life cycle cost, embodied energy and loss of power supply probability for the optimal design of hybrid power systems." *Mathematics and Computers in Simulation* 98:46-62.

Abed, KA, and AA El-Mallah. 1997. "Capacity factor of wind turbines." *Energy* 22 (5):487-491.

Ai, Bin, Hongxing Yang, Hui Shen, and X Liao. 2003. "Computer-aided design of PV/wind hybrid system." *Renewable Energy* 28 (10):1491-1512.

Akram, Umer, Muhammad Khalid, and Saifullah Shafiq. 2017. "Optimal sizing of a wind/solar/battery hybrid grid-connected microgrid system." *IET Renewable Power Generation* 12 (1):72-80.

Alberta Electric System Operator. 2016. "Transmission costs." accessed 2018. https://www.aeso.ca/grid/transmission-costs/.

Alberta Electric System Operator. 2017. 2016 Annual Market Statistics. https://www.aeso.ca/market/market-and-system-reporting/annual-market-statistic-reports/.

Alberta Electric System Operator. 2018. 2017 Annual Market Statistics. https://www.aeso.ca/market/market-and-system-reporting/annual-market-statistic-reports/.

Alberta Government. 2017a. "Alberta: Rebates to help Albertans tap solar resources." accessed 2018. https://www.alberta.ca/release.cfm?xID=463610A3269CE-0D2C-C140-6E391B3112A56664.

Alberta Government. 2017b. "Phasing out coal pollution." https://www.alberta.ca/climate-coal-electricity.aspx.

Alejandro, J, Alicia Arce, and Carlos Bordons. 2009. "Optimization strategy for element sizing in hybrid power systems." *Journal of Power Sources* 193 (1):315-321.

Alsayed, Mohammed, Mario Cacciato, Giuseppe Scarcella, and Giacomo Scelba. 2013. "Multicriteria optimal sizing of photovoltaic-wind turbine grid connected systems." *IEEE Transactions on Energy Conversion* 28 (2):370-379.

Amado, Miguel, and Francesca Poggi. 2012. "Towards solar urban planning: A new step for better energy performance." *Energy Procedia* 30:1261-1273.

Anderson, Kate H, Michael H Coddington, and Benjamin D Kroposki. 2010. "Assessing technical potential for city PV deployment using NREL's in my backyard tool." Photovoltaic Specialists Conference (PVSC), 2010 35th IEEE.

Ardakani, Fatemeh Jahanbani, Gholamhossein Riahy, and Mehrdad Abedi. 2010. "Optimal sizing of a grid-connected hybrid system for north-west of Iran-case study." In 2010 9th International Conference on Environment and Electrical Engineering, pp. 29-32. IEEE, 2010.

Arun, P, Rangan Banerjee, and Santanu Bandyopadhyay. 2009. "Optimum sizing of photovoltaic battery systems incorporating uncertainty through design space approach." *Solar Energy* 83 (7):1013-1025.

Ashok, S. 2007. "Optimised model for community-based hybrid energy system." *Renewable Energy* 32 (7):1155-1164.

Athari, MH, and MM Ardehali. 2016. "Operational performance of energy storage as function of electricity prices for on-grid hybrid renewable energy system by optimized fuzzy logic controller." *Renewable Energy* 85:890-902.

Atmaram, Gobind H, GovindaSamy TamizhMani, and Gerard G Ventre. 2008. "Need for uniform photvoltaic module performance testing and ratings." Photovoltaic Specialists Conference, 2008. PVSC'08. 33rd IEEE.

Aznar, Alexandra, Megan Day, Elizabeth Doris, Shivani Mathur, and Paul Donohoo-Vallett. 2015. City-Level Energy Decision Making. Data Use in Energy Planning, Implementation, and Evaluation in US Cities. National Renewable Energy Laboratory (NREL), Golden, CO (United States).

Besharat, Fariba, Ali A Dehghan, and Ahmad R Faghih. 2013. "Empirical models for estimating global solar radiation: A review and case study." *Renewable and Sustainable Energy Reviews* 21:798-821.

Bhandari, Binayak, Kyung-Tae Lee, Gil-Yong Lee, Young-Man Cho, and Sung-Hoon Ahn. 2015. "Optimization of hybrid renewable energy power systems: A review." *International Journal of Precision Engineering and Manufacturing-Green Technology* 2 (1):99-112.

Bilal, B Ould, V Sambou, PA Ndiaye, CMF Kébé, and M Ndongo. 2010. "Optimal design of a hybrid solar–wind-battery system using the minimization of the annualized cost system and the minimization of the loss of power supply probability (LPSP)." *Renewable Energy* 35 (10):2388-2390.

Boland, John, Lynne Scott, and Mark Luther. 2001. "Modelling the diffuse fraction of global solar radiation on a horizontal surface." *Environmetrics* 12 (2):103-116.

Borhanazad, Hanieh, Saad Mekhilef, Velappa Gounder Ganapathy, Mostafa Modiri-Delshad, and Ali Mirtaheri. 2014. "Optimization of micro-grid system using MOPSO." *Renewable Energy* 71:295-306.

Boz, Mesude Bayrakci, Kirby Calvert, and Jeffrey RS Brownson. 2015. "An automated model for rooftop PV systems assessment in ArcGIS using LIDAR." *AIMS Energy* 3 (3):401-420.

Brihmat, Fouzia, and Said Mekhtoub. 2014. "PV cell temperature/PV power output relationships homer methodology calculation." Conférence Internationale des Energies Renouvelables" CIER'13" International Journal of Scientific Research & Engineering Technology.

Byrne, John, Job Taminiau, Lado Kurdgelashvili, and Kyung Nam Kim. 2015. "A review of the solar city concept and methods to assess rooftop solar electric potential, with an illustrative application to the city of Seoul." *Renewable and Sustainable Energy Reviews* 41:830-844.

Cabral, Claudia Valéria Távora, Delly Oliveira Filho, Antônia Sônia Alves C Diniz, José Helvecio Martins, Olga Moraes Toledo, and B Lauro de Vilhena. 2010. "A stochastic method for stand-alone photovoltaic system sizing." *Solar Energy* 84 (9):1628-1636.

Camargo, Luis Ramirez, Roland Zink, Wolfgang Dorner, and Gernot Stoeglehner. 2015. "Spatio-temporal modeling of roof-top photovoltaic panels for improved technical potential assessment and electricity peak load offsetting at the municipal scale." *Computers, Environment and Urban Systems* 52:58-69.

Canada National Energy Board. 2018. "Canada's Renewable Power Landscape 2017 – Energy Market Analysis." https://www.neb-one.gc.ca/nrg/sttstc/lctrct/rprt/2017cndrnwblpwr/prvnc/ab-eng.html.

Canadian Solar Industries Association. 2018. Roadmap 2020: Powering Canada's Future with Solar Electricity. http://www.cansia.ca/roadmap-2020.html.

Canadian Solar Industries Association and Energy Efficiency Alberta. 2018. Alberta go solar guide. https://www.cansia.ca/gosolar.html.

Canadian Wind Energy Association. 2016. "Alberta Takes Action to Become Canada's Largest Market for New Wind Energy Investment." https://canwea.ca/news-release/2016/11/03/alberta-takes-action-become-canadas-largest-market-new-wind-energy-investment/.

Canadian Wind Energy Association. 2017. Powering Canada's Future. https://canwea.ca/wp-content/uploads/2018/08/Canada-Current-Installed-Capacity_e.pdf.

Canadian Wind Energy Association. 2018. "Alberta; Wind energy in Alberta." CanWEA, accessed December 2018. https://canwea.ca/wind-energy/alberta/.

Castellanos, Sergio, Deborah A Sunter, and Daniel M Kammen. 2017. "Rooftop solar photovoltaic potential in cities: how scalable are assessment approaches?" *Environmental Research Letters* 12 (12):125005.

Chauhan, Anurag, and RP Saini. 2014. "A review on integrated renewable energy system based power generation for stand-alone applications: configurations, storage options, sizing methodologies and control." *Renewable and Sustainable Energy Reviews* 38:99-120.

Chaves, Andrea, and AT Bahill. 2010. "Locating sites for photovoltaic solar panels." *Pilot study uses DEM derived from LiDAR, ArcUser* 13 (4).

Chow, Annie, Alan S Fung, and Songnian Li. 2014. "GIS modeling of solar neighborhood potential at a fine spatiotemporal resolution." *Buildings* 4 (2):195-206.

City of Lethbridge. 2017a. "About Lethbridge." accessed 2017. http://www.lethbridge.ca/Things-To-Do/About-Lethbridge/Pages/default.aspx.

City of Lethbridge. 2017b. "Census Results 2016." accessed 2017. http://www.lethbridge.ca/City-Government/Census/Pages/Census-Results-2015.aspx.

City of Lethbridge. 2017c. "City of Lethbridge Open Data Catalogue: Building Footprints." City of Lethbridge, accessed 2017. http://opendata.lethbridge.ca/datasets/7d32446fb333488598268bd4bc0c830d_0.

City of Lethbridge. 2017d. "City of Lethbridge Open Data Catalogue: City Boundary." accessed 2017. http://opendata.lethbridge.ca/datasets/3d37b1a4840d4eac88bb89a49672c2e7_1.

Clifton, Andrew, Aaron Smith, and Michael Fields. 2016. Wind Plant Preconstruction Energy Estimates. Current Practice and Opportunities. National Renewable Energy Lab.(NREL), Golden, CO (United States).

De Miguel, ABJARKH, J Bilbao, R Aguiar, H Kambezidis, and E Negro. 2001. "Diffuse solar irradiation model evaluation in the north Mediterranean belt area." *Solar Energy* 70 (2):143-153.

Del Cueto, JA. 2002. "Comparison of energy production and performance from flat-plate photovoltaic module technologies deployed at fixed tilt." Conference Record of the Twenty-Ninth IEEE Photovoltaic Specialists Conference, 2002.

Del Valle, Yamille, Ganesh Kumar Venayagamoorthy, Salman Mohagheghi, Jean-Carlos Hernandez, and Ronald G Harley. 2008. "Particle swarm optimization: basic concepts,

variants and applications in power systems." *IEEE Transactions on Evolutionary Computation* 12 (2):171-195.

Delucchi, Mark A, and Mark Z Jacobson. 2011. "Providing all global energy with wind, water, and solar power, Part II: Reliability, system and transmission costs, and policies." *Energy Policy* 39 (3):1170-1190.

Denholm, Paul, and Robert Margolis. 2008. "Supply curves for rooftop solar PV-generated electricity for the United States."

Despotovic, Milan, Vladimir Nedic, Danijela Despotovic, and Slobodan Cvetanovic. 2015. "Review and statistical analysis of different global solar radiation sunshine models." *Renewable and Sustainable Energy Reviews* 52:1869-1880.

Devabhaktuni, Vijay, Mansoor Alam, Soma Shekara Sreenadh Reddy Depuru, Robert C Green, Douglas Nims, and Craig Near. 2013. "Solar energy: Trends and enabling technologies." *Renewable and Sustainable Energy Reviews* 19:555-564.

Diaf, Said, Djamila Diaf, Mayouf Belhamel, Mourad Haddadi, and Alain Louche. 2007. "A methodology for optimal sizing of autonomous hybrid PV/wind system." *Energy Policy* 35 (11):5708-5718.

Dierauf, Timothy, Aaron Growitz, Sarah Kurtz, Jose Luis Becerra Cruz, Evan Riley, and Clifford Hansen. 2013. Weather-corrected performance ratio. National Renewable Energy Laboratory (NREL), Golden, CO.

Divya, KC, and Jacob Østergaard. 2009. "Battery energy storage technology for power systems— An overview." *Electric Power Systems Research* 79 (4):511-520.

Dodge David, and Thompson Dylan. 2016. "Financing critical for renewable energy projects." Green Energy Futures. http://www.greenenergyfutures.ca/episode/canada-germany-renewable-financing.

Doluweera, Ganesh, Allan Fogwill, Hossein Hosseini, Karen Mascarenhas, Experience Nduagu, Alpha Sow, and Evar Umeozor. 2018. A comprehensive guide to electricity generation options in Canada. Canadian Energy Research Institute.

Duffie, John A, and William A Beckman. 2013. *Solar Engineering of Thermal Processes*: John Wiley & Sons.

Eberhart, Russell, and James Kennedy. 1995. "A new optimizer using particle swarm theory." In MHS'95. Proceedings of the Sixth International Symposium on Micro Machine and Human Science, pp. 39-43. Ieee, 1995.

Ekren, Banu Y, and Orhan Ekren. 2009. "Simulation based size optimization of a PV/wind hybrid energy conversion system with battery storage under various load and auxiliary energy conditions." *Applied Energy* 86 (9):1387-1394.

Ekren, Orhan, and Banu Y Ekren. 2010. "Size optimization of a PV/wind hybrid energy conversion system with battery storage using simulated annealing." *Applied Energy* 87 (2):592-598.

Ekren, Orhan, and Banu Yetkin Ekren. 2008. "Size optimization of a PV/wind hybrid energy conversion system with battery storage using response surface methodology." *Applied Energy* 85 (11):1086-1101.

El-Sebaii, AA, FS Al-Hazmi, AA Al-Ghamdi, and Saud Jameel Yaghmour. 2010. "Global, direct and diffuse solar radiation on horizontal and tilted surfaces in Jeddah, Saudi Arabia." *Applied Energy* 87 (2):568-576.

Environment Lethbridge. 2017. Lethbridge State of the Environment. Environment Lethbridge Council. www.environmentlethbridge.ca (2017).

Erbs, DG, SA Klein, and JA Duffie. 1982. "Estimation of the diffuse radiation fraction for hourly, daily and monthly-average global radiation." *Solar Energy* 28 (4):293-302.

Erdinc, O, and M Uzunoglu. 2012. "Optimum design of hybrid renewable energy systems: Overview of different approaches." *Renewable and Sustainable Energy Reviews* 16 (3):1412-1425.

Esri. 2013. "ArcGIS Resources, ArcGIS Help 10.1- LAS dataset considerations." accessed 2017. http://resources.arcgis.com/en/help/main/10.1/index.html#/LAS_dataset_considerations/0 15w00000069000000/ESRI_SECTION1_104F85DA2EBC405E9EEBBFF61208759E/.

Esri. 2014. "ArcGIS Resources-ArcGIS Help 10.2, 10.2.1, and 10.2.2: How Slope works." accessed 2017. http://resources.arcgis.com/en/help/main/10.2/index.html#/How_Slope_works/009z00000 0vz000000/.

Esri. 2016a. "ArcMap- Area Solar Radiation." accessed 2016. http://desktop.arcgis.com/en/arcmap/10.3/tools/spatial-analyst-toolbox/area-solar-radiation.htm.

Esri. 2016b. "ArcMap- Creating raster DEMs and DSMs from large lidar point collections." accessed 2016. http://desktop.arcgis.com/en/arcmap/10.3/manage-data/las-dataset/lidar-solutions-creating-raster-dems-and-dsms-from-large-lidar-point-collections.htm.

Esri. 2016c. "ArcMap-Modeling solar radiation." accessed 2016. http://desktop.arcgis.com/en/arcmap/10.3/tools/spatial-analyst-toolbox/modeling-solar-radiation.htm.

Esri. 2017a. " ArcGIS Pro- Hillshade." accessed 2017. http://pro.arcgis.com/en/pro-app/tool-reference/3d-analyst/hillshade.htm.

Esri. 2017b. "ArcMap- How Raster Calculator works." accessed 2017. http://desktop.arcgis.com/en/arcmap/10.3/tools/spatial-analyst-toolbox/how-raster-calculator-works.htm.

Esri. 2019. "ArcMap- Storing lidar data." accessed 2019. http://desktop.arcgis.com/en/arcmap/10.3/manage-data/las-dataset/storing-lidar-data.htm.

Esri Canada Ed. 2013. "Canada Boundary." https://www.arcgis.com/home/item.html?id=dcbcdf86939548af81efbd2d732336db.

Fadaee, M, and MAM Radzi. 2012. "Multi-objective optimization of a stand-alone hybrid renewable energy system by using evolutionary algorithms: a review." *Renewable and Sustainable Energy Reviews* 16 (5):3364-3369.

Fath, Karoline, Julian Stengel, Wendelin Sprenger, Helen Rose Wilson, Frank Schultmann, and Tilmann E Kuhn. 2015. "A method for predicting the economic potential of (building-integrated) photovoltaics in urban areas based on hourly Radiance simulations." *Solar Energy* 116:357-370.

Fu, P, and PM Rich. 2000. *The solar analyst 1.0 user manual*, *Helios Environmental Modeling Institute*.

Gagnon, Pieter, Robert Margolis, Jennifer Melius, Caleb Phillips, and Ryan Elmore. 2016. *Rooftop solar photovoltaic technical potential in the United States: A detailed assessment*: National Renewable Energy Laboratory.

Garcia, Raquel S, and Daniel Weisser. 2006. "A wind–diesel system with hydrogen storage: Joint optimisation of design and dispatch." *Renewable Energy* 31 (14):2296-2320.

Gavanidous, ES, and AG Bakirtzis. 1992. "Design of a stand alone system with renewable energy sources using trade off methods." *IEEE Transactions on Energy Conversion* 7 (1):42-48.

González, Arnau, Jordi-Roger Riba, Antoni Rius, and Rita Puig. 2015. "Optimal sizing of a hybrid grid-connected photovoltaic and wind power system." *Applied Energy* 154:752-762.

Gooding, James, Holly Edwards, Jannik Giesekam, and Rolf Crook. 2013. "Solar City Indicator: A methodology to predict city level PV installed capacity by combining physical capacity and socio-economic factors." *Solar Energy* 95:325-335.

Government of Alberta. 2017. Climate Leadership Plan Progress Report 2016-17. https://www.alberta.ca/climate-leadership-plan.aspx.

Government of Alberta. 2018. "Electricity price protection." https://www.alberta.ca/electricity-price-protection.aspx.

Government of Canada. 2018. "Greenhouse gas sources and sinks: executive summary 2018." https://www.canada.ca/en/environment-climate-change/services/climate-change/greenhouse-gas-emissions/sources-sinks-executive-summary-2018.html.

Gueymard, Christian A. 2009. "Direct and indirect uncertainties in the prediction of tilted irradiance for solar engineering applications." *Solar Energy* 83 (3):432-444.

Handoyo, Ekadewi A, and Djatmiko Ichsani. 2013. "The optimal tilt angle of a solar collector." *Energy Procedia* 32:166-175.

Hemami, Ahmad. 2012. *Wind turbine technology*: Cengage Learning.

Herbert, GM Joselin, Selvaraj Iniyan, E Sreevalsan, and S Rajapandian. 2007. "A review of wind energy technologies." *Renewable and Sustainable Energy Reviews* 11 (6):1117-1145.

Hermann, Sebastian, Asami Miketa, and Nicolas Fichaux. 2014. Estimating the Renewable Energy Potential in Africa. International Renewable Energy Agency (IRENA), Abu Dhabi.

Hofierka, Jaroslav, and Marcel Suri. 2002. "The solar radiation model for Open source GIS: implementation and applications." Proceedings of the Open source GIS-GRASS users conference.

Horner, Robert M, and Corrie E Clark. 2013. "Characterizing variability and reducing uncertainty in estimates of solar land use energy intensity." *Renewable and Sustainable Energy Reviews* 23:129-137.

Huang, Yan, Zuoqi Chen, Bin Wu, Liang Chen, Weiqing Mao, Feng Zhao, Jianping Wu, Junhan Wu, and Bailang Yu. 2015. "Estimating roof solar energy potential in the downtown area using a gpu-accelerated solar radiation model and airborne lidar data." *Remote Sensing* 7 (12):17212-17233.

International Electrotechnical Commission. 2018. "The World's Online Electrotechnical Vocabulary." International Electrotechnical Commission (IEC). http://www.electropedia.org/iev/iev.nsf/6d6bdd8667c378f7c12581fa003d80e7?OpenForm.

International Energy Agency. 2015. Energy and climate change, world energy outlook special report. OECD, IEA, Paris, France.

International Energy Agency. 2016. Energy Technology Perspectives 2016. Annex H: Rooftop Solar PV Potential in Cities. http://www.iea.org/etp/etp2016/annexes/.

International Renewable Energy Agency. 2016. Renewable Energy in Cities. Abu Dhabi, *www.irena.org*: International Renewable Energy Agency (IRENA).

Izquierdo, Salvador, Marcos Rodrigues, and Norberto Fueyo. 2008. "A method for estimating the geographical distribution of the available roof surface area for large-scale photovoltaic energy-potential evaluations." *Solar Energy* 82 (10):929-939.

Jacobson, Mark Z, Mark A Delucchi, Zack AF Bauer, Savannah C Goodman, William E Chapman, Mary A Cameron, Cedric Bozonnat, Liat Chobadi, Hailey A Clonts, and Peter Enevoldsen. 2017. "100% clean and renewable wind, water, and sunlight all-sector energy roadmaps for 139 countries of the world." *Joule* 1 (1):108-121.

Jahanbani, Fatemeh, and Gholam H Riahy. 2011. "Optimum design of a hybrid renewable energy system." In *Renewable energy-trends and applications*. Dr. Majid Nayeripour (Ed.), ISBN: 978-953-307-939-4, InTech.

Jakubiec, J Alstan, and Christoph F Reinhart. 2013. "A method for predicting city-wide electricity gains from photovoltaic panels based on LiDAR and GIS data combined with hourly Daysim simulations." *Solar Energy* 93:127-143.

Jayachandran, M, and G Ravi. 2017. "Design and Optimization of Hybrid Micro-Grid System." *Energy Procedia* 117:95-103.

Jochem, Andreas, Bernhard Höfle, Martin Rutzinger, and Norbert Pfeifer. 2009. "Automatic roof plane detection and analysis in airborne lidar point clouds for solar potential assessment." *Sensors* 9 (7):5241-5262.

Journée, Michel, and Cédric Bertrand. 2011. "Quality control of solar radiation data within the RMIB solar measurements network." *Solar Energy* 85 (1):72-86.

Kammen, Daniel M, and Deborah A Sunter. 2016. "City-integrated renewable energy for urban sustainability." *Science* 352 (6288):922-928.

Kanters, Jouri, and Henrik Davidsson. 2014. "Mutual shading of PV modules on flat roofs: a parametric study." *Energy Procedia* 57:1706-1715.

Kausika, Bhavya, Wiep Folkerts, Wilfried van Sark, Bouke Siebenga, and Paul Hermans. 2014. "A big data approach to the solar PV market: design and results of a pilot in the Netherlands." 29th European Photovoltaic Solar Energy Conference and Exhibition.

Kellogg, W, MH Nehrir, G Venkataramanan, and V Gerez. 1996. "Optimal unit sizing for a hybrid wind/photovoltaic generating system." *Electric Power Systems Research* 39 (1):35-38.

Khalkhali, Abolfazl, Mohamadhosein Sadafi, Javad Rezapour, and Hamed Safikhani. 2010. "Pareto based multi-objective optimization of solar thermal energy storage using genetic algorithms." *Transactions of the Canadian Society for Mechanical Engineering* 34 (3-4):463-474.

Khare, Anula, and Saroj Rangnekar. 2013. "A review of particle swarm optimization and its applications in solar photovoltaic system." *Applied Soft Computing* 13 (5):2997-3006.

Khare, Vikas, Savita Nema, and Prashant Baredar. 2016. "Solar–wind hybrid renewable energy system: A review." *Renewable and Sustainable Energy Reviews* 58:23-33.

Kouhestani, Fariborz Mansouri, James Byrne, Dan Johnson, Locke Spencer, Paul Hazendonk, and Bryson Brown. 2018. "Evaluating solar energy technical and economic potential on rooftops in an urban setting: the city of Lethbridge, Canada." *International Journal of Energy and Environmental Engineering*:1-20.

Kuby Renewable Energy Ltd. 2018. "The Cost of Solar Panels." https://kubyenergy.ca/blog/the-cost-of-solar-panels.

L. Sawin, Janet , Jay Rutovitz , Freyr Sverrisson, Emma Aberg, Rana Adib, Fabiani Appavou, Adam Brown, Scott Dwyer, Barbel Epp, Flávia Guerra, Bozhil Kondev, Hannah E. Murdock , Evan Musolino, Jay Rutovitz , Janet L. Sawin, Kristin Seyboth, Jonathan Skeen, Freyr Sverrisson, Sven Teske , Stephanie Weckend, and Henning Wuester. 2018. Renewables 2018-Global status report. http://www.ren21.net/: Renewable energy policy network for the 21st century.

Lagorse, Jeremy, Damien Paire, and Abdellatif Miraoui. 2009. "Sizing optimization of a stand-alone street lighting system powered by a hybrid system using fuel cell, PV and battery." *Renewable Energy* 34 (3):683-691.

Lantz, Eric, Michael Leventhal, and Ian Baring-Gould. 2013. Wind power project repowering: financial feasibility, decision drivers, and supply chain effects. National Renewable Energy Laboratory (NREL), Golden, CO.

Lis, Natalia , Colette Craig, Ingrid Ektvedt, Nadew Michael, Ken Newel, Sara Tsang, and Cassandra Wilde. 2016. Canada's renewable power landscape energy market analysis 2016. http://www.neb-one.gc.ca/nrg/sttstc/lctrct/rprt/2016cndrnwblpwr/pblctn-nfrmtn-dwnlds-eng.html: Government of Canada, National Energy Board.

MacKinnon, Janice, and Jack Mintz. 2017. "Putting the Alberta budget on a new trajectory."

Mahesh, Aeidapu, and Kanwarjit Singh Sandhu. 2017. "A genetic algorithm based improved optimal sizing strategy for solar-wind-battery hybrid system using energy filter algorithm." *Frontiers in Energy*:1-13.

Maleki, Akbar, Mehran Ameri, and Farshid Keynia. 2015. "Scrutiny of multifarious particle swarm optimization for finding the optimal size of a PV/wind/battery hybrid system." *Renewable Energy* 80:552-563.

Maleki, Akbar, Marc A Rosen, and Fathollah Pourfayaz. 2017. "Optimal Operation of a Grid-Connected Hybrid Renewable Energy System for Residential Applications." *Sustainability* 9 (8):1314.

Margeta, Jure, and Zvonimir Glasnovic. 2010. "Feasibility of the green energy production by hybrid solar+ hydro power system in Europe and similar climate areas." *Renewable and Sustainable Energy Reviews* 14 (6):1580-1590.

Martín, Ana M, Javier Domínguez, and Julio Amador. 2015. "Applying LIDAR datasets and GIS based model to evaluate solar potential over roofs: a review." *AIMS Energy* 3 (3):326-343.

Mathew, Sathyajith. 2006. *Wind energy: fundamentals, resource analysis and economics*. Vol. 1: Springer.

McKenney, Daniel W., Sophie Pelland, Yves Poissant, Robert Morris, Michael Hutchinson, Pia Papadopol, Kevin Lawrence, and Kathy Campbell. 2008. "Spatial insolation models for photovoltaic energy in Canada." *Solar Energy* 82 (11):1049-1061. doi: https://doi.org/10.1016/j.solener.2008.04.008.

Melius, J, R Margolis, and Sean Ong. 2013. Estimating rooftop suitability for PV: a review of methods, patents, and validation techniques. National Renewable Energy Laboratory (NREL), Golden, CO.

Mellit, Adel, and Mohamed Benghanem. 2007. "Sizing of stand-alone photovoltaic systems using neural network adaptive model." *Desalination* 209 (1-3):64-72.

Mirmasoudi, Shaghayegh, James Byrne, Roland Kroebel, Daniel Johnson, and Ryan MacDonald. 2018. "A novel time-effective model for daily distributed solar radiation estimates across variable terrain." *International Journal of Energy and Environmental Engineering*:1-16.

Mitchell, Bruce. 2015. *Resource and environmental management in Canada*. Fifth ed. Canada: Oxford University Press.

Mohamed, Mohamed A, Ali M Eltamaly, and Abdulrahman I Alolah. 2016. "PSO-based smart grid application for sizing and optimization of hybrid renewable energy systems." *PloS one* 11 (8):e0159702.

Mohammed, Omar Hazem, Yassine Amirat, Gilles Feld, and Mohamed Benbouzid. 2016. "Hybrid Generation Systems Planning Expansion Forecast State of the Art Review: Optimal Design vs Technical and Economical Constraints." *Journal of Electrical Systems* 12 (1).

Mohanty, Parimita, Tariq Muneer, Eulalia Jadraque Gago, and Yash Kotak. 2016. "Solar radiation fundamentals and PV system components." In *Solar Photovoltaic System Applications*, 7-47. Springer.

Moore, Larry M, and Harold N Post. 2008. "Five years of operating experience at a large, utility-scale photovoltaic generating plant." *Progress in Photovoltaics: Research and Applications* 16 (3):249-259.

Mueller, S, P Frankl, and K Sadamori. 2016. "Next Generation Wind and Solar Power From Cost to Value." *International Energy Agency: Paris, France*.

Myers, Daryl R, Ibrahim Reda, Stephen Wilcox, and Afshin Andreas. 2004. "Optical radiation measurements for photovoltaic applications: instrumentation uncertainty and performance." Proceedings of SPIE.

Nafeh, Abd El-Shafy A. 2011. "Optimal economical sizing of a PV-wind hybrid energy system using genetic algorithm." *International Journal of Green Energy* 8 (1):25-43.

Natural Resources Canada. 2017a. About Renewable Energy. https://www.nrcan.gc.ca/energy/renewable-electricity/7295: Government of Canada.

Natural Resources Canada. 2017b. Photovoltaic and solar resource maps. http://www.nrcan.gc.ca/18366: Government of Canada.

Natural Resources Canada. 2018a. Electricity facts. https://www.nrcan.gc.ca/energy/facts/electricity/20068: Government of Canada.

Natural Resources Canada. 2018b. Energy and greenhouse gas emissions (GHGs). https://www.nrcan.gc.ca/energy/facts/energy-ghgs/20063: Government of Canada.

Nelson, DB, MH Nehrir, and C Wang. 2006. "Unit sizing and cost analysis of stand-alone hybrid wind/PV/fuel cell power generation systems." *Renewable energy* 31 (10):1641-1656.

Nguyen, Ha T, and Joshua M Pearce. 2013. "Automated quantification of solar photovoltaic potential in cities." *International Review for Spatial Planning and Sustainable Development* 1 (1):49-60.

Okinda, Victor O, and Nichodemus A Odero. 2015. "A review of techniques in optimal sizing of hybrid renewable energy systems." *International Journal of Research in Engineering and Technology* 4 (11):153-163.

Ong, Sean, Clinton Campbell, Paul Denholm, Robert Margolis, and Garvin Heath. 2013. Land-use requirements for solar power plants in the United States. National Renewable Energy Laboratory (NREL), Golden, CO.

Ordóñez, J, E Jadraque, J Alegre, and G Martínez. 2010. "Analysis of the photovoltaic solar energy capacity of residential rooftops in Andalusia (Spain)." *Renewable and Sustainable Energy Reviews* 14 (7):2122-2130.

Orgill, JF, and KGT Hollands. 1977. "Correlation equation for hourly diffuse radiation on a horizontal surface." *Solar Energy* 19 (4):357-359.

Owayjan, Michel, Adel Chit, Elie Abdo, and Chadi Fakhry. 2013. "Intelligent dump load controller for high power wind turbine." Microelectronics (ICM), 2013 25th International Conference on.

Pachauri, Rajendra K, Myles R Allen, Vicente R Barros, John Broome, Wolfgang Cramer, Renate Christ, John A Church, Leon Clarke, Qin Dahe, and Purnamita Dasgupta. 2014. *Climate change 2014: synthesis report. Contribution of Working Groups I, II and III to the fifth assessment report of the Intergovernmental Panel on Climate Change*: IPCC.

Pasqualetti, Martin J. 2011. "Social barriers to renewable energy landscapes." *Geographical Review* 101 (2):201-223.

Pelland, Sophie, Daniel W McKenney, Yves Poissant, Robert Morris, Kevin Lawrence, Kathy Campbell, and Pia Papadopol. 2006. "The development of photovoltaic resource maps for Canada." Proc. 31st Annual Conference of the Solar Energy Society of Canada (SESCI). Aug.

Pelland, Sophie, and Yves Poissant. 2006. "An evaluation of the potential of building integrated photovoltaics in Canada." Proceedings of the SESCI 2006 Conference, submitted.

People Power Planet Partnership. 2018. Alberta renewable energy and community energy overview. http://peoplepowerplanet.ca/alberta/resources/.

Perez, Richard, Pierre Ineichen, Robert Seals, Joseph Michalsky, and Ronald Stewart. 1990. "Modeling daylight availability and irradiance components from direct and global irradiance." *Solar Energy* 44 (5):271-289.

Perez, Richard, Robert Seals, Pierre Ineichen, Ronald Stewart, and David Menicucci. 1987. "A new simplified version of the Perez diffuse irradiance model for tilted surfaces." *Solar Energy* 39 (3):221-231.

Philipps, Simon, and Werner Warmuth. 2017. Photovoltaics report. Freiburg: Fraunhofer Institute for Solar Energy Systems, ISE.

Piragnolo, Marco, Andrea Masiero, Francesca Fissore, and Francesco Pirotti. 2015. "Solar irradiance modelling with NASA WW GIS environment." *ISPRS International Journal of Geo-Information* 4 (2):711-724.

Poissant, Y. , C. Baldus-Jeursen, CanmetENERGY, Natural Resources Canada, P. Bateman, and Canadian Solar Industries Association. 2017. National Survey Report of PV Power Applications in CANADA – 2016. International Energy Agency: Natural Resources Canada.

Poli, Riccardo, James Kennedy, and Tim Blackwell. 2007. "Particle swarm optimization." *Swarm Intelligence* 1 (1):33-57.

Power Advisory LLC. 2017. Independent assessment of renewable generation costs and the relative benefits of these projects compared to site C. https://canwea.ca/wp-content/uploads/2014/01/PowerAdvisory-AssessmentGenerationCostsBenefitsReSiteC-web.pdf: Power Advisory LLC.

Prasad, A Rajendra, and E Natarajan. 2006. "Optimization of integrated photovoltaic–wind power generation systems with battery storage." *Energy* 31 (12):1943-1954.

Quan, Pham, and Thananchai Leephakpreeda. 2015. "Assessment of wind energy potential for selecting wind turbines: an application to Thailand." *Sustainable Energy Technologies and Assessments* 11:17-26.

Ramachandra, TV. 2006. "Solar energy potential assessment using GIS." *Energy Education Science and Technology* 18 (1/2):101.

Ranjithan, S Ranji, S Kishan Chetan, and Harish K Dakshina. 2001. "Constraint method-based evolutionary algorithm (CMEA) for multiobjective optimization." International Conference on Evolutionary Multi-Criterion Optimization.

Redweik, P, Cristina Catita, and Miguel Brito. 2013. "Solar energy potential on roofs and facades in an urban landscape." *Solar Energy* 97:332-341.

Rehman, Naveed UR, and Mubashir Ali Siddiqui. 2012. "Development of Simulation Tool for Finding Optimum Tilt Angles for Solar Collectors."

Reich, Nils H, Bjoern Mueller, Alfons Armbruster, Wilfried GJHM Sark, Klaus Kiefer, and Christian Reise. 2012. "Performance ratio revisited: is PR> 90% realistic?" *Progress in Photovoltaics: Research and Applications* 20 (6):717-726.

Reindl, Douglas T, William A Beckman, and John A Duffie. 1990. "Diffuse fraction correlations." *Solar Energy* 45 (1):1-7.

Resch, Bernd, Günther Sagl, Tobias Törnros, Andreas Bachmaier, Jan-Bleicke Eggers, Sebastian Herkel, Sattaya Narmsara, and Hartmut Gündra. 2014. "GIS-based planning and modeling for renewable energy: Challenges and future research avenues." *ISPRS International Journal of Geo-Information* 3 (2):662-692.

Rich, P, RC Dubayah, W Hetrick, and S Saving. 1994. "Using viewshed models to calculate intercepted solar radiation: applications in ecology. American Society for Photogrammetry and Remote Sensing Technical Papers." American Society of Photogrammetry and Remote Sensing.

Richards, Garrett, Bram Noble, and Ken Belcher. 2012. "Barriers to renewable energy development: A case study of large-scale wind energy in Saskatchewan, Canada." *Energy Policy* 42:691-698.

Richardson, David B, and LDD Harvey. 2015. "Strategies for correlating solar PV array production with electricity demand." *Renewable Energy* 76:432-440.

Ritter, Matthias, Zhiwei Shen, Brenda López Cabrera, Martin Odening, and Lars Deckert. 2015. "Designing an index for assessing wind energy potential." *Renewable Energy* 83:416-424.

Ropp, ME, M Begovic, and A Rohatgi. 1997. "Determination of the curvature derating factor for the Georgia Tech Aquatic Center photovoltaic array." Photovoltaic Specialists Conference, 1997., Conference Record of the Twenty-Sixth IEEE.

Rosenbloom, Daniel, and James Meadowcroft. 2014. "Harnessing the Sun: Reviewing the potential of solar photovoltaics in Canada." *Renewable and Sustainable Energy Reviews* 40:488-496.

Rouhani, Ahmad, Hossein Kord, and Mahdi Mehrabi. 2013. "A comprehensive method for optimum sizing of hybrid energy systems using intelligence evolutionary algorithms." *Indian Journal of Science and Technology* 6 (6):4702-4712.

Rowlands, Ian H, Briana Paige Kemery, and Ian Beausoleil-Morrison. 2011. "Optimal solar-PV tilt angle and azimuth: An Ontario (Canada) case-study." *Energy Policy* 39 (3):1397-1409.

Ruiz-Arias, JA, Joaquín Tovar-Pescador, David Pozo-Vázquez, and Husain Alsamamra. 2009. "A comparative analysis of DEM-based models to estimate the solar radiation in mountainous terrain." *International Journal of Geographical Information Science* 23 (8):1049-1076.

Ryberg, David, and Janine Freeman. 2015. Integration, Validation, and Application of a PV Snow Coverage Model in SAM. National Renewable Energy Lab.(NREL), Golden, CO (United States).

Santosa, T, N Gomesb, S Freirea, MC Britoc, L Santosb, and JA Tenedório. 2014. "Applications of solar mapping in the urban environment [J]." *Applied Geography* 51:48-57.

Sauer, Dirk U, Georg Bopp, Andreas Jossen, Jürgen Garche, Martin Rothert, and Michael Wollny. 1999. "State of Charge–What do we really speak about." The 21st International Telecommunications Energy Conference.

Sawin, Janet L. , Kristin Seyboth, Freyr Sverrisson, Fabiani Appavou, Adam Brown, Ilya Chernyakhovskiy, Bärbel Epp, Lon Huber, Christine Lins, Jeffrey Logan, Lorcan Lyons, and Michael Milligan. 2017. Renewables 2017-Global Status Report. Paris: REN21

Schallenberg-Rodriguez, Julieta. 2013. "A methodological review to estimate techno-economical wind energy production." *Renewable and Sustainable Energy Reviews* 21:272-287.

Schmalensee, Richard. 2015. *The Future of Solar Energy: An Interdisciplinary MIT Study*: Energy Initiative, Massachusetts Institute of Technology.

Schnitzer, Marie, Christopher Thuman, and Peter Johnson. 2012. "Reducing Uncertainty in Solar Energy Estimates: Mitigating Energy Risk through On-Site Monitoring." *AWS True Power report, Albany, New York*.

SciPy.org. 2018. "numpy.std." https://docs.scipy.org/doc/numpy/reference/generated/numpy.std.html#numpy-std.

Seyboth, Kristin, F Sverrisson, F Appavou, A Brown, B Epp, A Leidreiter, C Lins, E Musolino, HE Murdock, and K Petrichenko. 2016. "Renewables 2016 Global Status Report." *REN21: Paris, France*.

Shahzad, Umair. 2012. "The Need for Renewable Energy Sources." *energy* 2:3.

Sharafi, Masoud, and Tarek Y ElMekkawy. 2014. "Multi-objective optimal design of hybrid renewable energy systems using PSO-simulation based approach." *Renewable Energy* 68:67-79.

Shi, Yuhui. 2001. "Particle swarm optimization: developments, applications and resources." In Proceedings of the 2001 Congress on Evolutionary Computation (IEEE Cat. No. 01TH8546). Vol. 1, pp. 81-86. IEEE.

Shukla, KN, Saroj Rangnekar, and K Sudhakar. 2015. "Comparative study of isotropic and anisotropic sky models to estimate solar radiation incident on tilted surface: A case study for Bhopal, India." *Energy Reports* 1:96-103.

Singh, Rhythm, and Rangan Banerjee. 2015. "Estimation of rooftop solar photovoltaic potential of a city." *Solar Energy* 115:589-602.

Skartveit, Arvid, and Jan Asle Olseth. 1986. "Modelling slope irradiance at high latitudes." *Solar Energy* 36 (4):333-344.

Skoplaki, E, AG Boudouvis, and JA Palyvos. 2008. "A simple correlation for the operating temperature of photovoltaic modules of arbitrary mounting." *Solar Energy Materials and Solar Cells* 92 (11):1393-1402.

Sohoni, Vaishali, SC Gupta, and RK Nema. 2016. "A Critical Review on Wind Turbine Power Curve Modelling Techniques and Their Applications in Wind Based Energy Systems." *Journal of Energy* 2016.

Solar Choice. 2016. "1.5kW solar PV systems: Pricing, outputs and payback." https://www.solarchoice.net.au/blog/1-5kw-solar-pv-systems-price-output-payback.

Sovacool, Benjamin K. 2009. "The cultural barriers to renewable energy and energy efficiency in the United States." *Technology in Society* 31 (4):365-373.

Staffell, Iain, and Richard Green. 2014. "How does wind farm performance decline with age?" *Renewable Energy* 66:775-786.

Statistics Canada. 2018. "Consumer Price Index, by province (Alberta)." accessed 2018. https://www.statcan.gc.ca/tables-tableaux/sum-som/l01/cst01/econ09j-eng.htm.

Steven, MD, and Michael H Unsworth. 1980. "The angular distribution and interception of diffuse solar radiation below overcast skies." *Quarterly Journal of the Royal Meteorological Society* 106 (447):57-61.

Stevens, David, and Jasmine Chung. 2017. "Energy Storage Developments in Canada, the U.S. and Beyond in the Last Twelve Months." energy insider. https://www.airdberlis.com/insights/blogs/energyinsider/post/ei-item/energy-storage-developments-in-canada-the-u.s.-and-beyond-in-the-last-twelve-months.

Strupeit, Lars, and Alvar Palm. 2016. "Overcoming barriers to renewable energy diffusion: business models for customer-sited solar photovoltaics in Japan, Germany and the United States." *Journal of Cleaner Production* 123:124-136.

Sun, Yanwei, Run Wang, Jialin Li, and Jian Liu. 2017. "GIS-based multiregional potential evaluation and strategies selection framework for various renewable energy sources: a case study of eastern coastal regions of China." *Energy Science & Engineering* 5 (3):123-140.

Ter-Gazarian, AG, and N Kagan. 1992. "Design model for electrical distribution systems considering renewable, conventional and energy storage units." IEE Proceedings C-Generation, Transmission and Distribution.

Thapar, Vinay, Gayatri Agnihotri, and Vinod Krishna Sethi. 2011. "Critical analysis of methods for mathematical modelling of wind turbines." *Renewable Energy* 36 (11):3166-3177.

Thevenard, Didier, and Sophie Pelland. 2013. "Estimating the uncertainty in long-term photovoltaic yield predictions." *Solar Energy* 91:432-445.

Tina, G, S Gagliano, and S Raiti. 2006. "Hybrid solar/wind power system probabilistic modelling for long-term performance assessment." *Solar Energy* 80 (5):578-588.

Tina, Giuseppe Marco, Cristina Ventura, and Sebastiano De Fiore. 2012. "Sub-hourly irradiance models on the plane of array for photovoltaic energy forecasting applications." Photovoltaic Specialists Conference (PVSC), 2012 38th IEEE.

Tooke, Thoreau Rory, Nicholas C Coops, Andreas Christen, Ozgur Gurtuna, and Arthur Prévot. 2012. "Integrated irradiance modelling in the urban environment based on remotely sensed data." *Solar Energy* 86 (10):2923-2934.

U.S. Energy Information Administration. 2016. International Energy Outlook 2016. Washington, DC: Office of Energy Analysis U.S. Department of Energy.

van der Hoeven, Maria. 2015. "Energy and climate change—world energy outlook special report." *Int. Energy Agency*.

Verso, A, A Martin, J Amador, and J Dominguez. 2015. "GIS-based method to evaluate the photovoltaic potential in the urban environments: The particular case of Miraflores de la Sierra." *Solar Energy* 117:236-245.

Vignola, Frank, Fotis Mavromatakis, and Jim Krumsick. 2008. "Performance of PV inverters." Proc. of the 37th ASES Annual Conference, San Diego, CA.

Vijayalekshmy, S, GR Bindu, and S Rama Iyer. 2014. "Estimation of Power Losses in Photovoltaic Array Configurations under Moving Cloud Conditions." Advances in Computing and Communications (ICACC), 2014 Fourth International Conference on.

Wang, Lingfeng, and Chanan Singh. 2008. "Hybrid Design of Electric Power Generation Systems Including Renewable Sources of Energy." *Bulletin of Science, Technology & Society* 28 (3):192-199.

Wang, Lingfeng, and Chanan Singh. 2009. "Multicriteria design of hybrid power generation systems based on a modified particle swarm optimization algorithm." *IEEE Transactions on Energy Conversion* 24 (1):163-172.

Weis, Tim, Alex Doukas, and Kristi Anderson. 2010. *Landowners' Guide to Wind Energy in Alberta*: Pembina Institute.

Whaley, Cass. 2016. Best practices in photovoltaic system operations and maintenance. National Renewable Energy Lab.(NREL), Golden, CO (United States).

Wiginton, LK, Ha T Nguyen, and Joshua M Pearce. 2010. "Quantifying rooftop solar photovoltaic potential for regional renewable energy policy." *Computers, Environment and Urban Systems* 34 (4):345-357.

Wirth, Harry, and Karin Schneider. 2016. "Recent facts about photovoltaics in Germany." *Fraunhofer ISE*:92.

World Energy Council. 2016. World Energy Resources | 2016. https://www.worldenergy.org/publications/2016/world-energy-resources-2016/.

Xu, Lin, Xinbo Ruan, Chengxiong Mao, Buhan Zhang, and Yi Luo. 2013. "An improved optimal sizing method for wind-solar-battery hybrid power system." *IEEE Transactions on Sustainable Energy* 4 (3):774-785.

Yang, Hongxing, Lin Lu, and Wei Zhou. 2007. "A novel optimization sizing model for hybrid solar-wind power generation system." *Solar Energy* 81 (1):76-84.